



UNIVERSIDADE ESTADUAL DE CAMPINAS  
FACULDADE DE ENGENHARIA MECÂNICA  
E INSTITUTO DE GEOCIÊNCIAS

DIANA MARÍA HERNÁNDEZ CASTRO

**INVESTIGATION OF DISSOLUTION  
EFFECTS ON CARBONATE ROCKS  
POROUS MEDIA UNDER CARBONATED  
WATER INJECTION**

**INVESTIGAÇÃO DOS EFEITOS DA  
DISSOLUÇÃO EM MEIOS POROSOS DE  
ROCHAS CARBONATICAS SOB INJEÇÃO DE  
ÁGUA CARBONATADA**

CAMPINAS

2018

**DIANA MARÍA HERNÁNDEZ CASTRO**

**INVESTIGATION OF DISSOLUTION EFFECTS ON  
CARBONATE ROCKS POROUS MEDIA UNDER  
CARBONATED WATER INJECTION**

**INVESTIGAÇÃO DOS EFEITOS DA DISSOLUÇÃO  
EM MEIOS POROSOS DE ROCHAS CARBONÁTICAS  
SOB INJEÇÃO DE ÁGUA CARBONATADA**

Dissertation presented to the Mechanical Engineering Faculty and Geosciences Institute of the University of Campinas in partial fulfillment of the requirements for the degree of Master in Petroleum Sciences and Engineering in the area of Reservoirs and Management.

Dissertação apresentada à Faculdade de Engenharia Mecânica e Instituto de Geociências da Universidade Estadual de Campinas como parte dos requisitos exigidos para a obtenção do título de Mestra em Ciências e Engenharia de Petróleo na área de Reservatórios e Gestão.

Orientador: Prof. Dr. Osvaldo Vidal Trevisan

Coorientador: Dra. Janeth Alina Vidal Vargas

Este exemplar corresponde à versão final da Dissertação defendida pelo aluno Diana Maria Hernandez Castro e orientada pelo Prof. Dr. Osvaldo Vidal Trevisan

---

Assinatura do Orientador

CAMPINAS

2018

Ficha catalográfica  
Universidade Estadual de Campinas  
Biblioteca da Área de Engenharia e Arquitetura  
Luciana Pietrosanto Milla - CRB 8/8129

C279i Castro Hernandez, Diana Maria, 1990-  
Investigation of dissolution effects on carbonate rocks porous media under carbonated water injection / Diana Maria Hernandez Castro. – Campinas, SP : [s.n.], 2018.

Orientador: Osvaldo Vidal Trevisan.

Coorientador: Janeth Alina Vidal Vargas.

Dissertação (mestrado) – Universidade Estadual de Campinas, Faculdade de Engenharia Mecânica.

1. Dissolução. 2. Rochas carbonáticas. 3. Tomografia computadorizada por raio x. 4. X-ray tomografia computadorizada. I. Trevisan, Osvaldo Vidal, 1952-. II. Vidal Vargas, Janeth Alina, 1983-. III. Universidade Estadual de Campinas. Faculdade de Engenharia Mecânica. IV. Título.

Informações para Biblioteca Digital

**Título em outro idioma:** Investigação dos efeitos da dissolução em meios porosos de rochas carbonáticas sob injeção de água carbonatada

**Palavras-chave em inglês:**

Dissolution

Carbonate rocks

X-ray computed tomography

**Área de concentração:** Reservatórios e Gestão

**Titulação:** Mestra em Ciências e Engenharia de Petróleo

**Banca examinadora:**

Janeth Alina Vidal Vargas [Coorientador]

Alessandro Batezelli

Edvaldo Sabadini

**Data de defesa:** 30-07-2018

**Programa de Pós-Graduação:** Ciências e Engenharia de Petróleo

**UNIVERSIDADE ESTADUAL DE CAMPINAS  
FACULDADE DE ENGENHARIA MECÂNICA  
COMISSÃO DE PÓS-GRADUAÇÃO EM ENGENHARIA  
MECÂNICA DEPARTAMENTO DE CIÊNCIAS E ENGENHARIA  
DE PETRÓLEO**

DISSERTAÇÃO DE MESTRADO ACADÊMICO

**INVESTIGATION OF DISSOLUTION EFFECTS ON  
CARBONATE ROCKS POROUS MEDIA UNDER  
CARBONATED WATER INJECTION**

**INVESTIGAÇÃO DOS EFEITOS DA DISSOLUÇÃO EM  
MEIOS POROSOS DE ROCHAS CARBONÁTICAS SOB  
INJEÇÃO DE ÁGUA CARBONATADA**

Autor: Diana María Hernández Castro

Orientador: Prof. Dr. Osvaldo Vidal Trevisan

A Banca Examinadora composta pelos membros abaixo aprovou esta Dissertação:

Prof. Dr. Janeth Alina Vidal Vargas, Presidente.  
Universidade Estadual de Campinas

Prof. Dr. Alessandro Batezelli  
Universidade Estadual de Campinas

Prof. Dr. Edvaldo Sabadini  
Universidade Estadual de Campinas

A Ata da defesa com as respectivas assinaturas dos membros encontra-se no processo de vida acadêmica do aluno.

Campinas, 30 de Julho de 2018

## **DEDICATION**

*To*

*My parents, Carlos and Diana, and my Sister, Catalina, for their love,  
support, invaluable advice and motivation.*

*I miss you every day and I love you!*

## ACKNOWLEDGEMENTS

Firstly, I would like to thank my thesis advisor Professor PhD. Osvaldo Vidal Trevisan, his door was always open whenever I ran into a trouble or motivation words were needed. Thank you for the guidance that inspires me to work on this thesis, I am grateful for your support and encouragement that motivates me to accomplish this project.

I would also like to thank the experts who were involved in the validation of this research: Dr. Erika Koroishi and Dr. Janeth Vidal. I would like to thank you for your excellent cooperation, you provided me with the tools needed to choose the right direction and successfully complete my dissertation, without your passionate participation and input, the thesis could not have been successfully conducted.

Also, want to thank Henrique Assis for his help during the preparation of the experiments, Emilia Medeiros, Tálisson Carvalho and Oswaldo Klinger for the long nights in the laboratory, your friendship, for providing me with unfailing support, and continuous encouragement throughout my years of study and through the process of researching and writing this thesis.

Finally, wish to thank the LMMR team at the University of Campinas, for their constructive discussions and feedbacks.

## RESUMO

Alguns reservatórios carbonáticos conhecidos por seu elevado conteúdo de  $\text{CO}_2$  no óleo. Uma das possibilidades para o uso do gás sem problemas ambientais é reinjetá-lo no reservatório. Injeção de água carbonatada tem atenção crescente em pesquisas por ser uma técnica mais vantajosa comparada à injeção de  $\text{CO}_2$  gasoso, dada a melhora da mobilidade. O objetivo deste estudo é avaliar o fenômeno da dissolução e precipitação durante a injeção de água carbonatada em rochas carbonáticas. Esses efeitos são identificados pela análise da variação da porosidade por meio de imagens computadorizadas de tomografia de raio-X e de permeabilidade, determinado indiretamente pelos transdutores de pressão que medem o diferencial de pressão do fluido no início e na saída do porta-testemunho. Ensaio de deslocamento foram realizados com dois porta-testemunhos em série para representar regiões diferentes do reservatório, por meio da injeção de solução salina saturada com 25% de  $\text{CO}_2$  em amostras de reservatório, compostas de dolomita, calcita e argila. Os testes foram realizados usando as seguintes condições de reservatório: 8500, 7500 e 8250 psi a  $70^\circ\text{C}$ , usadas para cada cenário.. Baseando-se nos dados experimentais fornecidos pelas imagens de CT, foi possível visualizar o aumento ou redução da porosidade durante a injeção de água carbonatada, devido à co-existência de dissolução (aumento de porosidade) e precipitação (redução de porosidade) ao longo das amostras. Esses fenômenos foram observados nas regiões com maior heterogeneidade de porosidade. Em adição, a mineralogia das amostras é composta por três minerais, que influenciam a capacidade de reação com água carbonatada. Para o primeiro experimento, a amostra localizada no primeiro porta-testemunho apresentou um aumento de porosidade, enquanto a do segundo apresentou uma redução. Por outro lado, a permeabilidade sofreu um aumento significativo para ambos porta-testemunhos, acreditasse que a injeção promoveu um fluxo por caminho preferencial que afetou consideravelmente a permeabilidade da rocha. Para o segundo experimento, a rocha localizada no primeiro porta-testemunho apresentou um aumento de porosidade para todo o comprimento e para a segunda amostra houve um aumento menor do que o da primeira. Nenhum aumento de permeabilidade foi observado nas amostras. Para

o terceiro experimento houve um aumento de porosidade médio na amostra do primeiro porta-testemunho e uma considerável redução de permeabilidade. Uma inovação da foi usar amostras de carbonato de reservatório do pré-sal brasileiro com mineralogia basicamente composta por dolomita, calcita e argila. Além disso, o trabalho experimental foi realizado em condições operacionais de reservatório.

**Palavras Chave:** Dissolução, Rochas Carbonáticas, Injeção de Água Carbonatada, Tomografia Computadorizada.



## ABSTRACT

Some carbonate reservoirs are known for their high CO<sub>2</sub> content in oil. One possibility to handle this gas without environmental problems is to reinject it into the reservoir. Injection of carbonated water has been drawing attention because it is an advantageous technique when compared to gaseous CO<sub>2</sub> injection, due to its improvement in mobility in the reservoir. The objective of this study is to evaluate the phenomenon of dissolution and precipitation during carbonated water injection in carbonate rocks. These effects are identified by analyzing the porosity variations through X-ray computer tomography images and permeability profile, determined indirectly by pressure transducers that measured the differential pressure by the fluid at the inlet and outlet of the core holders. Coreflooding tests were carried out with two core holders in series to represent different regions at the reservoir by the injection of brine saturated with 25% of CO<sub>2</sub> in reservoir samples, composed of dolomite, calcite and clay. The tests were performed using the following reservoir conditions of 8,500, 7500 and 8250 psi at 70°C were used for each scenario.. Based on the experimental data provided by CT images, it can be seen that the core porosity increases or decrease during carbonated water injection due to coexistence of dissolution (increase of porosity) and precipitation (decrease of porosity) along the samples. These phenomena are observed in regions with high heterogeneity in porosity. In addition, the mineralogy of the cores is composed by three minerals, which influence in the capacity of reaction with carbonated water. For the first experiment, the core placed in the core holder one presented a porosity increase and the second one decreased. On the other hand, the permeability showed a significant increase for both cores, it is believed that, the injection promoted a preferential way flow (wormhole) that affected considerably the permeability of the rock. For the second experiment, the core placed in the first core holder presented a porosity increase along all the sample length and the second one showed an increase lower than the first sample. The permeability does not show an increase for both samples. The third experiment reports an increase in the porosity average in the sample located in the first core holder and a considerable decrease in permeability. The novelty of the

investigation is that the experiments were carried out using Brazilian pre-salt carbonate reservoir rocks with mineralogy composed basically by dolomite, calcite and clay. Also, experimental work was performed at reservoir operational conditions.

**Key Word:** Dissolution, Carbonate rocks, Carbonated Water Injection, Computed tomography.

## FIGURE LIST

<b>Figure 2.1</b> Effect of Damköhler number on the channel network geometry generated by dissolution ((FOGLER, 1988)).....	35
<b>Figure 2.2</b> The ratios of the magnitude of $u$ at the voxel centers divided by the average pore velocity $U_{av}$ are colored using a linear scale where low velocity is blue, medium velocity is yellow, and high velocity is red.(MENKE et al., 2016).....	38
<b>Figure 2.3</b> Calcium concentration in 2000 ppm NaCl solution, during bulk test, versus time, 22°C, CO <sub>2</sub> -free environment, experimental + PHREEQC data. (OUDEN et al., 2015).....	41
<b>Figure 3.1</b> High Pressure Positive Displacement Pump. ....	43
<b>Figure 3.2</b> Oerlikon da Leybol vacuum pump ( <a href="http://www.idealvac.com/files/ManualsII">www.idealvac.com/files/ManualsII</a> )... ..	44
<b>Figure 3.3</b> Schematic of Core Holder. Nunez (2017).....	44
<b>Figure 3.4</b> Accumulator type piston .....	45
<b>Figure 3.5</b> Back Pressure ( <a href="http://www.corelab.com/cli/accessories/back-pressure-regulators-bp-bpr-series">www.corelab.com/cli/accessories/back-pressure-regulators-bp-bpr-series</a> ).....	46
<b>Figure 3.6</b> BB 2600T Series Pressure Transmitters. ....	46
<b>Figure 3.7</b> NOVOUS N1040 Temperature Controlled ( <a href="http://www.novus.com.br">www.novus.com.br</a> ).....	47
<b>Figure 3.8</b> Siemens Somatom Tomography .....	48
<b>Figure 3.9</b> UltraPore Porosimeter- Upore 300.....	49
<b>Figure 3.10</b> Permeameter Ultraperm-500 (Corelab).....	49
<b>Figure 3.11.</b> Chromatograph Thermo Scientific.....	50
<b>Figure 3.12</b> Quizix 5000 Series Pump.....	52
<b>Figure 3.13</b> Extrator Soxhlet .....	54
<b>Figure 3.14</b> Reservoir's rock after cleaning .....	55
<b>Figure 3.15</b> Applying Epoxi Resin at the sample contour.....	56
<b>Figure 3.16</b> Durepox (Epoxi Resin) .....	56
<b>Figure 3.17</b> Sand down of the reservoir rock .....	56
<b>Figure 3.18</b> Cemented and sand down reservoir's rocks.....	56
<b>Figure 3.19</b> OHAUS precision analytical balance.....	57
<b>Figure 3.20</b> Starrett Caliper .....	57
<b>Figure 3.21</b> Illustration of the Initial cell of the Sample.....	62

<b>Figure 3.22.</b> Example graph for the calculation of the dissolution rate.....	62
<b>Figure 3.23</b> Salts Mix Procedure .....	64
<b>Figure 3.24</b> Brine filtration Procedure.....	64
<b>Figure 3.25</b> Air removal Procedure. ....	65
<b>Figure 3.26.</b> The molality of CO <sub>2</sub> ( <a href="http://models.kl-edi.ac.cn">http://models.kl-edi.ac.cn</a> ).....	65
<b>Figure 3.27</b> Apparatus Carbonated Water Preparation.....	66
<b>Figure 3.28</b> Mechanic agitator with the cylinder with carbonated water. ....	67
<b>Figure 3.29</b> Rock Reservoir Isolate Process. ....	69
<b>Figure 3.30</b> Introduced into overburden system until reached 1000 psi.....	70
<b>Figure 3.31</b> A resistance heating type jacket is wrapping around the core holder .....	70
<b>Figure 3.32</b> Experiment Setup .....	71
<b>Figure 3.33</b> Experimental Setup .....	72
<b>Figure 4.1.</b> Porosity Media Values obtained from Tomographies DH1-A .....	75
<b>Figure 4.2</b> Porosity Media Values obtained from Tomographies DH1-B.....	75
<b>Figure 4.3</b> Porosity Variation along sample DH1-A .....	77
<b>Figure 4.4</b> Initial Porosity Variation along Sample DH1-B .....	78
<b>Figure 4.5</b> Porosity Variation along sample DH1-B in different times.....	79
<b>Figure 4.6</b> Behavior of the porosity at the sample DH1-B along the length 3cm to end of the rock. ....	79
<b>Figure 4.7</b> Saturated tomography CH2 (i=5).....	81
<b>Figure 4.8</b> Tomography #1 CH2 (i=5).....	81
<b>Figure 4.9</b> Tomography #2 CH2 (i=5).....	81
<b>Figure 4.10</b> Tomography #14 CH2 (i=5).....	81
<b>Figure 4.11</b> Tomography #15 CH2 (i=5).....	81
<b>Figure 4.12</b> Permeability of DH1-A and DH1-B samples throughout the experiment 1. The absence of permeability data present in the graph between the injected 40 and 47 VP is related to a stop at the Pump in the experiment.....	82
<b>Figure 4.13</b> Magnesium produced CH1 and CH2. ....	84
<b>Figure 4.14</b> Calcium produced CH1 and CH2.....	85
<b>Figure 4.15</b> Nunez 2017. Sample Porosity variation along the sample RV4 CH1.....	86
<b>Figure 4.16</b> Porosity Variation along sample DH1-A .....	86
<b>Figure 4.17</b> Sample Porosity variation along the sample RV6 CH2 .....	87
<b>Figure 4.18</b> Porosity Variation along sample DH1-B in different times.....	88
<b>Figure 4.19</b> Nuñez 2017. Permeability Variation RV4 CH1 .....	89

<b>Figure 4.20.</b> Nunez 2017. Permeability Variation RV6 CH2.....	89
<b>Figure 4.21</b> Permeability of DH1-A and DH1-B samples throughout the experiment 1. .....	90
<b>Figure 4.22</b> Average Porosity Values obtained from Tomographies DH2-A .....	92
<b>Figure 4.23</b> Average Porosity Values obtained from Tomographies DH2-B. ....	92
<b>Figure 4.24</b> Porosity Variation along the Sample DH2-A.....	93
<b>Figure 4.25</b> Porosity Variation Along the Sample DH2-B.....	94
<b>Figure 4.26</b> Porosity Variation Along the Sample ( 3 - 4.3 cm) DH2-B.....	95
<b>Figure 4.27</b> Porosities Rock DH2-B calculates at different times with the CT scan....	96
<b>Figure 4.28</b> Permeability Experiment #2.....	97
<b>Figure 4.29</b> Magnesium produced CH1 and CH2. ....	101
<b>Figure 4.30</b> Calcium produced CH1 and CH2.....	101
<b>Figure 4.31</b> Sample Porosity variation along the sample R2N CH1. Source: Nunez .	102
<b>Figure 4.32</b> Porosity Variation along the Sample DH2-A.....	103
<b>Figure 4.33</b> Nunez 2017. Sample Porosity variation along the sample R4N CH2.....	104
<b>Figure 4.34</b> Porosity Variation Along the Sample DH2-B.....	104
<b>Figure 4.35</b> Nunez 2017. Permeability Scatter Plot Sample R2N CH1. ....	105
<b>Figure 4.36</b> Permeability Scatter Sample Plot R4N CH2.....	106
<b>Figure 4.37.</b> Permeability Results Experiment 2 .....	106
<b>Figure 4.38</b> Average Porosity Values obtained from Tomographies DH3-A .....	108
<b>Figure 4.39</b> Porosity Variation along sample DH3-A .....	110
<b>Figure 4.40</b> Porosity Variation along sample DH3-B .....	111
<b>Figure 4.41</b> Permeability Experiment #3.....	112
<b>Figure 4.42</b> Permeability since 0 to 20 PVI - Experiment #3.....	112
<b>Figure 4.43</b> Permeability since 20 to 40 PVI - Experiment #3.....	113
<b>Figure 4.44</b> Permeability since 40 to 60 PVI - Experiment #3.....	113
<b>Figure 4.45</b> Permeability since 60 to 77 PVI - Experiment #3.....	114
<b>Figure 4.46</b> Magnesium produced CH1 and CH2 .....	115
<b>Figure 4.47</b> Calcium produced CH1 and CH2.....	116
<b>Figure 4.48</b> Nunez 2017. Sample Porosity variation along the Dolomite sample RN1 CH1.....	117
<b>Figure 4.49</b> Porosity Variation along sample DH3-A .....	117
<b>Figure 4.50</b> Nunez 2017. Sample Porosity variation along the Dolomite sample R3N CH2.....	118

<b>Figure 4.51</b> Porosity Variation along sample DH3-A .....	119
<b>Figure 4.53</b> Porosity Variation along sample DH3-A .....	119
<b>Figure 4.54</b> Permeability Scatter Plot of dolomite sample (R1N) CH1 by (Nuñez, 2017) .....	120
<b>Figure 4.55</b> Permeability Experiment #3.....	120
<b>Figure 4.55</b> Evolution of Dissolved moles of Kaolinite Sample DH1-A –Cell 1. ....	122
<b>Figure 4.56</b> Evolution of Dissolved moles of Calcite Sample DH1-A –Cell 1 .....	122
<b>Figure 4.57</b> Evolution of Dissolved moles of Dolomite Sample DH1-A –Cell 1 .....	123
<b>Figure 4.58</b> Evolution of Dissolved moles of Kaolinite Sample DH1-B –Cell 1 .....	124
<b>Figure 4.59</b> Evolution of Dissolved moles of Calcite Sample DH1-B –Cell 1 .....	125
<b>Figure 4.60</b> Evolution of Dissolved moles of Dolomite Sample DH1-B –Cell 1 .....	125
<b>Figure 4.61</b> Evolution of Dissolved moles of Kaolinite Sample DH2-A –Cell 1. ....	127
<b>Figure 4.62</b> Evolution of Dissolved moles of Calcite Sample DH2-A –Cell 1 .....	127
<b>Figure 4.63</b> Evolution of Dissolved moles of Dolomite Sample DH2-A –Cell 1 .....	128
<b>Figure 4.64</b> Evolution of Dissolved moles of Kaolinite Sample DH2-B –Cell 1 .....	129
<b>Figure 4.65</b> Evolution of Dissolved moles of Calcite Sample DH2-B –Cell 1 .....	129
<b>Figure 4.66</b> Evolution of Dissolved moles of Dolomite Sample DH2-B –Cell 1 .....	130
<b>Figure 4.67</b> Evolution of Dissolved moles of Kaolinite Sample DH3-A –Cell 1. ....	131
<b>Figure 4.68</b> Evolution of Dissolved moles of Calcite Sample DH3-A –Cell 1 .....	132
<b>Figure 4.69</b> Evolution of Dissolved moles of Dolomite Sample DH3-A –Cell 1 .....	132

## TABLE LIST

<b>Table 2.1</b> Properties Carbon Dioxide <a href="http://www.uigi.com">http://www.uigi.com</a> .....	28
<b>Table 2.2</b> Dissolution kinetics for calcite, dolomite and magnesite 25° C and 0-50 atm.(POKROVSKY et al., 2005) .....	33
<b>Table 3.1</b> The Dionex - Thermo Scientific multi anion.....	51
<b>Table 3.2</b> The Dionex - Thermo Scientific multi-cations .....	51
<b>Table 3.3</b> Mineralogy of samples used for experiments .....	52
<b>Table 3.4</b> Seawater Composition Utilized for the two Experiments .....	63
<b>Table 3.5</b> Operational parameters for each Experiments.....	73
<b>Table 4.1</b> Experimental conditions Test #1 .....	74
<b>Table 4.2.</b> Initial porosity (gas) and permeability (gas) of the samples for Experiment #1. ....	74
<b>Table 4.3</b> Calcium and Magnesium Ions Chromatography results.....	84
<b>Table 4.4</b> Experimental conditions Test #2 .....	91
<b>Table 4.5</b> Initial porosity (gas) and permeability (gas) of the samples for Experiment #2 .....	91
<b>Table 4.6</b> Position of the rock at the beginning, middle and end of the experiment CH1 .....	98
<b>Table 4.7</b> Position of the rock at the beginning, middle and end of the experiment CH2 .....	99
<b>Table 4.8</b> Calcium and Magnesium Ions Chromatography results.....	100
<b>Table 4.9</b> Experimental conditions Test #3 .....	107
<b>Table 4.10.</b> Initial porosity (gas) and permeability (gas) of the samples for Experiment #3 .....	108
<b>Table 4.11.</b> Calcium and Magnesium Ions Chromatography results.....	115
<b>Table 4.12</b> Mineral Reaction Rate at the Cell 1 in the Sample DH1-A.....	121
<b>Table 4.13</b> Mineral Percentage DH1-B located CH2 .....	123
<b>Table 4.14</b> Mineral Reaction Rates at the Cell 1 in the Sample DH1-B .....	124
<b>Table 4.15.</b> Mineral Percentage DH2-A located CH1 .....	126
<b>Table 4.16</b> Mineral Reaction Rate at the Cell 1 in the Sample DH2-A.....	126
<b>Table 4.17.</b> Mineral Percentage DH2-B located CH2 .....	128
<b>Table 4.18</b> Mineral Dissolution Rate at the Cell 1 in the Sample DH2-B.....	129

<b>Table 4.19</b> Mineral Percentage DH3-A located CH1 .....	130
<b>Table 4.20</b> Mineral Reaction Rate at the Cell 1 in the Sample DH3-A.....	131
<b>Table 4.21</b> Dolomite and Calcite rates measured at 25°C in rotaring disk experiments. .....	133
<b>Table 4.22</b> Dolomite and Calcite Rates measured at 70 °C in carbonate water injection experiment at CH1.....	133
<b>Table 4.23</b> Dolomite and Calcite Rates measured at 70 °C in carbonate water injection experiment at CH2.....	134



## **NOMENCLATURE**

### *Abbreviations*

CT Computed Tomography

CH1 Coreholder 1

CH2 Coreholder 2

CW Carbonated water

CWI Carbonated Water Injection

Da Damköhler Number

EOR Enhanced Oil Recovery

GCV Grubb's Critical Value

IC Ionic Chromatography

IQR Interquartile Range

OOIP Original Oil In Place

Pe Péclet Number

Ppm Parts Per Million

PVI Pore Volume Injected

SI Saturation Index

WAG Water Alternating Gas

WH Wormhole

XRD X-Ray Diffractogram

### *Symbols*

**A** Transversal sample area ( $cm^2$ )

***CTDry*** Dry reservoir rock outcrop sample attenuation coefficient (HU)

***CTDry-N<sub>2</sub>*** Reservoir rock outcrop sample saturated with  $N_2$  attenuation coefficient (HU)

***CTRock*** Rock attenuation coefficient (HU)

***CTN<sub>2</sub>*** Nitrogen attenuation coefficient (HU)

***CTS<sub>at</sub>-CO<sub>2</sub>*** Reservoir Rock outcrop sample saturated with  $CO_2$  attenuation coefficient (HU)

***CTS<sub>at-Sw</sub>*** Reservoir Rock outcrop sample saturated with sea water attenuation coefficient (HU)

***CT<sub>sw</sub>*** Seawater attenuation coefficient (HU)

***Dissolved Moles*** dissolved moles at different times

***K<sub>abs</sub>*** Absolute Permeability (mD)

**L** Sample length (Cm)

***mCO<sub>2</sub>*** Carbon dioxide molality (mol/Kg)

***Mineral Mol*** Mols of Calcite, Dolomite or Kaolinite

***PM Mineral*** Molar mass

***VT*** Outcrop sample total volume (*cm*<sup>3</sup>)

***V<sub>cell</sub>*** Cell volume (*cm*<sup>3</sup>)

*Greeks*

$\phi$  Porosity

$\phi_i$  Initial Porosity

$\phi_x$  Average Porosity

$\mu$  Viscosity (Cp)

$\Delta P$  Drop pressure (Psi)

$\rho$  Density of the mineral

% Mineral Percentage of the mineral at the rock

# CONTENTS

1	INTRODUCTION.....	21
1.1	Motivation .....	22
1.2	Objectives .....	22
2	LITERATURE REVIEW.....	24
2.1	Carbonates .....	24
2.2	Enhance Oil Recovery (EOR) in Carbonate Rock .....	25
2.3	CO <sub>2</sub> Injection as EOR Technique .....	26
2.4	CO <sub>2</sub> Properties .....	27
2.5	EOR by Carbonated Water Injection.....	28
2.6	Permeability and porosity changes due to the Carbonated Water Injection 30	
2.7	Factors Influencing Dissolution Phenomena.....	32
2.7.1	Influence of Pressure and Temperature in the Dissolution. ....	32
2.7.2	Influence of Injection Rate in the Dissolution .....	34
2.7.3	Influence of Rock Composition in the Dissolution.....	38
2.7.4	Influence of Water Composition in the Dissolution.....	40
2.7.5	Influence of Flow Orientation.....	41
3	EQUIPMENT AND METHODS.....	42
3.1	Equipment.....	42
3.1.1	Positive Displacement Pump.....	42
3.1.2	Vacuum Pump .....	43
3.1.3	Core Holder .....	44
3.1.4	Accumulators .....	45
3.1.5	Back Pressure .....	45
3.1.6	Pressure Data Acquisition .....	46
3.1.7	Temperature Controller .....	47

3.1.8	X-Ray Computed Tomography .....	47
3.1.9	UltraPore porosimeter .....	48
3.1.10	Permeameter.....	49
3.1.11	Ions Chromatograph Thermo Scientific (ICS-5000+) .....	50
3.1.12	Quizix 5000 Series Pump.....	51
3.2	Methods .....	52
3.2.1	Characterization and preparation of the rock .....	52
3.2.2	Sample Cleaning .....	53
3.2.3	Cementing core process .....	55
3.2.4	Basic Petrophysics.....	56
3.2.5	Porosity Evolution Using X-Ray Computed Tomography .....	58
3.2.6	Dissolved Moles Evolution .....	60
3.2.7	Fluids Characterization .....	63
3.2.8	Carbonated Water Preparation .....	65
3.2.9	Determination of ionic composition of the fluids .....	67
3.2.10	Core Holder (CH) Assembly.....	69
3.3	Experimental Setup .....	71
3.3.1	Experimental Conditions for Experiments.....	72
4	CARBONATED WATERFLOODING RESULTS .....	74
4.1	Experiment #1 – Dissolution near to well .....	74
4.1.1	Porosity Results.....	74
4.1.2	Permeability Results.....	81
4.1.3	Ion Chromatography Result .....	83
4.1.4	Discussion on Experiment 1.....	85
4.2	Experiment #2 – Dissolution Near to Wellbore After two production years	
	90	
4.2.1	Porosity Results.....	90

4.2.2	Permeability Results.....	96
4.2.3	Ion Chromatography Result Experiment #2.....	100
4.2.4	Discussion on Experiment 2.....	102
4.3	Experiment #3 – Represents a region 100 m away from the injector well 107	
4.3.1	Porosity Results.....	107
4.3.2	Permeability Results.....	111
4.3.3	Ion Chromatography Result Experiment #3.....	114
4.3.4	Discussion on Experiment 3.....	116
4.4	Dissolved Moles Results for Experiments 1, 2, and 3.....	121
4.4.1	Experiment #1 .....	121
4.4.2	Experiment #2 .....	125
4.4.3	Experiment #3 .....	130
4.4.4	Discussion of Results .....	132
5	CONCLUSIONS .....	135
6	REFERENCES.....	137

# 1 INTRODUCTION

The petroleum industry has been using the carbon dioxide injection as an advanced recovery method for over 50 years. Laboratory data and field experience have shown CO<sub>2</sub>- enhance oil recovery is the most widely used process to increase the recovery factor. It is a desirable option due to increasing production and represents an alternative to reduce CO<sub>2</sub> emissions into the atmosphere (VERMA, 2015). One of the techniques that shows a suitable alternative for using the CO<sub>2</sub> and improves the recovery is the method of carbonated water injection (CWI). This method reduces problems of gravitational segregation and low sweep efficiency and concerning to storage, large volumes of carbon dioxide can be injected into the reservoir through the injection of carbonated water without risk of leakage by the cap rock (SOHRABI et al., 2011).

In recent years, many studies have focused on the importance of understanding the changes in porosity and permeability of carbonate rocks resulting from the interaction between carbonated water and minerals from the rocks. EGERMANN et al., 2005 studied dissolution experiments in limestone cores. ZEKRI et al., 2009 injected CO<sub>2</sub> into limestone cores at 4000 psi and 25°C. YASUDA et al., 2013 performed static experiments in Italian travertine outcrop rocks. SHOGENOV et al., 2015 present the results of a CO<sub>2</sub>-rich brine injection experiments in reservoir samples. YASUDA et al., 2016 studied the effects of water injection with dissolved CO<sub>2</sub> in an extended core of outcrop coquina. VAZ et al., 2017 and NUNEZ et al., 2017 performed an experimental investigation of dolomite rocks during carbonated water injection with 100% and 21,5% saturation of CO<sub>2</sub> respectively.

As a result, no clear carbonated water injection experiment has been done with real reservoir conditions and carbonate reservoir rocks. The present work presents the experimental results aiming to reproduce the injection of carbonated water in the region next to the injector well and far away from it. It was selected reservoir rocks from a pre-salt Brazilian reservoir composed basically of dolomite, calcite, and clay. The porosity and the permeability behavior were monitored. The experiments were carried out under conditions of high pressure for the range 7500

8250 and 8500 psi and 70°C, like those expected for pre-salt Brazilian reservoirs. The injection fluid was a brine with a composition similar to seawater enriched with 25% of CO<sub>2</sub>, and the injected flow rate was one cc/min and 0,1 cc/min.

## 1.1 Motivation

Particularly, the reservoir engineering area in petroleum companies has been proved interested and new requirements to understand the consequences of porous media changes resulting from reactions between the carbonate minerals and CO<sub>2</sub>. To meet this challenge, it is crucial to study in laboratory evaluating the carbonate dissolution and precipitation due to interactions between the carbonate minerals and CO<sub>2</sub> taking into account the porosity and permeability changes at reservoir real conditions. In addition, in view of such encouraging and greatly promising scenario, it is extremely important to develop researches concerning to carbon dioxide injection for enhanced oil recovery. Also, The sequestration and injection in oil and gas reservoirs have been showed a feasible alternative to reduce the gas emission in the atmosphere (IZGEC et al., 2005).

Experimental data obtained by experimental researches considering the carbonate reservoirs are limited in the literature. The studies are well established for sandstone, however for carbonate rocks can be considered a challenge to understand the complexity of these type of rock mainly the presence of heterogeneity concerning to petrophysical properties and mineralogy in this case with three type of minerals calcite, dolomite, and clay. The present work characterizes as a significant advance to meet the needs of oil companies to apply laboratory data to simulate field data. Laboratory data can be very promising and provided crucial information for the success of the reservoir performance.

## 1.2 Objectives

The objective of this study is to evaluate the phenomenon of dissolution and precipitation during carbonated water injection saturated with 25% of CO<sub>2</sub> in Brazilian pre-salt carbonate rocks composed by calcite dolomite and clay at three reservoir conditions. The first condition represents a region near to injector well at an initial production instant. The second represents a region near to the injector

well at an instant of two years of production and, the third one represents a region 100 m away from the injector well.



## 2 LITERATURE REVIEW

In this section, an overview of the essential concepts of carbonate water injection and carbonates rocks are presented.

### 2.1 Carbonates

WRIGHT W. et al., 1984 stated that the sedimentary carbonate rocks differ from siliciclastic sedimentary rocks in several ways. Siliciclastic came from sediments that suffer the process of displacement, deposition, and lithification to generate a stable rock. Carbonate rocks came through biogenetics sediments formed from geologic activities such as reef creation and organic material accumulation at the bottom of the sea. Others factors as deposition texture, grain or pore type, rock composition or diagenesis process allow comparing to carbonate sedimentary rocks and siliciclastic sedimentary rocks.

CHILINGARIAN et al., 1992 stated that carbonate rocks are a class of sedimentary rocks which are formed mainly by carbonate minerals. Some examples of carbonates are calcite, aragonite, and dolomite. Also, the origin follows a marine depositional environment that comprises tidal-flat, sebkha, and associated lagoonal, beach, and eolian deposits, which can be source rocks, seals, and reservoirs for hydrocarbons.

MANRIQUE et al., 2007. indicated that carbonates are classified into two major types of rock: limestone, and dolostone. Limestones are composed of more than 50% carbonate minerals, of which 50 % or more consist of calcite and/or aragonite ( $\text{CaCO}_3$ ). They are composed mainly of skeletal fragments of marine organisms, such as corals, foraminifers, and mollusks. This kind of rock may be white, gray, dark gray, yellowish, greenish, blue, and, sometimes, black. The principal varieties of limestones include chalks, coquina, fossiliferous limestone, oolitic limestone, and travertine. Due the content of calcium carbonate present in limestone an easy way to identify them is through reaction with a cold solution of 5% hydrochloric acid that produces a effervesces reaction in limestone surface.

Also discussed that dolomite is an anhydrous carbonate mineral composed of calcium magnesium carbonate, ideally  $\text{CaMg}(\text{CO}_3)_2$ . An alternative name sometimes used for the dolomitic rock type is dolostone. The mineral dolomite is

rarely observed forming in sedimentary environments. For this reason, it is believed that most dolomites form when post-depositional chemical change modifies lime muds or limestones. Dolomite and limestone are forming an environment characterized by shallow, calm, warm marine waters, this is the type of environment where the organisms are capable of forming calcium carbonate shells, and skeletons can easily extract the needed ingredients from ocean water (MANRIQUE et al., 2007)

## **2.2 Enhance Oil Recovery (EOR) in Carbonate Rock**

A large number of EOR fields projects in carbonate reservoirs has been made since the 1970s. However, for the oscillation with the oil price, most of the projects have been abandoned. The EOR processes for carbonate reservoirs are Carbon dioxide (CO<sub>2</sub>) flooding (continuous or water alternating gas (WAG)) is the first EOR process used in the United States. This is because CO<sub>2</sub> has a low-cost. Also, EOR chemical like polymers flooding.

In the case, carbonate reservoirs are naturally fractured geologic formations characterized by heterogeneous porosity and permeability. Also, they are oil to mixed wet rock for that reason, usually result in lowered hydrocarbon recovery. When EOR strategies began, the injected fluids will likely flow through the fracture and bypass the rock with oil. The high permeability of the fracture will result in breakthrough of the injected fluids, and in most those cases almost 50% of the original oil in place (OOIP) is not produced and the recovery strategy is not economically viable. For this reason, the last decade EOR by gas injection (specially CO<sub>2</sub>) had been dominant recovery method for crude oil reservoirs for carbonate reservoirs with low permeability and polymer flooding had been limited in carbonate reservoirs. AL ADASANI and BAI, 2011 described that there are 143 active projects with EOR using gas injection and thermal methods. Gas injections refer to CO<sub>2</sub>. Of the 143 active EOR projects, 57 have been implemented in carbonated reservoirs. The CO<sub>2</sub> is the most common recovery process with 48 active projects followed by six projects of air injection, 2 of nitrogen injection, 1 of steam injection and one surfactant stimulation.

## 2.3 CO<sub>2</sub> Injection as EOR Technique

MONGER et al., 1991 stated that CO<sub>2</sub> mass transfer to oil is the mechanism that provides more mobility for the oil; this mobilization is converted into an incremental oil recovery. Also, CO<sub>2</sub> presents a higher solubility in oil phase compared with water phase, for this reason, CO<sub>2</sub> moved to oil causing swelling and viscosity decreasing, which results in a higher oil recovery factor. Moreover, injection of CO<sub>2</sub> into the oil zone of the reservoir can lead to changes in the solubility of asphaltenes present in petroleum. Raising the gas, by increasing the methane content of an oil system routinely causes the precipitation of asphaltenes.

Carbon dioxide injection had been used like enhance oil recovery (EOR) since 1950. The first carbonated water floods were tested in 1951 and slugs of CO<sub>2</sub> for oil displacement were tested in 1963 (MCPHERSON and LICHTNER, 2001). Also, the first field-wide application took place in 1972 in the Permian Basin where the CO<sub>2</sub> was transported via a 200 mile – long pipeline from the Delaware – Val Verde Basin . The process proved to be a technical success but required optimization of the CO<sub>2</sub> slug size or the volume of CO<sub>2</sub> injected (KANE, 1979).

GOZALPOUR et al., 2005 suggested that the critical point is to allow enough time for the most significant amount of CO<sub>2</sub> to be absorbed by the oil when the miscibility is carried out. This causes a reduction in the viscosity of the oil, and a reduction in the surface tension between the oil and the pores of the rock is increasing the mobility of oil and, consequently, an increase in the production rate.

PICHA, 2007 stated that the main reactions that occur when CO<sub>2</sub> contacts the oil-water-rock system are associated with chemical and physical alteration in the reservoir and are divided into two primary reactions:

- The reaction between CO<sub>2</sub> and the water formation produces carbonic acid.
- When the carbonic acid (H<sub>2</sub>CO<sub>3</sub>) reacts with calcium carbonate (CaCO<sub>3</sub>) present in the rock surface, causing the dissolution phenomena, which improves the flow channels in the reservoir, through an increase in porosity and permeability.

Also, PICHA, 2007 indicated that there are numerous aspects of the injection of large amounts of CO<sub>2</sub> into the subsoil. Among them, it is emphasized

that the injection of CO<sub>2</sub> inside a salt aquifer can result in the precipitation of minerals. The reason for this process is that saline water typically contains aqueous calcium, so adding CO<sub>2</sub> can lead to the precipitation of calcite. Also, the CO<sub>2</sub> injected may react further with calcium minerals in the subsoil.

VERMA, 2015 observed that experimental and field data showed oil recovery rates close to 22 % of OOIP with Carbonated injection water. Moreover, this process has two significant advantages: firstly, an additional hydrocarbon recovery promotes energy independence and the second one is related to reduce storage emissions of CO<sub>2</sub>.

There are two primary methods of CO<sub>2</sub> injection. The first method consists in the injection of CO<sub>2</sub> and water alternately (WAG - Water Altering Gas). WAG process involves the injection of CO<sub>2</sub> to the reservoir through an injector well; the injection rates vary depending on fluids mobility relations and the permeability of the zone. The second method is the Huff and Puff technique (Cyclic CO<sub>2</sub> Injection) that consists of injecting a volume of CO<sub>2</sub> in gaseous phase into the formation through a production well. Once the CO<sub>2</sub> gas is in the formation, the well is closed to allow gas miscibility with the gas, the formation of carbonic acid, which reacts with the CaCO<sub>3</sub> of the reservoir rock increasing the permeability (VERMA, 2015)

## 2.4 CO<sub>2</sub> Properties

Carbon dioxide (CO<sub>2</sub>) is a slightly toxic, odorless, colorless gas with a slightly pungent, acid taste. CO<sub>2</sub> is a small but essential constituent of air. It is a necessary raw material for most plant life, which remove carbon dioxide from air using the process of photosynthesis. This gas is formed by combustion and by biological processes. These include decomposition of organic material, fermentation, and digestion (VERMA, 2015).

The critical pressure and temperature of CO<sub>2</sub> are (73.82 kPa ) and (31.1 °C ), respectively, and at this point, CO<sub>2</sub> gas and liquid coexist. At higher than critical pressures and temperatures, CO<sub>2</sub> is in the supercritical state and forms a phase whose density is close to that of a liquid, even though its viscosity remains quite low (0.05–0.08 cP). This dense phase CO<sub>2</sub> can extract hydrocarbon components

from oil more efficiently than gaseous CO<sub>2</sub> and is in this supercritical state for CO<sub>2</sub>-EOR. Although the low CO<sub>2</sub> viscosity is detrimental to oil sweep, with the CO<sub>2</sub> dissolution in oil, the oil viscosity is also lowered, which in turn helps improve oil recoveries. Liquid CO<sub>2</sub> exists between its critical temperature and pressure and its triple-point temperature (-69.9 °F [-56.6 °C]) and pressure (75.1 psi [517.8 kPa]) and is usually transported as a liquid for economic and operational considerations (VERMA, 2015).

**Table 2.1** Properties Carbon Dioxide <http://www.uigi.com/carbondioxide.html#Properties>.

Metric Units			Boiling Point @ 101.325 kPa		Gas Phase Properties @ 0° C & @ 101.325 kPa			Liquid Phase Properties @ B.P., & @ 101.325 kPa		Triple Point		Critical Point		
			Temp.	Latent Heat of Vaporization	Specific Gravity	Specific Heat (Cp)	Density	Specific Gravity	Specific Heat (Cp)	Temp.	Pressure	Temp.	Pressure	Density
Substance	Chemical Symbol	Mol. Weight	°C	kJ/kg	Air = 1	kJ/kg ° C	kg/m <sup>3</sup>	Water = 1	kJ/kg ° C	°C	kPa abs	° C	kPa abs	kg/m <sup>3</sup>
Carbon Dioxide	CO <sub>2</sub>	44.01	-78.5	571.3	1.539	0.85	1.9789	1.18 <sup>o</sup>	--	-56.6	517.3	31.1	7382	468

## 2.5 EOR by Carbonated Water Injection

Carbonate water injection (CWI) is a combination of CO<sub>2</sub> with a waterflooding process, in where quantities of CO<sub>2</sub> are used efficiently to EOR from oil reservoirs.

MARTIN, J.W., 1959 studied the potential of CWI for EOR through a series of core-flood experiments. He reported 12 % additional oil recovery during CWI compared to waterflooding.

HOLM, 1959 studied the oil recovery mechanisms of CWI at pore scale. The experiments were made with a pressure of 2000 psi and 100 °F. They concluded that the primary oil recovery mechanism is oil swelling that causes coalescence of trapped oil leading to local flow to an unswept area of the porous medium and oil viscosity reduction.

KECHUT et al., 2010 made a core flood experiments and compositional simulations to study the performance of CWI. The experiments used N-Decane and crude oil and un-aged cores. They showed that CWI had high potential as CO<sub>2</sub> storage strategy with around 50% of the total volume of the injected CO<sub>2</sub> being stored by the end of their test.

DONG et al., 2011 studied the performance of the CWI like secondary and tertiary by experiments in sands conducted at 600 psi and 104 °F.

CWI presents some advantages associated mainly with the eliminating the problem of gravity segregation, gas fingering and poor sweep efficiency due to high CO<sub>2</sub> mobility, which are characteristics of a typical CO<sub>2</sub> injection project. CWI also provides the opportunity to use CO<sub>2</sub> for sequestration purposes. One of the primary motivations to use CWI is that CO<sub>2</sub> dissolved in the water reacts with the fluid and porous media in the reservoir causing chemical and physics reactions allowing to enhance oil recovery. In the CWI-Fluids system, a high amount of CO<sub>2</sub> is dissolved in the oil phase causing oil swelling and a reduction in the viscosity, therefore a mobility increase in the oil phase. For CWI-Rock system, the principal reaction is associated with the rock dissolution effect due to the carbonic acid present during the flood; this rock dissolution entails an increase in porosity and permeability allowing a more efficient porous media to produce oil (SOHRABI et al., 2011).

SHU et al., 2014 used dead oil and un-age core for experiments that showed that injecting one pore volume of carbonated water before CO<sub>2</sub> flooding can alleviate lead to a better oil recovery during CWI process.

MOSAVAT and TORABI, 2014 investigated the performance of Carbonated water injection at various operating pressure (0,7 – 10,3 MPa). Also, the CO<sub>2</sub> solubility in brine was measured using a high-pressure visual cell. Results showed that the recovery with CWI could be increased about 19% as compared to the conventional waterflooding. The results, as expected, showed the solubility of CO<sub>2</sub> in brine increases with increased pressure at constant temperature and salinity. Therefore, the solubility of CO<sub>2</sub> increases more rapidly at lower pressures than higher pressure. Moreover, the solubility of CO<sub>2</sub> in brine decreases when temperature increases from 25 to 40 °C at constant pressure 4,1 MPa and salinity of 0.3492 mol NaCl/ kg water.

MOSAVAT and TORABI, 2016 indicated a possibility of wettability change with CWI process. They experimented with low pressure 304 psi and low temperature 19°C, and dead oil.

## 2.6 Permeability and porosity changes due to the Carbonated Water Injection

Egermann et al., 2005 performed dissolution experiments in two limestones cores to evaluate the effects of permeability and porosity due to an acid treatment. It was injected CO<sub>2</sub>-rich brine (acid solution, pH=1), the overall permeability improvements reach 30% and 70%, respectively. Samples showed permeability increase from 468 mD to 762 mD and 1.76 mD to 2.35 mD, respectively. Porosity increment also was observed in the samples. It was concluded that CO<sub>2</sub> induced dissolution in the sample surface, causing the modification in the sample petrophysical parameters.

André et al., 2006 stated that massive injection of CO<sub>2</sub> into an aquifer reservoir would alter the geochemical system equilibrium between the porous rock and the formation water. Dissolution of supercritical CO<sub>2</sub> into brine will control the rate of dissolution and precipitation of minerals constituting the porous media. Volume changes of the solid phase will modify the pore structure, affecting both the porosity and permeability of the porous media.

Zekri et al., 2009 reported a significant drop in permeability values for limestone samples during CO<sub>2</sub> flooding at 4000 psi and 250°C; samples exhibited permeability losses of 65%, this drop of permeability was associated to the high presence of calcite in the samples. Also, it was concluded that the dissolution and precipitation could occur in the core during a given experiment resulting in an opposite effect on the measured permeability and porosity. Calcite dissolution is the primary reason for the improvement of permeability and precipitation of the calcite can plug the flow channels and impairs the permeability.

Yasuda et al., 2013 performed static experiments to determine the kinetics of carbonate dissolution and its effects on the porosity and permeability of consolidated porous media. Results showed a mass loss ( $8.3 \times 10^{-4}$  g/h) in an Italian travertine outcrop rocks after subjected to conditions of high pressure and temperature (9000 psi and 64 °C) in a carbonate solution during 250 hours. Results also showed an increase in porosity and permeability values; this behavior was associated with the sample dissolution.

Shogenov et al., 2015 presented results for dissolution experiments in reservoir samples under the effects of a CO<sub>2</sub>-rich brine, with 10 bar and 60°C, as

experimental conditions. Results showed a significant dissolution of the pore-filling carbonate cement (ankerite and calcite) causing a high increase in effective porosity and permeability and a decrease in the weight of samples, bulk and matrix density.

YASUDA et al., 2016 studied the effects of water injection with dissolved CO<sub>2</sub> on the petrophysical properties of carbonate rocks. It was evaluated experimentally by an extended core of outcrop coquina. The work emphasizes the evaluation of permeability variations along the extension of the core. The experiments were performed at T=22°C and P=2,000 psi and flow rates of 0.5, 1 and 2 cc/min. The mean porosity indicated a considerable change in the test. Initially, the outcrop porosity was 13%, and in the last test, it showed 17% representing a considerable change for a whole reservoir. Permeability remained the same, up to 120 PV.

Yasuda et al., 2017 also made an experimental investigation on the permeability and porosity changes of a pressurized carbonate rock with the injection of saturated CO<sub>2</sub> brine. Tomography was used to observe the behavior of any wormholes created during the test. The experiment was performed at 2,000 psi, 18°C and four different flow rates of 0.025, 0.075, 0.1 and 2 cc/min. The porosity results showed a linear increase at the first 6 pore volumes injected (5,300 mins), but after that, the permeability suffers more significant changes at the injection rate of 2 cc/min reaching values of 4D, an indicator of a wormhole in some regions

Nunez et al., 2017 studied carbonated water injection through the investigation of the phenomenon of rock dissolution that was carried out using dolomite core samples with carbonated water saturated with 21.5%. Also, was performed two different experiments to evaluate how different experimental conditions influenced dolomite dissolution. For both experiments porosity and permeability decreased in the second core holder, this behavior could be associated with pore throat blockage due to mineral precipitation coming from the first core holder. Sample heterogeneity plays an important role regarding the amount of dissolved mineral. It can be seen the occurrence of dissolution-precipitation phenomena in both regions of higher and lower values of initial porosity, respectively.



Vaz et al., 2017 performed an experimental investigation of the effects of porosity and permeability of dolomite rock. During a carbonated water injection process with a high concentration of CO<sub>2</sub> at high pressure (8500 and 7500 psi) and temperature 70 °C. It was aimed to reproduce the flow conditions observed in different regions of the reservoir and at different times of field production. It was possible to identify that the effect of the dissolution predominates the region of the rock in which the injection initiates, that is marked by the increase of the porosity of the rock. On the contrary, the second region, a little more distant to the injection of carbonated water is already close to the chemical equilibrium with the rock, and the phenomena of dissolution and precipitation coexist. In this way, the second region is marked by periodic variations of the porosity, both positive and negative, but, in general, less significant than the variations observed in the first region. The author concluded that the total porosity of the rock in the region near the face of injection tends to increase, while the total porosity of the rock in regions distant from the point of injection tends to remain constant or decrease.

## **2.7 Factors Influencing Dissolution Phenomena**

### **2.7.1 Influence of Pressure and Temperature in the Dissolution.**

Pokrovsky et al., 2005 realized experiments to determine the dissolution kinetics of calcite, dolomite, and magnesite at 25°C and 0 to 50 atm (**Table 2.2**). Results showed that the dissolution rates for dolomite and calcite increase as the same time pressure system increase; it could be related with the fact that at high pressures, the amount of CO<sub>2</sub> to be dissolved in the brine system is higher.

**Table 2.2** Dissolution kinetics for calcite, dolomite and magnesite 25° C and 0-50 atm.(POKROVSKY et al., 2005)

$R_{\text{mgmol/cm}^2/\text{s}}$	pCO <sub>2</sub> , atm (1,2)	pCO <sub>2</sub> , atm (10)	pCO <sub>2</sub> , atm (35)	pCO <sub>2</sub> , atm (50)
Dolomite	$3.77e^{-10}$	$1.21e^{-09}$	$1.07e^{-09}$	$1.02e^{-09}$
Calcite	$4.74e^{-09}$	$2.13e^{-08}$	$1.80e^{-08}$	$1.70e^{-08}$
Magnesite	$1.24e^{-12}$	$1.52e^{-12}$	$1.47e^{-12}$	$1.82e^{-12}$

IZGEC et al., 2005 stated that temperature did not change the behavior trends of porosity and permeability of limestone samples under the injection of carbonated water. They pointed the exposure time to the rock and the area contacted by CO<sub>2</sub> as parameters more impacting for the injection rate concerning the evolution of the permeability observed in the experiments.

LUQUOT and GOUZE, 2009 performed a set of carbonate water flow experiments on limestone samples to evaluate the mass transfer processes occurring at different distances from the injector well. To represent these different locations, the researchers varied two properties: the partial pressure of CO<sub>2</sub> (P<sub>CO2</sub>) and the composition of brine. As expected, the dissolution of calcite was more significant in the localities whose reproduced conditions were the one of more excellent proximity to the injector well, corresponding to higher values of P<sub>CO2</sub>.

BACCI et al., 2011 performed an experimental work to investigate the mechanisms of dissolution and precipitation of carbonate minerals during the injection of an acid solution in the presence of pressure and temperature gradients, thus analyzing regions near and far to the injector well. The gradient of temperature showed a significant impact. However, in a real case of injection, when the acidic solution flows into the reservoir, it is expected that the temperature increases and the pressure decreases, it will lead to decrease the solubility of carbonates, generating an environment more conducive for precipitation. This is aggravated by the release of CO<sub>2</sub> in the water, promoting an increase in the pH of the solution. Besides, the authors reported the dissolution effects on limestone cores during CWI at two different temperatures (25°C and 65°C). It was used an experiment set up with two samples connected in serial; the first sample was heated at 25°C to simulate the wellbore temperature, while the

second sample was heated at 65°C to mimic reservoir temperature. Results showed a significant permeability increase in the first sample compared with the second sample, gas permeability showed an increase from 2.64 to 522.45 mD in the first sample, this increase was related with the interconnected created by dissolution through the entire core, while for the second sample was 2.71 to 2.97 mD.

COTO et al., 2012 evaluated the dissolution effects of CaCO<sub>3</sub> at different temperatures in a CO<sub>2</sub>-rich brine. Effluents were analyzed to quantify the number of moles Ca<sup>2+</sup> at a temperature range (25°C to 95°C). Results showed an amount of  $2 \times 10^{-4}$  moles Ca<sup>2+</sup> for 95°C, while for 25°C the amount was  $5.3 \times 10^{-4}$  moles Ca<sup>2+</sup>. Thus it was concluded that CaCO<sub>3</sub> suffered a more significant dissolution at low temperatures, it is related with the amount of acid carbonic in the injection fluid.

MOSAVAT and TORABI, 2014 performed oil recovery experiments in sand packs during CWI at two different temperatures (25°C and 40°C). It was found that the tertiary CW flooding performed at 40°C resulted in lower ultimate oil recovery factor (RF) of 66.5% compared to RF of 68.8% at 25°C. At constant pressure, a relatively less amount of CO<sub>2</sub> dissolves in the brine at 40°C (i.e.,  $m_{CO_2} = 0.7303$  mol/kg) compared to the solubility of  $m_{CO_2} = 0.9775$  mol/kg at 25°C.

### 2.7.2 Influence of Injection Rate in the Dissolution

All experimental studies of CO<sub>2</sub> flow in carbonates presented here showed the occurrence of dissolution and precipitation of carbonate minerals. These phenomena could be observed at small distances from one another on a laboratory scale, and in some cases, they coexisted at the same sample site. However, in general, the regions closer to the injector well constitute an environment more conducive to the dissolution of carbonate minerals and increased permeability.

FOGLER, 1988 performed the acid injection experiments on limestone and dolomite samples to investigate the influence of parameters such as fluid velocity and reaction rate on the evolution of the permeability, including the structure and rate of evolution of wormholes. Different injection rates and acid reaction rates were used to assess the impact of varying Damköhler number (Da) values. In Figure 2.1, it was observed that high values of Da result in a rapid and localized

consumption of the acid near the face of the injection, generating wormholes without branching, whereas low values of  $Da$  favour a more distributed dissolution and more branched channels that reach a higher volume in the formation. Thus, it was found that the process of dissolution of the porous medium is controlled by the number of Damköhler. The authors used a metallic alloy to shape the network of channels generated by the dissolution of the samples, which makes clear the influence of  $Da$ .

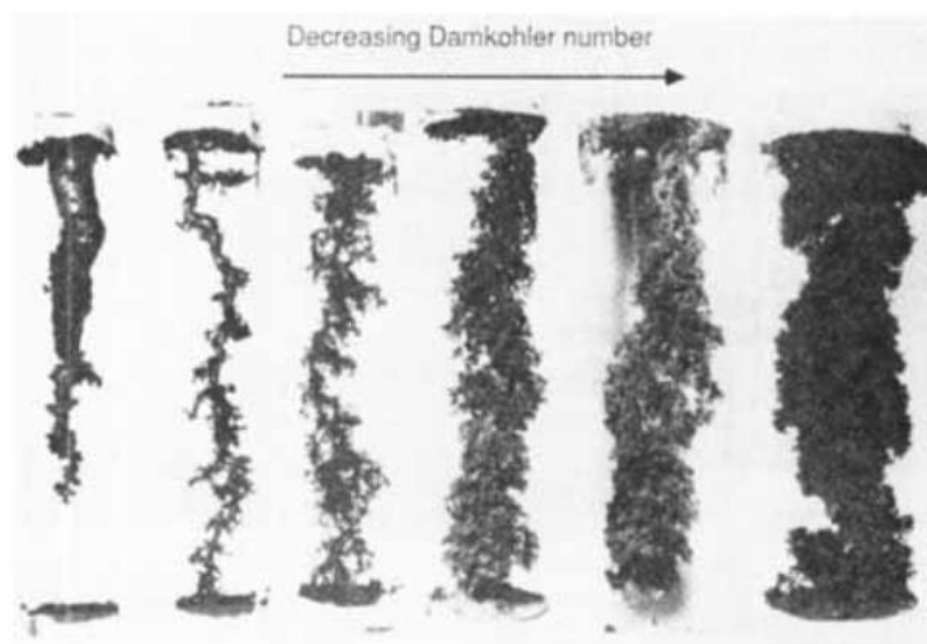


**Figure 2.1** Effect of Damköhler number on the channel network geometry generated by dissolution ((FOGLER, 1988)).

GOLFIER et al., 2002 showed that high injection rates create an environment less conducive to the precipitation of carbonate minerals, even as it causes a shorter residence time of the fluids in the rock, showing that the flow rate is one of the most impacting attributes to the rock-fluid interaction. Also, the dissolution regimes can be characterized by Péclet ( $Pe$ ) and Damköhler ( $Da$ ) numbers. Being the ratios of advective to diffusive transport rates **Equation 2.1**, and the ratio of the overall dissolution rate to the advective transport rate **Equation 2.2**. For  $Pe$  and  $Da$  numbers above  $10^{-2}$  a wormhole (WH) dominant dissolution regime is expected.

**Equation 2.1**

$$Pe = u * l D$$

With  $u$  being the fluid velocity,  $l$  representing the pore length scale, and  $D$  being the diffusion coefficient.

**Equation 2.2**

$$Da = k * l D$$

with  $k$  being the overall reaction rate,  $l$  representing the pore length scale, and  $D$  being the diffusion coefficient.

Egermann et al., 2005 developed CWI studies on carbonates . They found the same dissolution tendencies as a function of injection rates, indicating that the dissolution phenomenon is strongly dependent on the flow regime. Besides, the authors showed that the high injection rates create an environment less conducive for the precipitation of carbonate minerals, even as it causes a shorter residence time of the fluids in the rock. They concluded that the flow rate is one of the most impacting attributes in the processes rock-fluid interaction.

IZGEC et al., 2005 pointed the exposure time to the rock and the area contacted by  $\text{CO}_2$  as parameters more impacting for the injection rate concerning the evolution of the permeability observed in the experiments.

LUQUOT and GOUZE, 2009 stated that the mechanism of rock dissolution occurs in three distinct steps: firstly, the transport of the reactant to the surface of the mineral occurs, the second one regards to the rock-fluid reaction and the third, the transport of the products away from the reaction surface happens. If the rock surface reaction is the slowest step in the process, the dissolution is classified as limited-by-reaction, whereas if the renewal of reagent on the mineral surface is what limits the process, then the kinetics is said Limited-by-transportation. To investigate the relationship between the flow of the reactants and the chemical reactions, some authors use the number of Damköhler ( $Da$ ), which represents the ratio between the relative contribution of the advective transport and the chemical reaction in the mass transfer process. Thus, high  $Da$  values are associated with

high dissolution rates or low injection rates, while low Da values are observed at low reaction rates and high injection rates.

Lasaga, 1984 defined the Damköhler number:

**Equation 2.3**

$$Da(t) = \frac{\overline{v(t)L}}{\bar{u}}(t), \quad \text{for } Pe > 1$$

Where,  $v$  is the velocity of reaction ( $s^{-1}$ ),  $L$  is the sample length (m),  $u$  is the mean velocity of infiltration ( $m s^{-1}$ ) and  $Pe$  (**Equation 2.1**) is the Peclet number that characterizes the reagent renewal at the fluid/rock interface. For values of  $Da < 1$ , the dissolution is limited-by-reaction, whereas, for values of  $Da > 1$ , the dissolution is limited-by-transport.

Gouze and Luquot, 2011 concluded that the experimental work performed with a low Damköhler in which the dissolution was homogeneous resulting in a decrease in tortuosity, while the experiment carried out with higher  $Da$  (heterogeneous porosity development) also resulted in a tortuosity decrease, but accompanied by an increase in hydraulic radius. They proposed a porosity-permeability relationship, Equation 2.2, based on a percolation threshold in which a critical porosity,  $\phi_c$ .

**Equation 2.4**

$$K(t) = K_0[\theta(t) - \theta_c]^\alpha \left(\frac{Bt}{t}\right)$$

$t$  where  $\alpha$  is the power dependence of the relationship that typically varies over time,  $\tau$  is the tortuosity and  $Bt$  is an experimentally determined coefficient.

MENKE et al., 2016 investigated the impact of initial pore structure and the velocity field heterogeneity on the dynamics of fluid/solid reaction at high  $Pe$  (fast flow) and low  $Da$  (relatively slow reaction rates). Experimental procedure consisted in the injection of  $CO_2$ -saturated brine in two limestone samples at two different flow rates for two hours. Each sample was scanned to evaluate the changes in porosity, permeability and reaction rate. It was concluded that the

injection flow rates play an essential role during rock dissolution process, in this case, the flow rate of 0.5 ml/ min showed the most significant impact in the properties alterations as porosity and permeability compared with the flow rate of 0.1 ml/min. Also, it was observed that the high flow rates have more opportunity to present wormhole (WH) dissolution regime.

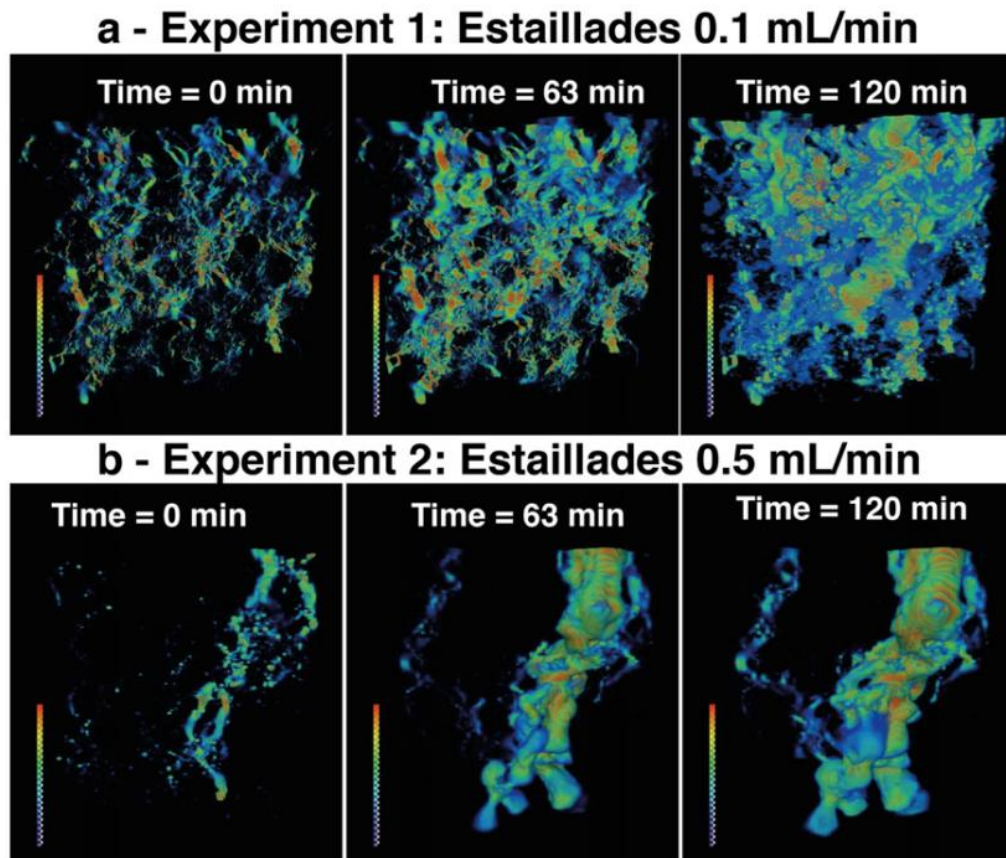


**Figure 2.2** The ratios of the magnitude of  $u$  at the voxel centers divided by the average pore velocity  $U_{av}$  are colored using a linear scale where low velocity is blue, medium velocity is yellow, and high velocity is red.(MENKE et al., 2016)

### 2.7.3 Influence of Rock Composition in the Dissolution

FOGLER, 1988 compared the dissolution processes in calcite and dolomite under injection of acid solutions. The reaction rate of the acid solution with calcite was much higher than with dolomite. Due to this difference, the value of the  $Da$  in dissolution in calcite at a constant injection rate is higher than the  $Da$  value in samples of dolomite.

TAYLOR et al., 2006 on the other hand, carried out a series of flow tests with a group of carbonate samples of different compositions and showed that the presence of impurities usually found in carbonate reservoirs could drastically change the dissolution rate of the acid when compared to pure carbonates. It was reported that the presence of small amounts of clay (1 to 2 wt%) reduced the rate of dissolution of calcite samples by 25 times under experimental conditions, caused by the formation of a clay layer that reduces the reaction surface.

ZEKRI et al., 2009 showed that the increase in permeability caused by the CO<sub>2</sub> injection in samples previously saturated with water is higher than in oil-saturated samples, probably due to the higher CO<sub>2</sub>-rock contact in the first. The authors evaluated in what way the amount of calcite presents in the rock surface influences the dissolution and precipitation phenomena. Also, they compared the petrophysical properties of two samples with different percentage of calcite (C-S1: 20% calcium - D-S4: 11% calcium) which are affected by CWI. Results showed that the sample permeability C-S1 had an increase concerning its initial value. Meanwhile, the sample D-S4 exhibited permeability losses of 65%. The authors concluded that calcite dissolution is the primary reason for the evolution of permeability and precipitation, can be able to plug the flow channels, and impairs the permeability indicating that the permeability alteration due to rock–CO<sub>2</sub>– water interaction is not consistent and could change from one part of the field to another.

POKROVSKY et al., 2005 concluded that the calcite presented a higher dissolution rate in comparison with the dolomite dissolution rate. Experiments reported  $1.70e^{-08} \text{ mol /seg cm}^2$  as dissolution rate for calcite, while the dolomite  $1.02e^{-09} \text{ mol /seg cm}^2$ , under same conditions of pressure and temperature.

YASUDA et al., 2013 compared the mass variation rate for a sample with a travertine sample composed of 86.53% of carbonaceous mineral of calcite and 13.47% against pure calcium carbonate, reacting with hydrochloric acid ( $2 \text{ l xl}^{-1}$ ). Results showed that an exponential decay could represent the mass variation for both samples, but the mass loss for travertine sample is slower than compared with the pure CaCO<sub>3</sub>. That due to the difference in the consolidation state of the samples and the resistance to the flow into the sample pores, avoiding the contact between rock and acid solution.



#### 2.7.4 Influence of Water Composition in the Dissolution

IZGEC et al., 2005 evaluated the effect promoted in permeability on carbonate samples provided by variation of sodium bromide in CWI. Three brines, with different concentration of sodium bromide (0% , 2,5 %, 5%), at 18°C and 60 ml/min, were performed. It was observed that the sample flooded with 0% showed a permeability increase 40%, compared to salinity cases, where permeability only can reach 20%. As salt content of the brine increased, the permeability drop was more pronounced.

EGERMANN et al. 2005 investigated the impact of the brine composition on carbonate water injection into carbonates. The comparison between two brines, which differed only by the presence of Na<sub>2</sub>SO<sub>4</sub>, showed that the presence of sulphates favours a more compact dissolution, which may suggest a tendency of salt precipitation in a SO<sub>4</sub><sup>2-</sup> rich environment, leading to a reduction of permeability. They concluded that the composition of the fluids initially presents in the rock and the flow rate were the most striking attributes in the processes of rock-fluid interaction.

IZGEC et al., 2005 evaluated the effects of brine composition on rock-fluid interactions during CO<sub>2</sub> injection. The authors observed that the more significant gain and less permeability loss was observed in the absence of the salt.

ZEKRI et al., 2009 verified that through the chemical analysis of the water, produced in similar experimental procedures, some chemical elements, like Na and Cl, were retained in the rock, indicating their precipitation and consequent damage to the formation.

OUDEN et al., 2015 measured the calcium concentration in effluents for three chalk samples under CWI process with different brines varying the NaCl concentration. **Figure 2.3** showed the data of three different bulk experiments performed with 2000 ppm NaCl at environment temperature. The three experiments were made with different types of grounded carbonate material such as chalk, limestone and pure calcite crystals. The results showed that the calcite dissolution at equilibrium matched the dissolution at equilibrium conditions pure calcite for pure calcite. The calcite concentration from the limestone bulk test was almost 50% higher. This shows that mineralogy has an effect on the interactions between rock and brines.

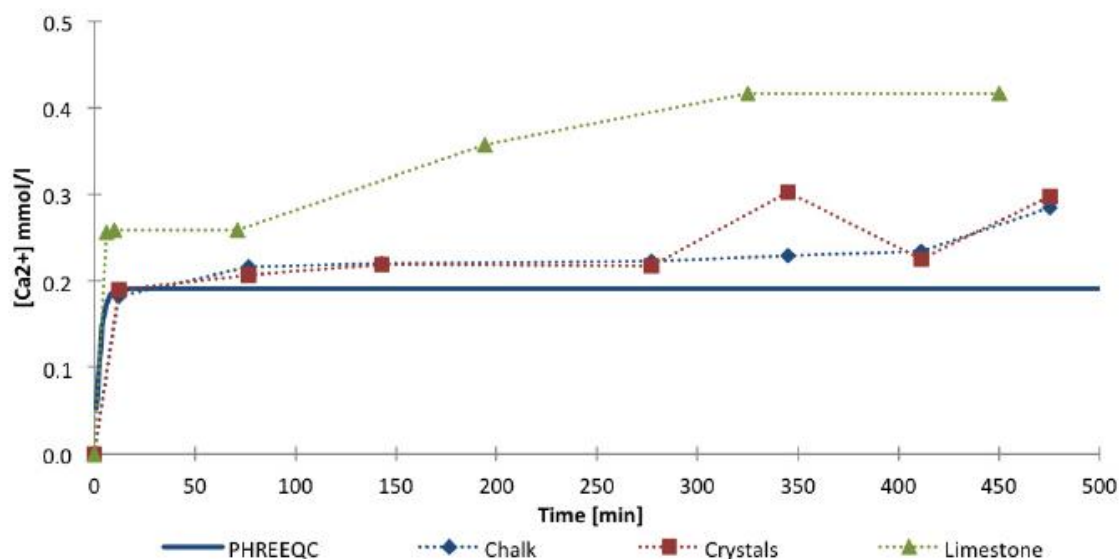


**Figure 2.3** Calcium concentration in 2000 ppm NaCl solution, during bulk test, versus time, 22°C, CO<sub>2</sub>-free environment, experimental + PHREEQC data. (OUDEN et al., 2015)

### 2.7.5 Influence of Flow Orientation

IZGEC et al., 2008 showed that the flow orientation plays a vital role in the design of the carbonate properties during injection of CO<sub>2</sub>. In cases of vertical injection of CO<sub>2</sub>, the authors observed an increase in the permeability and a subsequent reduction of the same property while the horizontal injection. They observed an initial drop in permeability until it stabilized around the same value. It is believed that in vertical injection, due to gravitational forces, CO<sub>2</sub> flows more easily to the top of the sample, causing an early eruption. In horizontal injection, CO<sub>2</sub> is concentrated near the injection face, causing an increase in porosity in this region. More significant precipitation of heat was observed in the case of horizontal injection.

### 3 EQUIPMENT AND METHODS

NUÑEZ et al., 2017 and VAZ et al., 2017 created an experimental setup for core flooding tests in dolomite rocks. For our experiments with carbonate rocks, it was used the same setup with some adaptations. The first adaptation in the setup was injected just one carbonated water accumulator. This change was made because when it was injected two accumulators, at the moment of close one accumulator to pass to the other one for injection, it generated a pressure disturbance. The second adaptation was the new pressure transducers at the setup, described in the equipment section; this change was due to the last transducers did not allow to measure a low drop pressure required for the lower values of permeability from the reservoir rocks.

The equipment section of this chapter aims to describe the equipment and the main features of the devices employed on the core-flooding test. The methods section discusses all the procedures and methodology that were used to carry out this work; since the description of the experimental conditions used, characterization and preparation of rocks and fluids and assembly of the apparatus.

#### 3.1 Equipment

##### 3.1.1 Positive Displacement Pump

A pump can be defined as a mechanical device that adds energy to a fluid to increase flow rate and overcome static pressure. High Pressure Positive Displacement pumps are devices where liquid is positively displaced from fixed volume. Commonly, these pumps are referred to as a constant volume.

A DRB Pump supplied by Schlumberger (**Figure 3.1**) was used during the experimental work, especially in the viscosity measurements. The device includes two operation modes: constant pressure and constant flow. The technical operation includes pressure and flow rate up to 20,000 psi and 1,000 cm<sup>3</sup>/h, respectively, the volumetric capacity of 500 cm<sup>3</sup> and the accuracy of +/- 0.02% .

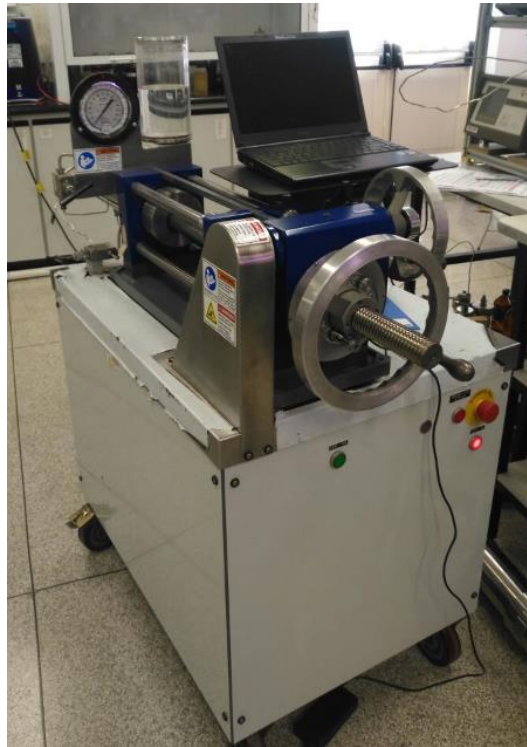


**Figure 3.1** High Pressure Positive Displacement Pump.

### **3.1.2 Vacuum Pump**

An Oerlikon da Leybol vacuum pump, with the flow rate of  $22.7 \text{ m}^3/\text{h}$  was used for core saturation stage, where firstly, the reservoir rocks were submitted to vacuum in order to remove the gas molecules to ensure a better saturation at the moment that the fluids are in contact with the rock. In addition, the pump was used for the stage that involves the brine (synthetic seawater) preparation to remove the presence of gases to ensure just one phase during the rock saturation.



**Figure 3.2** Oerlikon da Leybol vacuum pump  
([www.idealvac.com/files/ManualsII](http://www.idealvac.com/files/ManualsII))

### 3.1.3 Core Holder

Core Holders (**Figure 3.3**) are metallic cells on which the reservoir rocks are placed and confined to displace fluids through them. The core holder body is made by aluminium due to compatibility with X-rays.

The caps are made by stainless steel 316L, a material resistant to corrosion and they are able to work by 15,000 Psi and 150 °C. The core holder has inlet and outlet of 1/8" for injection and production fluid and has control by measuring variables like temperature and overburden pressure.

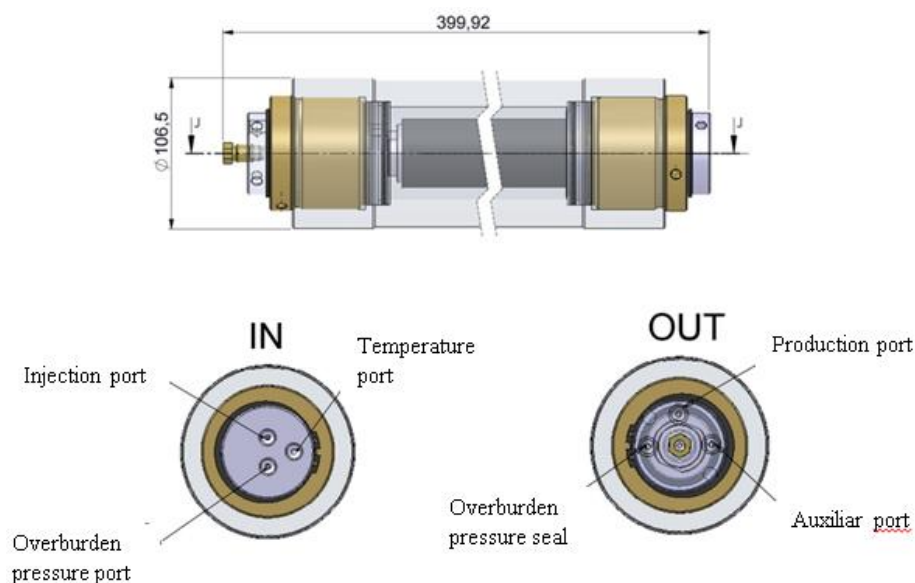


**Figure 3.3** Schematic of Core Holder. Nunez (2017)

### 3.1.4 Accumulators

Injection fluids, such as brine and carbonated water, are placed in type piston accumulators (**Figure 3.4**). This equipment has an operating principle of floating piston that is pushed by hydraulic fluids coming mainly from the positive displacement pump.

The type piston accumulator used in the experiments is made of steel 316L with the volumetric capacity of 750 cm<sup>3</sup> and the limiting operational conditions up to 12,000 Psi and 120° C.



**Figure 3.4** Accumulator type piston

### 3.1.5 Back Pressure

ZINSMEYER et al., 1993 offered an idea that the Back pressure regulator model BPR-150 is a dome-loaded type, which controls the upstream back pressure to whatever pressure is applied to its dome. It is design to operate using compressed gas in the dome, and water and oil in the body. A diaphragm separates the two sections.

The Back pressure operates based on the principle of balanced pressure. First, the dome camera is charged with nitrogen or a compressible gas at a specific pressure. When the flowing pressure is less than exposed to the dome pressure, the diaphragm closes. In order to reach production fluid, the flowing pressure need to overcome the dome pressure generated by the nitrogen over the diaphragm and by pushing this, it allows the contact between production fluid and the outline.

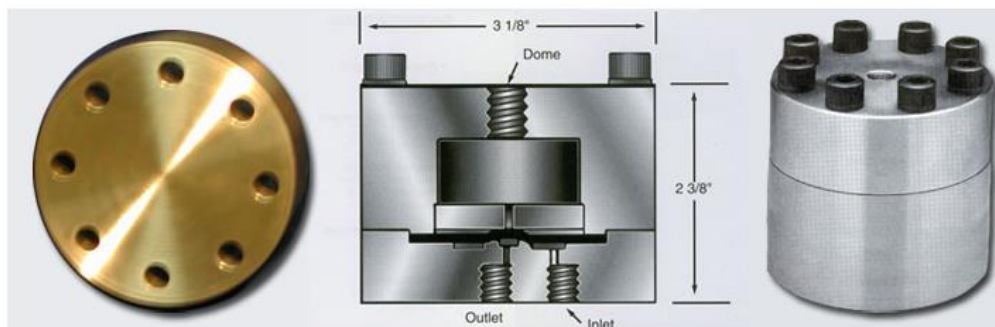


**Figure 3.5** Back Pressure ([www.corelab.com/cli/accessories/back-pressure-regulators-bp-bpr-series](http://www.corelab.com/cli/accessories/back-pressure-regulators-bp-bpr-series))

### 3.1.6 Pressure Data Acquisition

Pressure transducers are devices for pressure measurement of gas and liquid. This instrument is used to control and monitor the process, moreover they can also be used to indirectly measure other variables such as liquid flow, gas flow or permeability. For the experimental setup of this work, it was used an ABB 2600T Series Pressure Transmitters (**Figure 3.6**). This transmitter is connected to the process through impulse lines and can measure pressure, differential pressure or absolute pressure.

The software used for the data collection of pressure in the entrance and the exit of each core holder is called Laboratory Virtual Instrument Engineering Workbench (LabVIEW), which is a platform design system used for data acquisition, instrument control and industrial automatization on a variety of operating system (TRAVIS et al., 2007)



**Figure 3.6** BB 2600T Series Pressure Transmitters.

### 3.1.7 Temperature Controller

Temperature is an important parameter in this work, because it has to be controlled and maintained in the core holder and accumulator. The first dispositive requires to reply the reservoir temperature in order to achieve a better approach to the real conditions. The second one demands to ensure a constant thermodynamic equilibrium between the CO<sub>2</sub> and the brine. For both apparatus, it was used the heater system like the resistance heating jacket, wrapped in their bodies. Also, it was used a temperature controller NOVOUS N1040, that presents a thermocouple type with operation range -110 to 950 °C.



**Figure 3.7** NOVOUS N1040 Temperature Controlled  
([www.novus.com.br](http://www.novus.com.br))

### 3.1.8 X-Ray Computed Tomography

X-ray computed tomography (CT) is a medical imaging technique that produces images of trans axial planes along human body. When compared with a conventional radiography, which is an image of many planes superimposed on each other, a CT image exhibits a significantly improved contrast, although this is at the expense of reduced spatial resolution (KALENDER, 2006).

A medical tomography Siemens SOMATOM Spirit (**Figure 3.8**) was used for fluids and cores samples for the CT determination. CT-scan technique provides investigation of the porosity evolution along the tests.

X-ray computed tomography (CT) was used to determinate the core sample porosity evolution and fluids attenuation coefficients. It was necessary separated in transversal sections along the sample for analysis a data generated. Each section represents an image formed by pixel 512 x 512 matrix. For image treatment and analysis, a MATLAB routine was used.





**Figure 3.8** Siemens Somatom Tomography

### **3.1.9 UltraPore porosimeter**

Porosity was measured using the UltraPore Porosimeter – Upore 300, which is a nitrogen gas expansion porosimeter. It can be used for cores of 1'' or 1 ½ '' diameter and 3'' in length. Moreover, the system can be used in a grain volume or pore volume measurement mode depending on the configuration of the core holder used.

The nitrogen is confined into at a known pressure and the pressure drop measures the volume of the solid (core). The grain density is calculated from the core dry mass and the volume of the solid.



**Figure 3.9** UltraPore Porosimeter- Upore 300

### 3.1.10 Permeameter

The gas permeability was measured on a digital permeameter Ultraperm-500 (Corelab). On this type of equipment, the nitrogen flowed through the Hassler type holder where the rock was mounted. The pressure difference between upstream and downstream was obtained from transducers. The permeability is calculated from Darcy's Law.



**Figure 3.10** Permeameter Ultraperm-500 (Corelab).

### 3.1.11 Ions Chromatograph Thermo Scientific (ICS-5000+)

For this research, chromatography analyses were performed with effluents samples taken at the exit of each core holder during the experiment. The analyses were done with the following chromatographic equipment and materials:

- Chromatograph Thermo Scientific (ICS-5000+)
- Ultra-purification water system
- Millipore- Model Direct Q 3 UV
- Multications standard sample six components 10000 ppm - Specsol-lot F16C0093C
- Multianions standard sample 100 ppm - Specsol-lot F16B0572C

All equipment located in the laboratory of Miscible Methods of Recovery (LMMR).. **(Figure 3.11)**

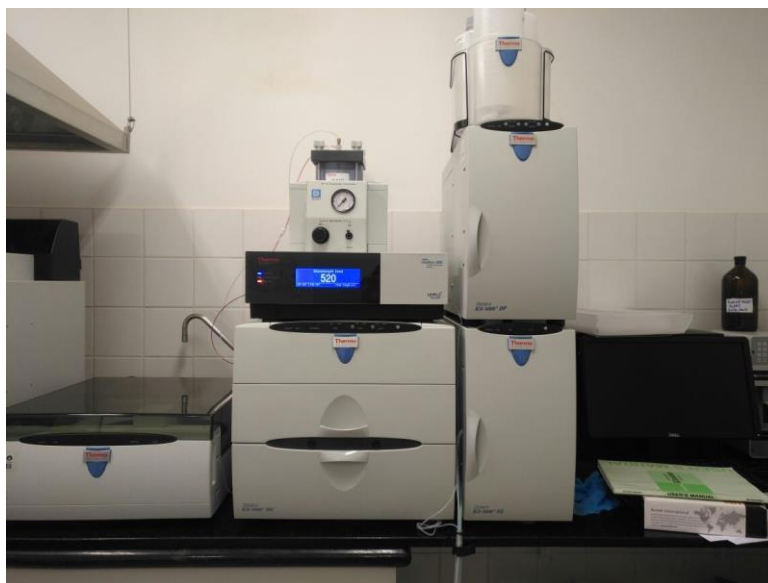


**Figure 3.11.** Chromatograph Thermo Scientific

The Chromatograph analyzed Potassium ( $K^+$ ), Magnesium ( $Mg^{+2}$ ) and Calcium ( $Ca^{+2}$ ) ions for a 100-fold dilution in type 1 demineralized water and Sodium ( $Na^+$ ) and Chloride ( $Cl^-$ ) ions at a 10,000-fold dilution.

The chromatograph analysis used the Dionex - Thermo Scientific multi-anion standard with seven components (**Table 3.1**) and the multi-cations standard with six components (**Table 3.2**)

**Table 3.1** The Dionex - Thermo Scientific multi anion

Components	mg/L
Fluoride	20
Chloride	30
Bromide	100
Nitrate	100
Nitrate	100
Phosphate	150
Sulfate	150

**Table 3.2** The Dionex - Thermo Scientific multi-cations

Components	mg/L
Lithium	49
Sodium	199
Ammonium	248
Potassium	499
Magnesium	249
Calcium	498

The ion chromatography procedure consists in calculating the volume for each dilution, and with the micropipettor, the effluent is transferred to a volumetric flask and filled with Milli-Q water.

### 3.1.12 Quizix 5000 Series Pump

Quizix 5000 Series Pump is a high-pressure syringe pump that provides pulse-free pumping. It is a positive displacement pump ideal for handling aqueous solutions, brines, hydrocarbons and gases such as CO<sub>2</sub>.

It has a pair of cylinders that can work together to pump for a long time. It can pump fluid at a constant flow rate or a constant pressure or constant delta pressure. Besides, the pump system is operating using Pump Works Software, which runs on a computer with Windows operating system.

The features of the Quizix pump are:

- Pressure up to 20,000 psi
- Flow rate up to 60 ml/min

- Ultra-low flow rate option available
- High-temperature option up to 545°F (285°C)
- Multiple options for temperature control, from -10°C to 285°C

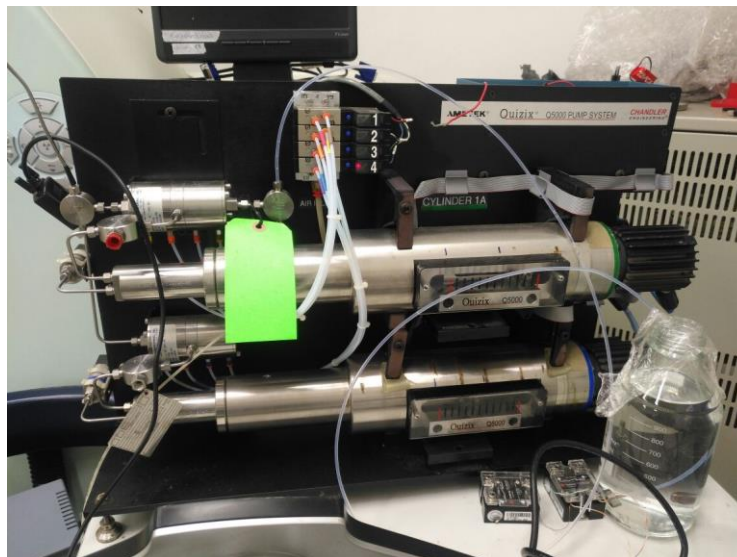


**Figure 3.12** Quizix 5000 Series Pump

## 3.2 Methods

### 3.2.1 Characterization and preparation of the rock

For each experiment were used samples of reservoir rock from the Brazilian pre-salt carbonate formations. The samples were screened to identify the most suitable to be used in the study using the X-ray Computed Tomography. That was because of the difficulty in choosing the best representative pairs for each experiment. This screening was initially performed in visual analysis of the porous medium and samples with the most homogeneous porous medium without large fractures or vugs were selected.

At the end of this analysis, it was selected samples that indicated the relatively homogeneous porous medium, excluding the samples that presented significant alterations in their environment. Also, it was discussed the importance of the mineralogical composition of the samples. For that reason, it was decided to use six rocks with similar mineralogical composition and with a diameter of 3.8 cm and a length varying between 4 and 8 cm.

**Table 3.3** Mineralogy of samples used for experiments

<b>Experiment</b>	<b>Clay (%)</b>	<b>Calcite (%)</b>	<b>Dolomite (%)</b>	<b>Others (%)</b>
DH1-A	1.6	52.92	41.78	3.7
DH1-B	1.34	45.17	37.79	15.7
DH2-A	3.68	77.22	9.8	9.3
DH2-B	4.76	64.31	18.74	12.19
DH3-A	4.3	84.1	5.3	6.3
DH3-B	2.94	48.2	35.9	12.96

It was necessary to carry out the cleaning procedure to remove all possible contaminants from the rocks.

### 3.2.2 Sample Cleaning

The aim of cleaning is to remove all liquids or contaminants from the core so that porosity, permeability, and fluid saturations can be measured (API, 1998).

For this work, the cleaning process was carried out with toluene and methanol, in furtherance of removing the presence of organic and inorganic compounds present in the sample. The cleaning process was performed using a Soxhlet Extractor (**Figure 3.13**), which consists of the following parts: bottom flask to store cleaning solvent, condenser, extraction chamber, electric heating mantle and thermostatic bath. In the Soxhlet Extractor, the samples go through cycles of immersion in solvent (methanol/ Toluene) at high temperature. After two days of this process, the samples are transferred to the hood so that the methanol evaporates and then they are taken to the greenhouse for drying. The cleaning process has the following steps:

#### **Toluene Cleaning**

Prepare 200ml of Toluene and place it in the volumetric container.

Put the volumetric container and the solvent in the heating mantle.

Attach the reflux chamber to the volumetric container.

Attach the condenser to the reflux chamber.

Connect a water source to the lower part of the condenser.

Connect a hose to the upper part of the condenser.

Turn on the heating mantle.

Let the reflux process continue until no more color change can be seen in condense solvent.

### **Methanol Cleaning**

Prepare 200ml of methanol and place it in the volumetric container.

Put the volumetric container and the solvent in the heating mantle.

Attach the reflux chamber to the volumetric container.

Attach the condenser to the reflux chamber.

Connect a water source to the lower part of the condenser

Connect a hose to the upper part of the condenser.

Turn on the heating mantle.

Let the reflux process continue until no more color change can be seen in condense solvent.



**Figure 3.13** Extrator Soxhlet

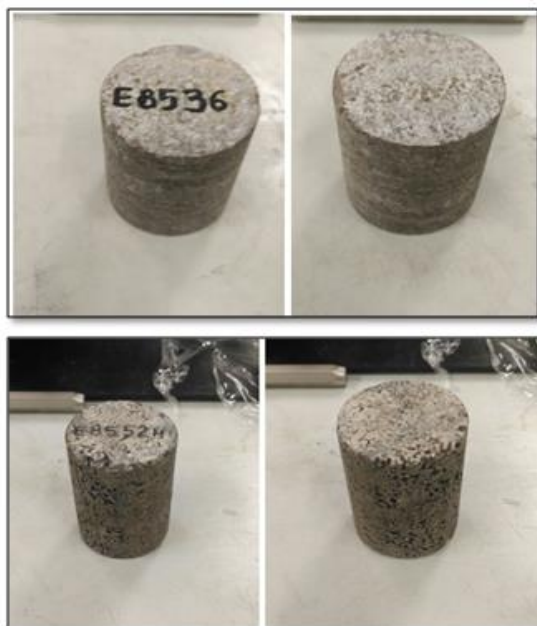


**Figure 3.14** Reservoir's rock after cleaning

### 3.2.3 Cementing core process

The cementing procedure aims to seal vugs and eliminate imperfections present on the lateral surface of the samples. It was observed that the presence of this type of structure, under conditions of high temperature and effective high pressure, allows some regions of the rubber, used to mount the bearing case, to penetrate the rock, resulting in leaks and, consequently, failure in the injection test.

As observed in the works carried out by Vaz (2017) and Nuñez (2017), a common form of cementing the rock is using cement, which is used on the lateral surfaces of the samples in a thin and uniform layer to avoid exposition to vugs. In that case, the samples used in their work were composed 100% by mineral dolomite and the lateral surfaces did not present considerable vugs, causing that the use of the cement did not present interference in the results. However, in this work was used reservoir rocks with complex mineralogical composition and constituted of several minerals such as: calcite, dolomite, sandstone, clay, among others.

Due to its complexity and the presence of large irregularities on the surface of the samples, a material of inert composition to its covering was sought to minimize any type of reaction during the experimental test. For that reason, the Epoxi resin (**Figure 3.15**) was used, and it was applied at the sample contour, in



order to seal the possible vugs present in the rock. After the cementing process, the samples were sand down to remove the excessive cement. **Figure 3.17**

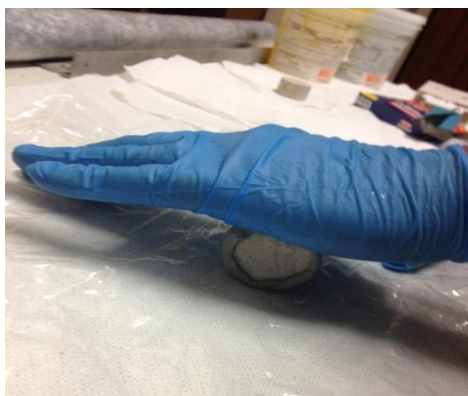


**Figure 3.15** Applying Epoxi Resin at the sample contour.



**Figure 3.16** Durepox (Epoxi Resin)



**Figure 3.17** Sand down of the reservoir rock



**Figure 3.18** Cemented and sand down reservoir's rocks

## 3.2.4 Basic Petrophysics

### 3.2.4.1 Rock dimensions

#### 3.2.4.1.1 Analytical Balance.

An OHAUS precision analytical balance (Adventurer Pro-**Figure 3.19**) was used for determination of the sample mass and the salts weights in order to prepare the synthetic seawater (brine) used for injection and for the saturation of reservoir rocks. Specs (Max: 260g; Min: 0.01g; Error: +/-0.001g).



**Figure 3.19** OHAUS precision analytical balance

#### **3.2.4.1.2 Starrett Caliper**

The caliper was used to measure the core dimensions. (Range (mm): 0-150mm; Graduations (mm): 0.02mm; Accuracy (mm): +/- 0.025mm per 300mm).



**Figure 3.20** Starrett Caliper

#### **3.2.4.2 Inicial Porosity Determination**

Measurements of initial porosity was taken in order to classify and select the rocks that will be used in the carbonated water flooding experiments. Tests were conducted in UltraPore Porosimeter - UPore 300 using nitrogen. The porosity calculations was based in the Boyle's law double-cell method, that is a technique for measuring the grain volume of a core sample by observing the change in pressure of gas introduced into a chamber containing the sample. The

core plug was placed in the sample chamber; nitrogen is admitted into the reference chamber at predetermined pressure, typically 200 psi, and then P1 (Pressure indicated by the transducer digital readout) should be recorded. The gas is allowed to expand into the sample chamber. The resulting lower pressure P2 is measured after the system has reached equilibrium. The grain volume is calculated using the pressure drop produced during the nitrogen expansion in the chamber sample.

### **3.2.4.3 Gas permeability Determination**

Permeability measures were performed using the permeameter Ultraperm-500 and Darcy's law. The rock was placed in the Hassler cell (1.5 inch) and the overburden pressure was set at 600 psi, aided by a manual hydraulic pump (Enerpac). In addition, the upstream and downstream flow lines were connected to the Hassler cell, to allow the gas flow through the core sample. Using a pressure control valve, the nitrogen was injected into the core sample; the pressure drop along the sample was measured by a digital pressure transducer. In addition, once gas (nitrogen) flowed through the sample and the steady-state was established, the permeability was calculated using Darcy's law.

### **3.2.5 Porosity Evolution Using X-Ray Computed Tomography**

Porosity evolution was performed using the attenuation coefficient values of the sample initially dry, and next, the values for the saturated sample at pre-established time. For treatment and analysis of the images was used a MATLAB routine that allows the rock attenuation values. After that, it was necessary to obtain the attenuation values for each image, the dry sample attenuation value (CTDry) and the saturated sample attenuation value (CTSAT).

For experimental procedures performed for carbonated water waterflooding, the porosity evolution was determined by the next equations:

**Equation 3.1**

$$CT_{\text{Dry-N}_2} = CT_{\text{Rock}} (1 - \phi_i) + CT_{\text{N}_2} * \phi_i$$

**Equation 3.2**

$$CT_{\text{Sat-Sw}} = CT_{\text{Rock}} (1 - \phi_i) + CT_{\text{Sw}} * \phi_i$$

**Equation 3.3**

$$\phi_i = \frac{CT_{\text{dry-N}_2} - CT_{\text{Sat-sw}}}{CT_{\text{N}_2} - CT_{\text{Sw}}}$$

The rock CT ( $CT_{\text{Rock}, i}$ ) was obtained for each section  $i$  of the sample according to Equation 3.4

:

**Equation 3.4**

$$CT_{\text{Rock}} = \frac{CT_{\text{Dry-N}_2} - CT_{\text{N}_2} * \phi_i}{(1 - \phi_i)}$$

Finally, it was possible to calculate the porosity value for each position  $i$ , at time ( $t$ ) according to **Equation 3.5**

**Equation 3.5**

$$\phi_{1,2,3\dots} = \frac{CT_{\text{sat-CW}} - CT_{\text{sat-Sw}} - \phi_i * (CT_{\text{rock}} - CT_{\text{Sw}})}{CT_{\text{CW}@P,T} - CT_{\text{rock}}}$$

Where,

$CT_{\text{dry-N}_2}$  = is the coefficient of the sample saturated  $\text{N}_2$ .

$CT_{rock}$  = is the coefficient of the rock;

$\phi_i$  = is the initial porosity of the sample;

$CT_{N_2}$  = is the coefficient of  $N_2$ ;

$CT_{sat-S_w}$  = is the coefficient of the sample saturated with brine;

$CT_{S_w}$  = is the coefficient of the synthetic brine;

$CT_{sat-CW}$  = is the coefficient of the sample saturated with carbonated water;

$CT_{CW@P,T}$  = is the coefficient of carbonated brine under specific P, T conditions;

$\phi_{1,2,3...}$  = is the mean porosity of each section of the sample (1, 2, 3 ...).

### 3.2.6 Dissolved Moles Evolution

The dissolved moles for the three experiments were calculated based on porosity values of each sample, core properties and dimensions. The following mathematical development presented in **Equation 3.6** to **Equation 3.9**

Firstly, the total sample volume  $V_T$  was calculated, where  $l$  is sample length and  $D$  the diameter

**Equation 3.6**

$$V_T = \pi * l * \frac{D^2}{4}$$

Next, the cell volume  $V_{cell}$  was determined. For Core holder 1 and Core holder 2. The ( $\# Images$ ) is is the total number of images along the sample.

**Equation 3.7**

$$V_{cell} = \frac{V_T}{\# Images}$$

**Equation 3.8** was used to determine the dolomite, calcite, and kaolinite initial moles. The dolomite, calcite and kaolinite moles were calculated using the molar mass (*PM Mineral*) and the density of each mineral ( $\rho$  *Mineral*) and for each cell volume.  $\phi_x$  corresponds to obtained porosity value for each image.

**Equation 3.8**

$$\text{Mineral Mol} = \frac{V_{\text{cell}} * (1 - \phi_x) * \% \text{ Mineral} * \rho \text{ Mineral}}{\text{PM Mineral}}$$

Finally, **Equation 3.9** was used for calculation of dissolved moles at different porous injected volume.

**Equation 3.9**

$$\text{Dissolved Moles (t} \neq 0) = \text{Mineral Mol (Initial)} - \text{Mineral Mol (t} \neq 0)$$

After the calculation of dissolved moles at different times, the calculation of the dissolution rate of each mineral was done by estimating the quantities average of each mineral that compose the rock (Calcite, Dolomite and Clay). These rates are an estimative because the quantities of each mineral are an average of the mineral in the rock.

In order to analyse the rocks, the samples were divided into cells. Each cell is a relation between total core volume and the number of images made by tomography of the rock. The first cell of the rock cell was chosen, which each represents an initial position in the porous medium (along the rock length). **Figure 3.21**

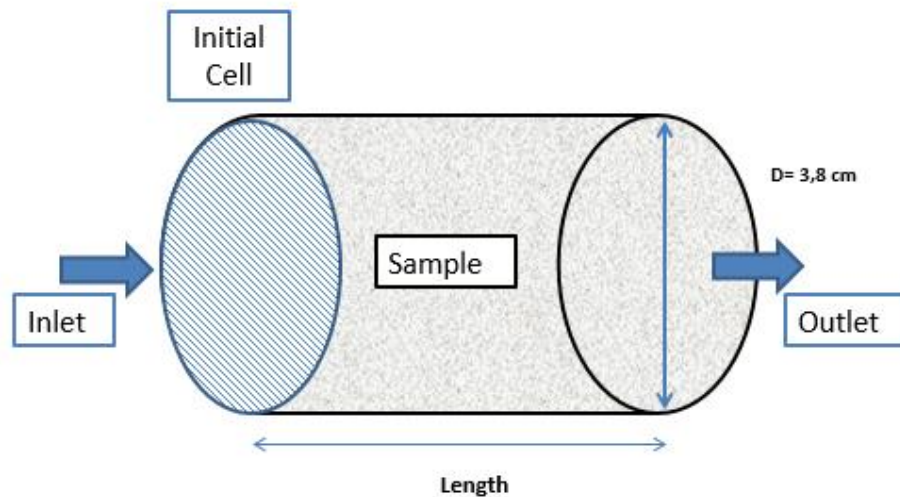


**Figure 3.21** Illustration of the Initial cell of the Sample

After that, we can graph the dissolved moles in the cell at different times. Then, knowing the slope of the tendency line of the graph that relates the dissolved moles and time, we could estimate the dissolution rate of each mineral. We can observe in the next example:

Example for calculation of dissolution rate:

First step is to graph the dissolved moles Vs Porous volume injected. After having the graph, we draw the trend line of this graph, and we can know the slope that is equivalent to the dissolution rate of the chosen mineral. In this case, the dissolution rate is  $5 \times 10^{-8}$

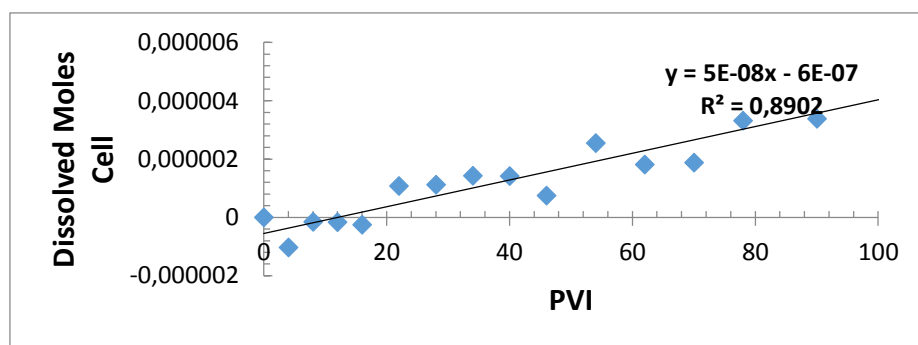


**Figure 3.22.** Example graph for the calculation of the dissolution rate

### 3.2.7 Fluids Characterization

For the Experiment, it was necessary to prepare three fluids, two Synthetic Seawaters, and one Carbonated Water.

#### 3.2.7.1 Synthetic seawater preparation

Synthetic seawater was used as flooding fluid for all experiments performed in this work. Besides, the injection fluid used on the core-flooding tests was brine enriched with 25% CO<sub>2</sub>. The seawater composition is showed in **Table 3.4** and it was utilized for the two experiments.

**Table 3.4** Seawater Composition Utilized for the two Experiments

<b>Brine (1000 ml Solution)</b>	
Potassium Chloride (KCl)	0.9534
Sodium Sulfate (Na <sub>2</sub> SO <sub>4</sub> )	0.0591
Magnesium Chloride Hexahydrate ( MgCl <sub>2</sub> .6H <sub>2</sub> O)	14.2197
Strontium Chloride Hexahydrate (SrCl <sub>2</sub> .6H <sub>2</sub> O)	0.0274
Calcium Chloride Dihydrate (CaCl <sub>2</sub> .2H <sub>2</sub> O)	1.8341
Sodium Chloride (NaCl)	24.8009
Sodium Hydrogen Carbonate (NaHCO <sub>3</sub> )	0.1389
Sodium Carbonate (Na <sub>2</sub> CO <sub>3</sub> )	0.0547
<b>TOTAL CONCENTRATION</b>	<b>42.0882</b>

The synthetic seawater preparation process followed next steps:

Use of a volumetric flask to mix 500 ml of deionized water with the salts presented in **Figure 3.23** Which are added in the same order presented in the **Table 3.4**. Sodium sulfate (Na<sub>2</sub>SO<sub>4</sub>) and the Sodium Hydrogen Carbonate (NaHCO<sub>3</sub>) need to be mixed in a different volumetric flask with 100 ml of deionized water to avoid the salt precipitation.

Once the salt dissolution process has occurred in the volumetric flask, it was necessary to mix it with a magnetic bar to obtain just one solution.

Use of a 0.22 micrometers filter and borosilicate filter vacuum system to filter the brine and remove the possible presence of contaminant particles, **Figure 3.24**.



After filtration process, an air removal procedure is realized, for this, the brine is placed in a Kitasato flask and connected to the vacuum pump during 20 minutes, **Figure 3.25**



**Figure 3.23** Salts Mix Procedure



**Figure 3.24** Brine filtration Procedure

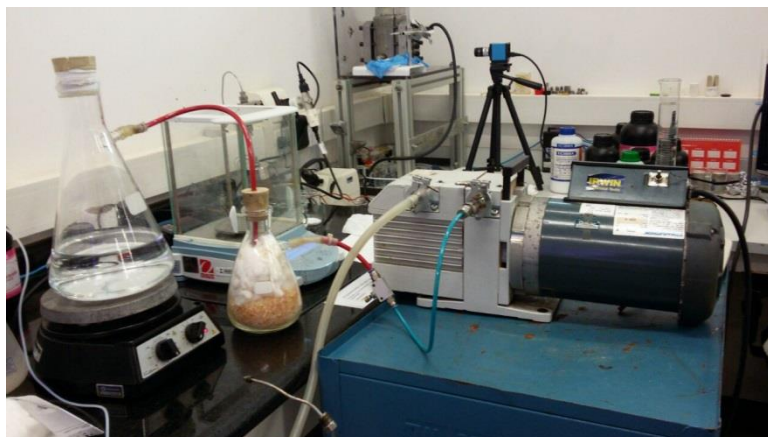


**Figure 3.25** Air removal Procedure.

### 3.2.8 Carbonated Water Preparation

For the experiments it will be used a carbonated water saturated with 25% of  $\text{CO}_2$  due to this value is the average production of  $\text{CO}_2$  from the Pre-salt fields.

The carbonated water was prepared based on  $\text{CO}_2$  solubility in the seawater with salinity of approximately 42 kppm. The preparation was performed in two steps, the first one determine the solubility of  $\text{CO}_2$  at reservoir conditions (8,500 psi@70°C), for this calculation was used an online software (<http://models.kl-edi.ac.cn>) that reported the molality of  $\text{CO}_2$  under specific conditions for temperature, pressure and brine weight percentage (**Figure 3.26**).

T-P condition		
Temperature:	293.15	K
Pressure:	137.8951	bar
Seawater composition		
Salinity:	4.2	wt ‰
m $\text{CO}_2$ :	1.5335	mol/kg

**Figure 3.26.** The molality of  $\text{CO}_2$  (<http://models.kl-edi.ac.cn>)

After that, the second step consisted in finding out the volume of  $\text{CO}_2$  necessary to be injected in  $750 \text{ cm}^3$

$$\frac{1.5335 \text{ mol de } \text{CO}_2}{\text{Kg de } \text{\'agua}} * 0.750 \text{ Kg de } \text{\'agua} * 25\% = 0.2875 \text{ mol de } \text{CO}_2$$

Knowing that the molar volume of 2,000 psi and 20 ° C is 49.6608 mL / mole, then the required volume of that gas to achieve maximum solubility in the brine is:

$$\frac{49.6608 \text{ mL}}{\text{mol de CO}_2} * 0.2875 \text{ mol de CO}_2 = \mathbf{14.27 \text{ mL de CO}_2}$$

Thus, 14.27 cm<sup>3</sup> of CO<sub>2</sub> were necessary to be injected in 750 cm<sup>3</sup> of brine to obtain carbonated water saturated at 25% CO<sub>2</sub>.

Carbonated water was prepared using an apparatus mounted according to the **Figure 3.27** and followed the following procedure:

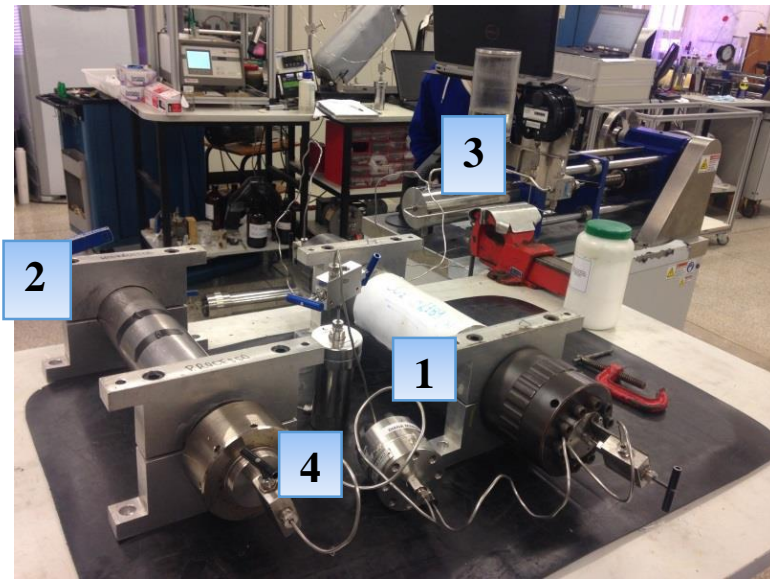


**Figure 3.27** Apparatus Carbonated Water Preparation.

- Fill up the cylinder with CO<sub>2</sub> until 2,000 Psi. (1)
- Fill up the cylinder type piston with 750 cc of brine. (2)
- The cylinder with brine has a sphere in order to mix the CO<sub>2</sub> with brine.
- Connect the pump to the cylinder with CO<sub>2</sub> and inject CO<sub>2</sub> at 2,000 psi through the cylinder with brine.(3)

- Connect the back pressure at the top of the cylinder with brine in order to guarantee CO<sub>2</sub> entering into the cylinder with 2,000 psi of pressure. (4)
- Inject the volume of CO<sub>2</sub> in order to enrich the brine with 21.5 % of CO<sub>2</sub>.
- The heating mantle is placed at the contour of the cylinder with brine in order to increase the temperature until 70°C.
- Connect the pump for pressurization until 8,500 Psi and place in the mechanic agitator during 24 hours to completed CO<sub>2</sub> solubilization

**Figure 3.28.**



**Figure 3.28** Mechanic agitator with the cylinder with carbonated water.

### **3.2.9 Determination of ionic composition of the fluids**

Chromatography analysis was performed in the saturation fluid and samples that were taken at both outputs of the system during the experiment. The first sample collect point was placed between the core holders, for the collect process was used a micrometer valve in order to control the volume of sample. The second collect point was at the output system line, placed at the back pressure system. For this research, these effluents were analysed with ionic chromatography.

These analyses were made by the Thermo Scientific Ion Chromatograph (ICS-5000 +), water ultra-purification system the Millipore (Direct Q 3UV), and for analyses of columns of cations (IonPacCS12A) and for anions (IonPacAS18).

The equipment is located in the Laboratory of Miscible Methods of Recovery (LMMR) of the Center for Petroleum Studies (CEPETRO), at University of Campinas.

The analyzed ions were Potassium ( $K^+$ ), Magnesium ( $Mg^{2+}$ ) and Calcium ( $Ca^{2+}$ ). For in type 1, water demineralized 100 times, and sodium ( $Na^+$ ) and chloride ( $Cl^-$ ) of 10,000 times. The ions  $SO_4^{2-}$  and  $Br^-$  were not identified because their concentrations were lower than the lower limit of the calibration curve.

The ionic Chromatography procedure followed the next steps:

1. Cations Standard Sample: with the aid of a micropipette (100-1000  $\mu$ L), it was transferred 1,000  $\mu$ L of standard solution to a volumetric flask (50 mL), the rest of volume was completed with Milli-Q water (standard cations stock solution). A 1,000  $\mu$ L aliquot of the standard stock solution cations was transferred to a 10 mL volumetric flask with the aid of a micropipette (100-1000  $\mu$ L), the volume was completed with Milli-Q water, the resulting solution was filtered with 0.22  $\mu$ m and taken for analysis.
2. Anions Standard Sample: with the aid of a micropipette (100-1000  $\mu$ L), it was transferred 1000  $\mu$ L of standard solution to a volumetric flask (50 mL), the rest of volume was completed with Milli-Q water (standard anions stock solution). A 750  $\mu$ L aliquot of the standard stock solution cations was transferred to a 5 mL volumetric flask with the aid of a micropipette (100-1000  $\mu$ L), the volume was completed with Milli-Q water, the resulting solution was filtered with 0,22  $\mu$ m and taken for analysis.
3. Samples Preparation: with the aid of a micropipette (100-1000  $\mu$ L), it was transferred 500  $\mu$ L of standard solution to a volumetric flask (10 mL), the rest of volume was completed with Milli-Q water (standard anions stock solution). A 750  $\mu$ L aliquot of the standard stock solution cations was transferred to a 5 mL volumetric flask with the aid of a micropipette (100-1000  $\mu$ L), the volume was completed with Milli-Q water, the resulting solution was filtered with 0,22  $\mu$ m and taken for analysis.

### 3.2.10 Core Holder (CH) Assembly

When the core sample completed the preparatory task (Cleaning-Drying-Cementing and sanding down) and characterization (Dimensions-Porosity-Permeability), the process described previously was ready to be placed and mounted in the core holder. After the sand down process was completed, the sample was wrapped with a series of layers in order to isolate and protect the rubber Viton sleeve from the corrosive action of carbonated water. The sample was wrapped firstly with Teflon tape. Subsequently, an aluminium paper sleeve was placed in the sample contour, and finally, a thermoplastic sleeve was positioned in the sample (**Figure 3.29**). Once the sample was isolated, it was placed in the coreholder. After the sample was placed into the coreholder, the deionized water was introduced into overburden system until reached 1,000 psi with the aid of a positive displacement pump (**Figure 3.30**). A resistance heating type jacket was wrapped around the coreholder in order to heat the complete system until 70°C. A vacuum pump was connected to the injection port in the cap, in order to remove the air contained in the sample; the vacuum procedure was performed during 12 hours.

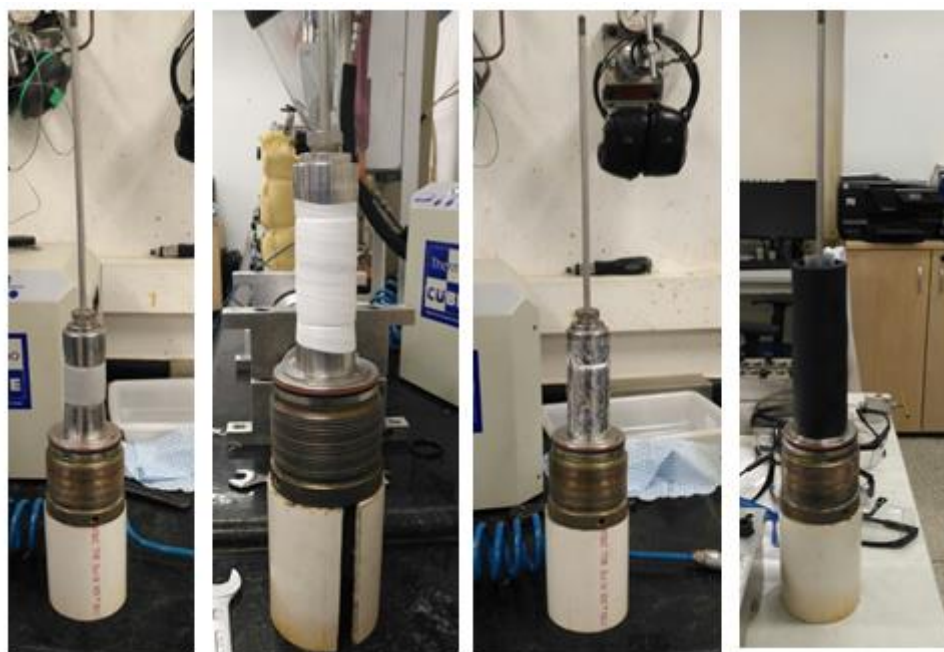


**Figure 3.29** Rock Reservoir Isolate Process.



**Figure 3.30** Introduced into overburden system until reached 1000 psi



**Figure 3.31** A resistance heating type jacket is wrapping around the core holder

After vacuum process was completed, the core holders were placed into the tomograph table, to proceed acquisition images processing. The first step is obtaining the dry sample images; for this process, a nitrogen accumulator was connected to the production port, the sample was filled with nitrogen until reach 500 psi. The nitrogen was in gaseous state at 500 psi and 70°C. At this point, the system conditions present 1,000 psi of effective pressure, at 70°C is ready to begin proceeding with the computed tomography. Once the sample dry images were acquired, the sample was saturated to proceed with the acquisition images process. An accumulator was filled with the brine, described and prepared in the previous

chapter. Using a positive displacement pump, the brine was injected into the sample at a constant flow rate (0.5 cc/min). During the saturation process, the overburden and injection pressure were raised gradually until reach an effective pressure value of 1,000 psi.



**Figure 3.32** Experiment Setup

### 3.3 Experimental Setup

Core flooding tests were performed in an apparatus showed in **Figure 3.32**. Experimental setup is composed of the following devices: positive displacement pump, accumulators, core holders, pressure transducers, backpressure system, valves, tubes and temperature controllers.



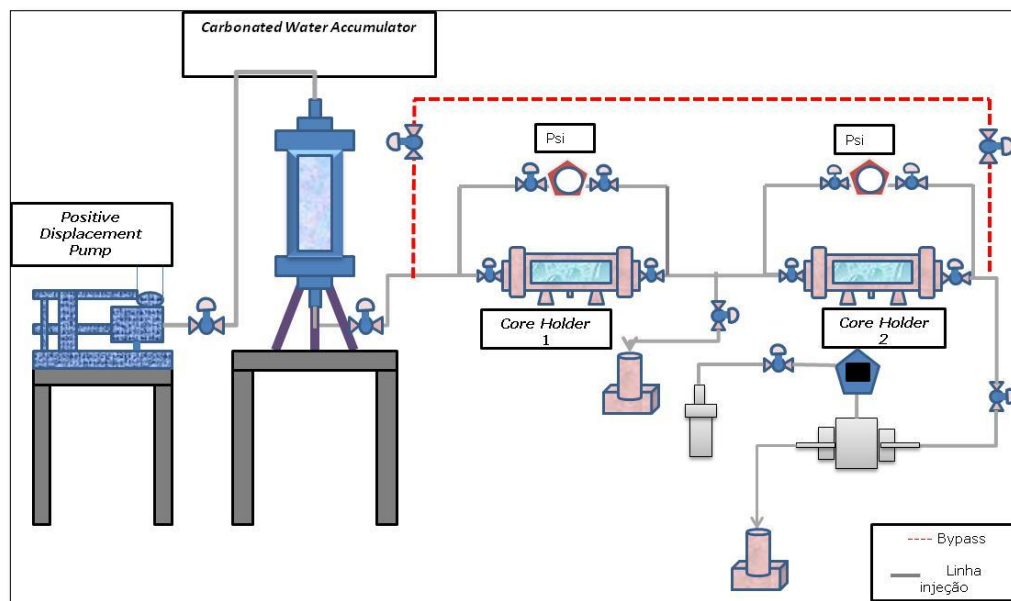


**Figure 3.33** Experimental Setup

As illustrated in **Figure 3.33** carbonated water was previously prepared and stored in the accumulator, pumped and heated up, according to the test procedure and particular conditions, via steel tubing network and flows to set of serially core holders (CH). and carbonated water accumulators were wrapped with a thermal blanket controlled by an electronic temperature device. Sample cores were covered with an aluminium paper and a thermoplastic sleeve in a way to protect the Viton sleeve for the possible wear caused by the carbonated water. A micrometer valve was used between the two coreholders to collect water samples, which were analyzed by an ionic chromatographer. Pressure transducers were connected to each coreholder in order to record the pressure drop data during the test, the backpressure system also has a pressure transducer in favour to control the outlet system pressure. The backpressure provided for nitrogen supply via the Teflon diaphragm maintains the CO<sub>2</sub> in solution. All the experimental setup mentioned previously was placed into a tomography equipment to perform images acquisition, which allowed the evaluation of the porosity evolution in the samples.

### 3.3.1 Experimental Conditions for Experiments

This work proposed to perform three dissolution tests with the following experimental conditions. The conditions are different in the three tests due to they

are simulating distinctive reservoir regions and productions moments (**Table 3.5**). The pressures and temperature used in the experiment was reservoir conditions from the pre- salt fields. Initially, the flow rate was defined at 2 cc/min; however, when the experiment began the pressure transducer equipment did not measure the pressure drop due to it was out of range. Therefore, it was necessary to raise the flow rate up to 1 cc/min.

1. Experiment I represent a region near to injector well at an initial production instant.
2. Experiment II represents a region near to the injector well at an instant of two years of production.
3. Experiment III represents a region 100 m away from the injector well.

**Table 3.5** Operational parameters for each Experiments

	<b>Injection Pressure (psi)</b>	<b>Flow Rate (cc/min)</b>	<b>Temperature (°C)</b>	<b>Injection Brine</b>
<b>Experiment I</b>	8.500	1	70	Brine with 25 % CO <sub>2</sub>
<b>Experiment II</b>	7.500	1	70	Brine with 25 % CO <sub>2</sub>
<b>Experiment III</b>	8.250	0,1	70	Simulated Brine with CO <sub>2</sub>

## 4 CARBONATED WATERFLOODING RESULTS

This chapter presents the results of the carbonated waterflooding experiments. Results include the porosity changes, dissolved moles and permeability changes for the experiments introduced in **Table 3.5**. The Matlab and Osiris Software were tools used to determinate the porosity values.

### 4.1 Experiment #1 – Dissolution near to well

#### 4.1.1 Porosity Results

The first experiment was carried out to reply the rock dissolution that can occur near to wellbore during carbonated water injection. The operational conditions performed at the experiment are in **Table 4.1**

**Table 4.1** Experimental conditions Test #1

Experiment #1	
Parameter	Experimental Condition
Injected Fluid	Brine 42 Kppm - 25% CO <sub>2</sub>
Flow Rate	1 cc /min
Injection Pressure	8500 psi
Overburden Pressure	9500 psi
Temperature	70 °C

The carbonated water injection test had a total of 15 tomography scans and 102 porous volumes injected. In addition, the porosity analysis was performed using tomography images. Each scan provided 47 images for the core holder 1 and 39 images for the core holder 2.

**Table 4.2** shows the initial values of porosity and permeability measured with the porosimeter and the permeabilimeter at the laboratory.

**Table 4.2.** Initial porosity (gas) and permeability (gas) of the samples for Experiment #1.

Sample	Porosity %	Permeability (mD)
DH1-A	10.1	18
DH1-B	11.3	10

**Figure 4.1** and **Figure 4.2** show the behaviour of the porosity media for DH1-A and DH1-B along the experiment #1. The sample DH1-A began with a porosity value of 6.75 % and finished with a 7.03 % of porosity after 102 porous volume injected (PVI). The rock DH1-B began with a porosity value of 7.63% and finished with 7.46%. It can conclude that the sample DH1-A had an increment of the 4.1 % of the porosity media in the rock, and the dissolution phenomenon is predominant in this sample. The DH1-B did not have an increment in the finish of the test but after 12 VPI had an increment of the 3.93% of the porosity media in the rock, and this suggests the coexistence of phenomena of dissolution and precipitation.

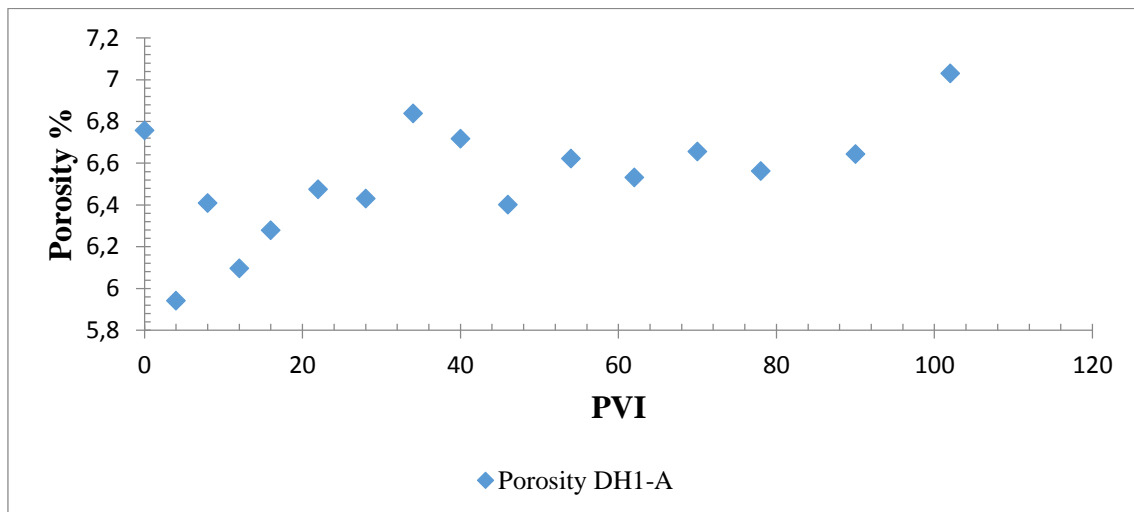


**Figure 4.1.** Porosity Media Values obtained from Tomographies DH1-A

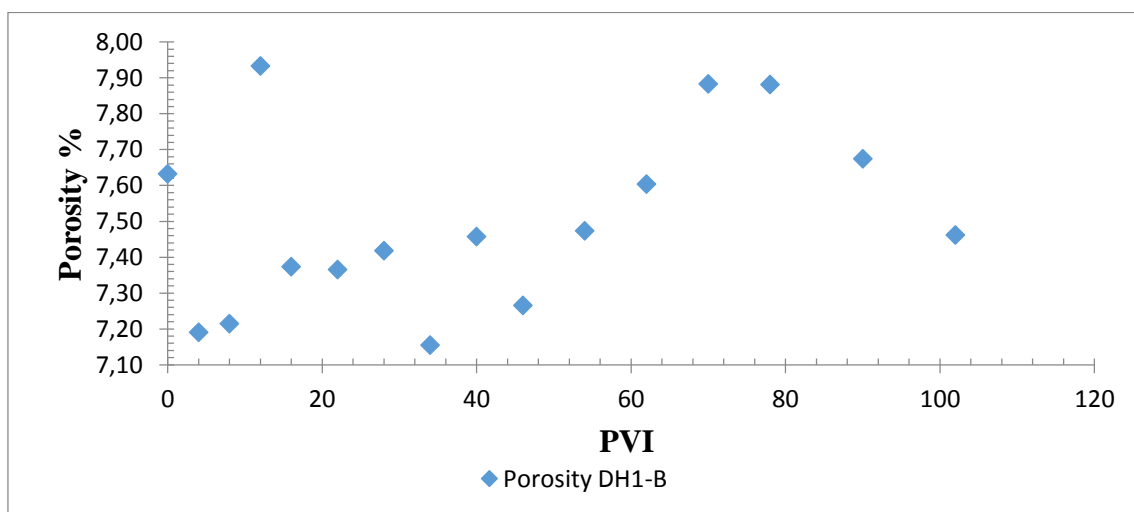


**Figure 4.2** Porosity Media Values obtained from Tomographies DH1-B

#### 4.1.1.1 Core Holder 1 with the Sample DH1-A

**Figure 4.3** shows the distribution of the porosity along the sample DH1-A located at Core holder 1 (CH1). The blue line at the figure represents the initial porosity calculated using **Equation 3.3** and the red line shows the final porosity obtained with the last tomography (#15) using **Equation 3.5**

At **Figure 4.3**, it is possible to notice four regions with different porosity behaviours. The first region (A, blue line) is located at the first 0.5 centimeters of the sample DH1-A. This region shows the highest favorable variations of the porosity, reaching a 9.39% after 102 PVI. The first region indicates that the dissolution shows a substantial increase near to the injection point due to reactive fluid presents a greater quantity of reagents to promote this reaction.

The second region, (B, green line), centimeters 0.5 -1.5, shows a heterogeneity zone concerning porosity due to the range of initial porosity values oscillate from 4,69% to 9,46%. After 102 PVI, the points with high porosity (peaks) presents an increase in porosity and the lowest points of porosity do not show any change in porosity.

The third region (C, black line), between 1.5 cm and 4.2 cm, has a porosity variation from 5,67% to 7,93%. The range from centimeters 2 to 3.6 presented small changes in the porosity where peaks show dissolution (increase in porosity) and lowest points show precipitation (decrease porosity) after 102 PVI. Finally, the range from centimeters 3.6 to 4.2 does not present significant changes at porosity.

In the last region (D, red line), from 4.2 cm to 4.7cm, the initial porosity presents a predominant decrease with porosity values of 4.8% to 6.75%. This region exhibited a reduction of porosity approximately 20% compared with the initial values which indicate precipitation.

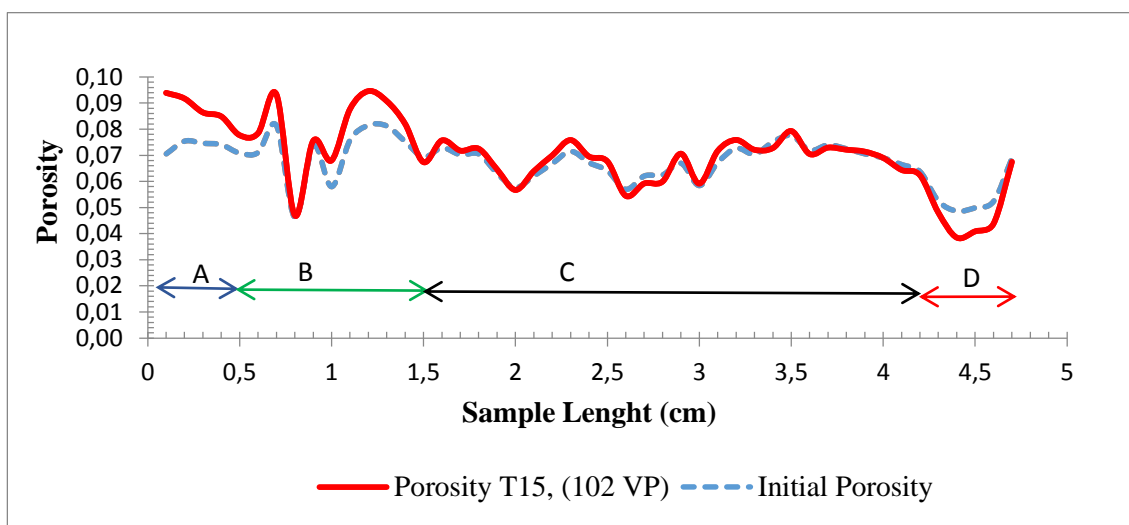


**Figure 4.3** Porosity Variation along sample DH1-A

#### 4.1.1.2 Core Holder 2 with the Sample DH1-B

Based on the initial porosity presents in the **Figure 4.4**, it was possible to identify four regions in the sample. Each one describes the presence of different heterogeneities related to porosity along DH1-B sample.

The first region (A, black line), the centimeter 0 until 1.37 cm, shows a porosity variation from 6.58% to 9.51%. This region presents three peaks (high porosity) and one valley (low porosity). This zone can be considered of high heterogeneity since the porosity varies over a wide range.

The region 2 (B, Blue line), from the 1.37cm to 2 cm, presents a homogeneous porosity zone with the values varying from 7.10% to 7.31%.

The third region (C, green line), between centimeters 2 - 2.96 cm, presents a heterogeneous porosity zone with the values varying in the range from 6.17% to 7.99%.

The end of the sample (D, red frame) shows the initial porosity values varying between from 6.25% to 8.85%. This zone presents different peaks and valleys from the position of 2.96 cm to 4.11 cm.

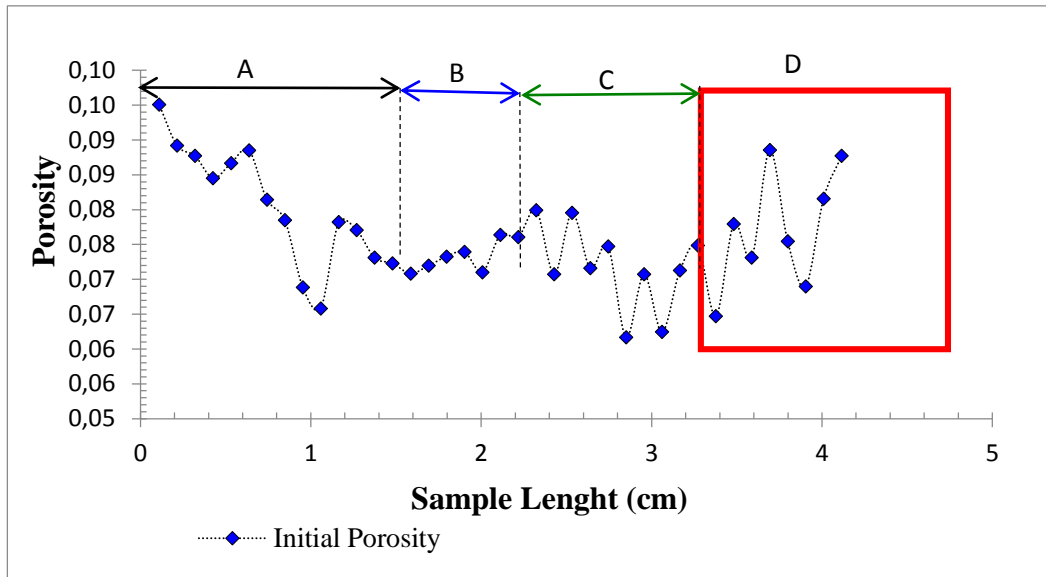


**Figure 4.4** Initial Porosity Variation along Sample DH1-B

**Figure 4.5** shows the porosity along the length of the sample DH1-B for the tomography scans number 1, 2, 14 and 15. Each line represents the porosity profile for its respective tomography. It is possible to identify the tomography as follows: the blue dashed line is the initial porosity, the green line is the porosity calculated from the tomography 1 after four PVI. From the tomography 2 with eight porous volumes injected calculated the solid blue line, the green line is from tomography 14 with 90 PVI and, the red line is the final porosity number 15 with 102 PVI.

It was observed that the regions A, B and C (**Figure 4.4**) follow the trend behavior of the initial porosity profile, peaks increasing and valleys decreasing throughout the sample at the different porous volumes injected. However, the D region presents a definite change in the porosity profile trends in the different PVIs concerning the initial porosity profile, causing a random behavior in this zone.

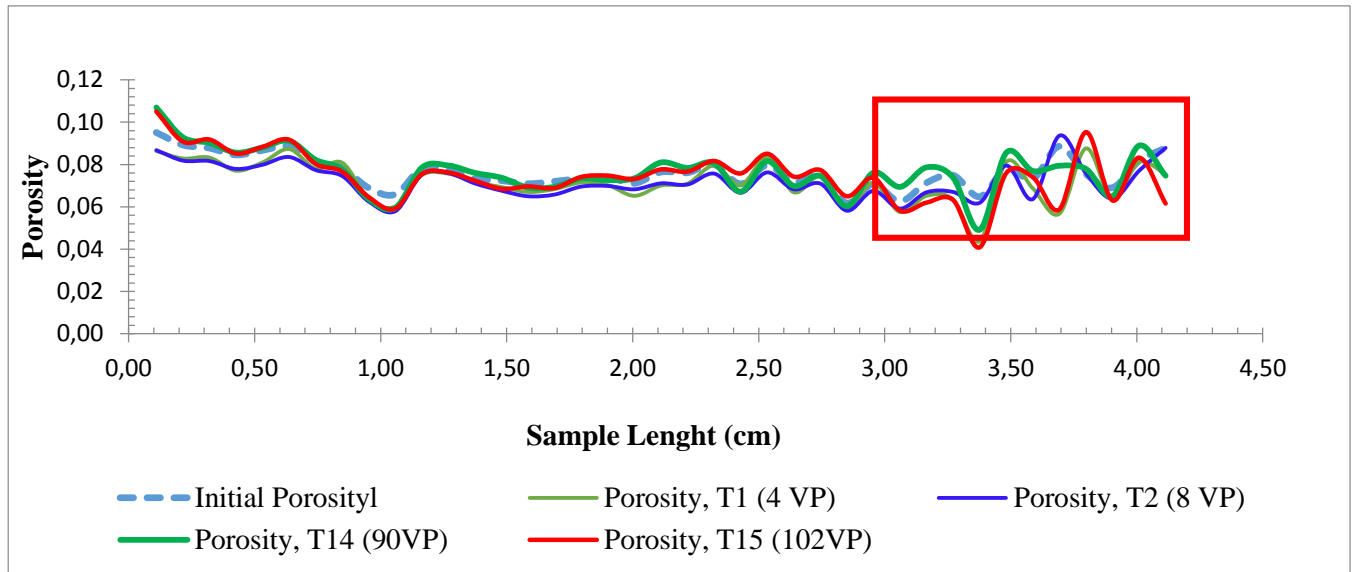


**Figure 4.5** Porosity Variation along sample DH1-B in different times.

Due to the change of the trend (red frame **Figure 4.5**), it was decided to make a detailed treatment for tomography images referring to this region in the **Figure 4.6**.

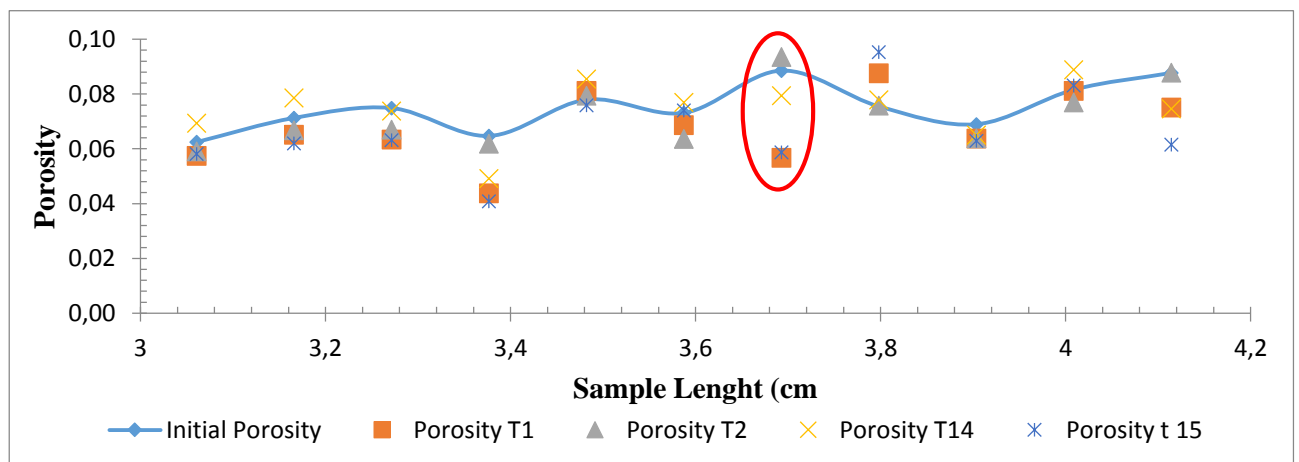


**Figure 4.6** Behavior of the porosity at the sample DH1-B along the length 3cm to end of the rock.

**Figure 4.6** shows the initial porosity profile (blue line) and the porosity profiles calculated from tomography scans 1, 2, 14 e 15 from 3 cm to end of the sample. We took a point at the 3.8 cm of the sample (red circle) like an example. At that point, it can observe that at different times of injection the porosity values increase and decrease or come back to initial value. For the first tomography (T1) the rock presented dissolution because the porosity value is above of the initial



porosity value. For the second tomography (T2), the rock precipitated because the porosity value came back to initial porosity. For the Tomography 14, the rock dissolved a little, and finally, for the tomography 15, the rock dissolved again.

The 3.7 cm value taken in **Figure 4.6** (red circle) correspond to Image 5 (i=5). The next figures correspond to Image 5 (i=5) for each tomography in different injection times. We chose a referent point that showed the variation of the attenuation coefficient.

The attenuation coefficient (CT) is defined with the next equation:

#### **Equation 4.1**

$$CT_{VALUE} = CT_{Rock} (1 - \phi_i) + CT_{FLUID} * \phi_i$$

With the **Equation 4.1** it can observe that for high porosity values the number CT decrease. In others words, the relationship between CT values and porosity is inversely proportional.

With next figures, it is possible to identify:

- The CT increased from 1959 HU (**Figure 4.7**) to 2019 HU (**Figure 4.8**) in the same point (reference point) indicating precipitation or decreasing porosity. The attenuation coefficient above 2000 HU indicates presence of rock matrix.
- **Figure 4.8** and **Figure 4.9** show a decrease in the CT from 2019 HU to 1948 HU indicating an increase in the porosity or rock dissolution.
- **Figure 4.10** and **Figure 4.11** show increase at the CT suggesting precipitation.

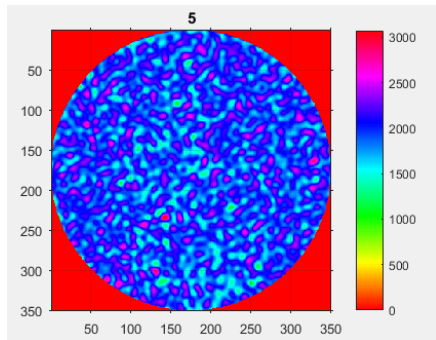


**Figure 4.7** Saturated tomography CH2 (i=5)

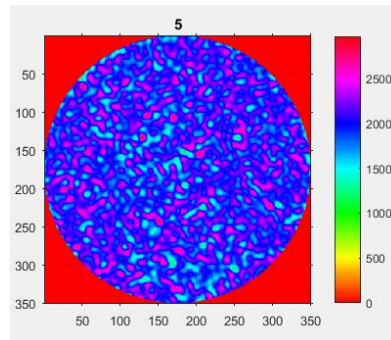


**Figure 4.8** Tomography #1 CH2 (i=5)

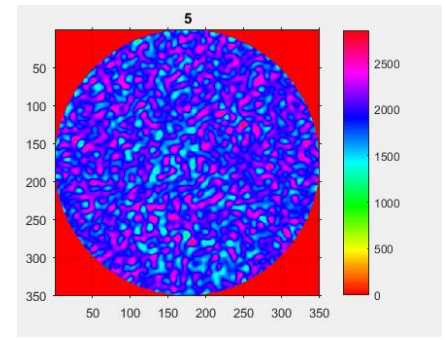


**Figure 4.9** Tomography #2 CH2 (i=5)

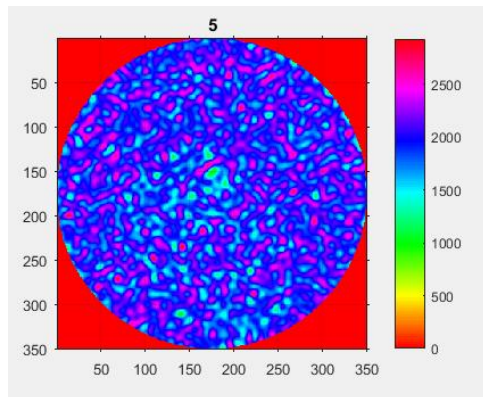


**Figure 4.10** Tomography #14 CH2 (i=5)

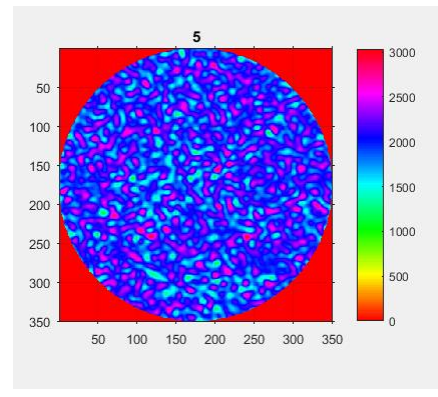


**Figure 4.11** Tomography #15 CH2 (i=5)

#### 4.1.2 Permeability Results

Pressure drops registered along the test allowed to monitor the permeability behaviour. It was used two pressure transducers. Each one recorded the data every 30 seconds for its respective sample. The experiment lasted 795 minutes, and approximately 102 PV of carbonated water was injected during the test.

The first permeability data calculated from the first pressure drop recorded by pressure transducer for DH1-A provided a value of 13.25 mD. However, the permeability measured in the gas permeabilimeter was 18 mD. This happens because the measurements were carried out under different operational conditions and specific fluids. Moreover, the experimental conditions in the two procedures were different. For the first measurement mentioned, the effective pressure was 1000 psi at 70° C. On the other hand, the measurement obtained using gas permeabilimeter, the effective pressure was 550 psi at 20 °C. The reason is

because the effective pressure has a direct influence on the permeability of the porous media.

**Figure 4.12** shows the evolution of the permeability as a function of pore volumes injected in the samples DH1-A assembled in the Core Holder 1 and DH1-B in the Core Holder 2. The sample DH1-A in the Core holder 1 presented increase at the permeability during the test and at the end of the experiment, the permeability increased 80%. The sample DH1-B located in the Core Holder 2 also increased 70% compared with the initial permeability.

It is assumed that one of the reasons for the lowest permeability increment is regarding precipitation observed in region D after 102 PVI (**Figure 4.4**). It could blockage the flow channels impairing the permeability measurements obtained from the pressure drops registered at inlet and outlet sample. Furthermore, the porosity profiles at the samples in CH1 and CH2 end showed that sample in the CH2 exhibited heterogeneity referred to porosity that provided the dissolution in this region and increase the permeability.

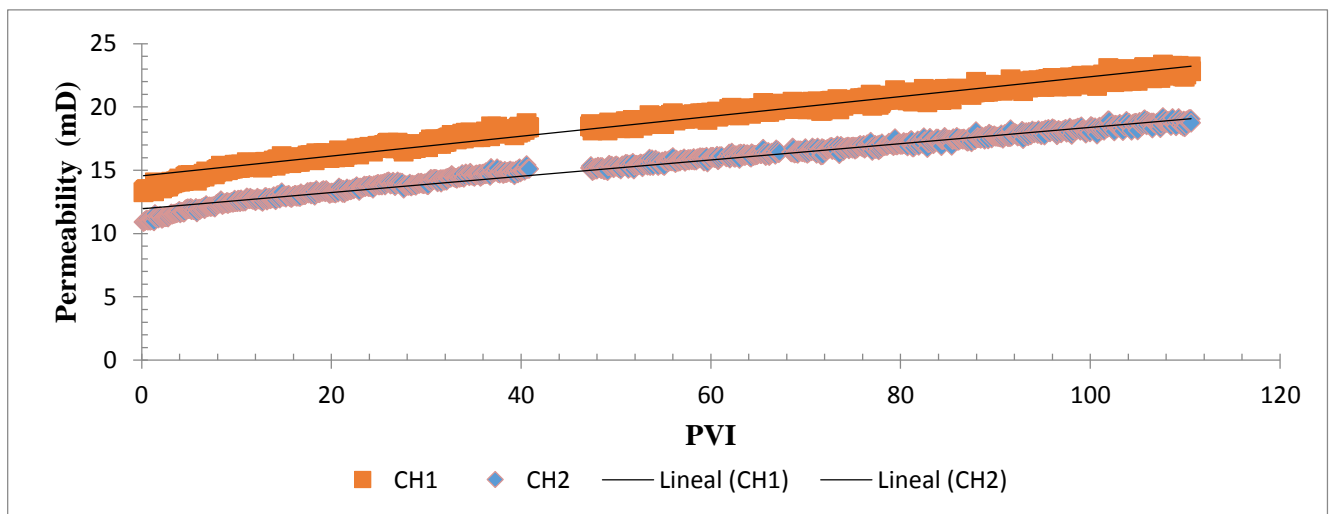


**Figure 4.12** Permeability of DH1-A and DH1-B samples throughout the experiment 1. The absence of permeability data present in the graph between the injected 40 and 47 VP is related to a stop at the Pump in the experiment

### 4.1.3 Ion Chromatography Result

Ionic Chromatography results are presented in **Table 4.3** with the ion concentration mg/L of magnesium and calcium. **Figure 4.13** and **Figure 4.14** show the production curve for each ion: Mg and Ca.

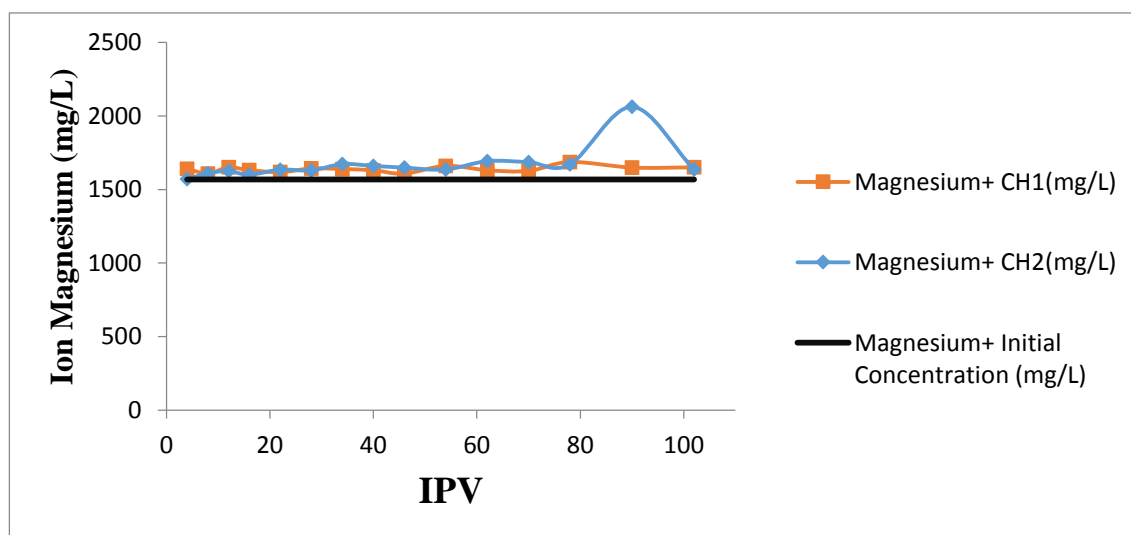
Results obtained from the ionic chromatography were used as input data to perform the simulations using PHREEQC, in order to determine the brine composition to be used in the third experiment. The simulation was performed by research group to project the brine composition at 100 meters away from the wellbore.

**Figure 4.13** presented the magnesium production between CH1 and CH2. The results show that magnesium does not have relevant dissolution or precipitation along to the experiment 1.

**Figure 4.14** showed the comparative calcium production between both core holders and the saturation brine. The significant calcium production increase is evident after a few pore volumes were injected. The production increase is related to the calcium released from the reservoir rock during the dissolution process. Besides, calcite is the mineral with the highest dissolution rate at the two core holder in Experiment 1. After, 80 pore volumes injected, calcium decrease in the CH1. If the behavior is compared with porosity decrease in the CH1 showed in **Figure 4.3**, the precipitation at the end of the sample DH1-A happened at the same time that production decreased meaning that precipitation had occurred, causing the calcium production lessening.

**Table 4.3** Calcium and Magnesium Ions Chromatography results

IPV	Mg (mg/L)		Ca (mg/L)	
	CH1	CH2	CH1	CH2
4	1641.81	1571.43	1231.56	1180.15
8	1608.48	1609.86	684.68	1201.33
12	1651.20	1626.78	1250.21	1195.44
16	1632.42	1600.71	1198.63	1181.39
22	1618.44	1635.44	1193.76	1194.21
28	1643.46	1630.45	1188.53	1180.63
34	1639.87	1673.27	941.49	1208.61
40	1631.00	1660.94	1173.97	877.01
46	1608.39	1648.90	1208.76	1222.64
54	1661.33	1636.70	1193.28	1148.83
62	1631.94	1693.24	1176.95	1219.54
70	1626.92	1686.63	1177.17	1231.31
78	1687.62	1670.83	1219.07	1213.61
90	1649.74	2062.45	1074.84	1492.67
102	1651.18	1637.19	914.54	1200.87

**Figure 4.13** Magnesium produced CH1 and CH2.

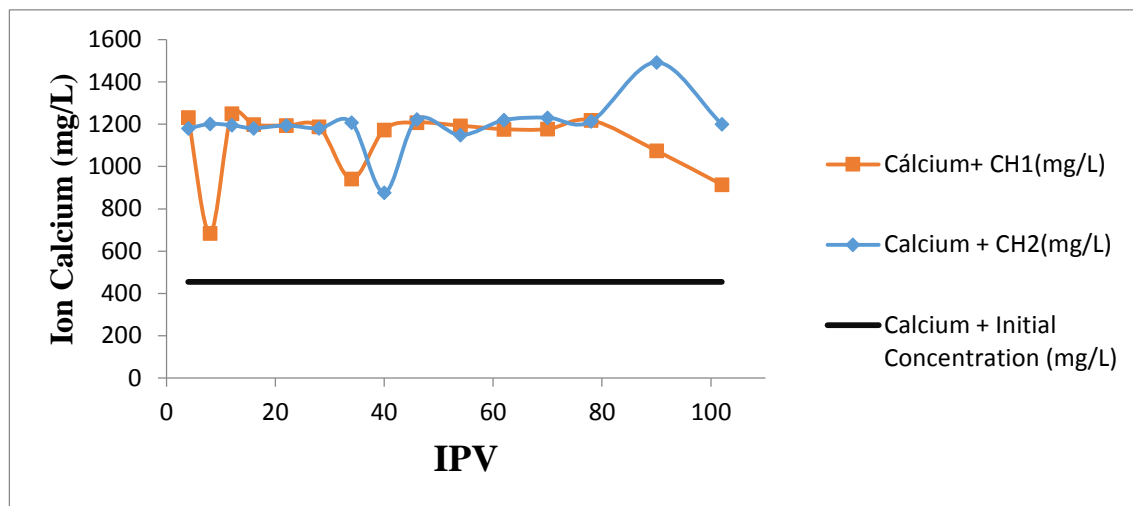


**Figure 4.14** Calcium produced CH1 and CH2

#### 4.1.4 Discussion on Experiment 1

In this section, we are going to compare the results obtained during the work of injection of carbonated water to 25% of CO<sub>2</sub> in reservoir rocks, and a work with the same methodology but they injected carbonate water enrich with 21,5% in dolomite rock, work done by Nuñez 2017. **¡Error! No se encuentra el origen de la referencia.** to Figure 4.20 are from the first experiment of Nuñez 2017 and the nomenclature RV4 and RV6 are the samples names used for the experiment.

##### 4.1.4.1 Porosity

The Results of porosity in the first experiment (8500 Psi injection) can be compared with those obtained by Nuñez 2017. They injected seawater enriched with 21.5% of CO<sub>2</sub> in 100% Dolomite rock. **Figure 4.15** and **Figure 4.17** describe the sample porosity along the sample RV4, and RV6 located in CH1 and CH2. The experiments with dolomite and reservoir rock show the rock dissolution in the first centimeters of rock in the CH1. For the dolomite rock (**Figure 4.15**), the dissolution is higher than in reservoir rock because, dolomite presented dissolution from the initial point to the 1 centimeter of the rock, and reservoir rock presented jus the first 0.5 cm of the rock (**Figure 4.16**).

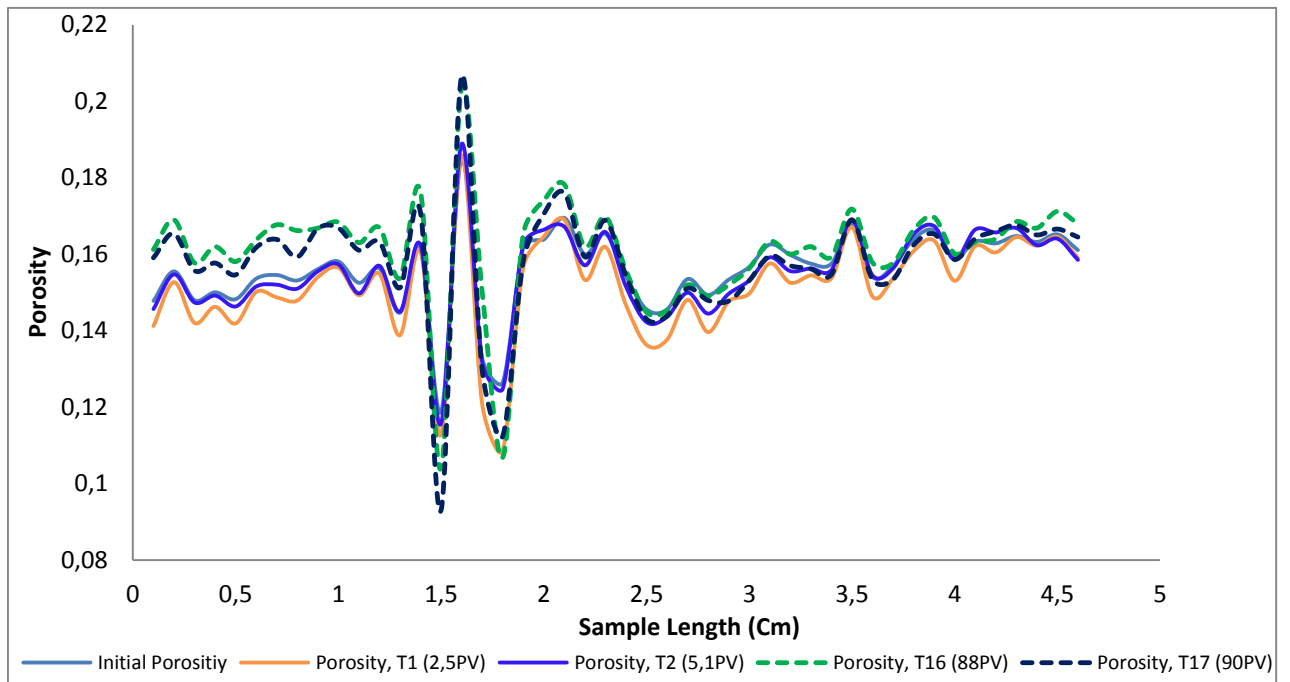


Figure 4.15 Nunez 2017. Sample Porosity variation along the sample RV4 CH1

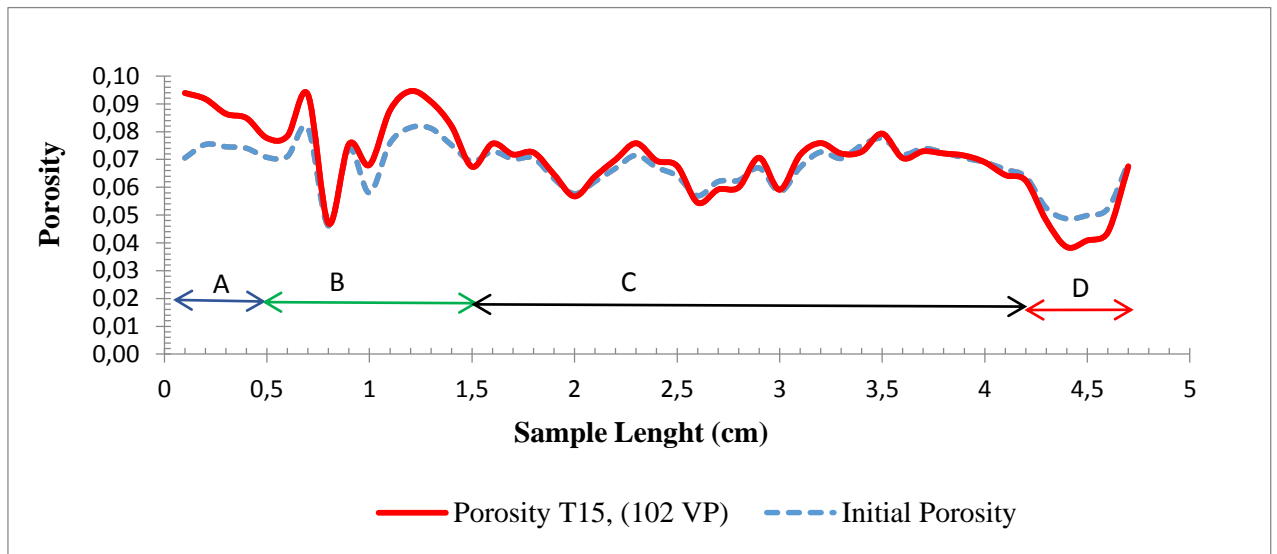


Figure 4.16 Porosity Variation along sample DH1-A

For the experiments with Dolomite and reservoir rock at the same conditions for CH2, it can be seen that in the first centimetres of the rock high dissolution occurs. Besides, some low porosity locations show a decrease in porosity that can

be related with mineral precipitation in the rock surface, whereas in high porosity locations the rocks suffer an increase in porosity, which indicates dissolution.

However, due to the mineralogy in the reservoir Rock, it is more complex than the dolomite rock, the porosity graph (**Figure 4.18**) presented a behavior that it did not see at Nuñez 2017 (**Figure 4.17**). In **Figure 4.18**, it can be seen that there was the region D that it could be observed a definite change in the porosity profile trends in the different PVIs concerning the initial porosity profile, causing a random behavior in this zone.

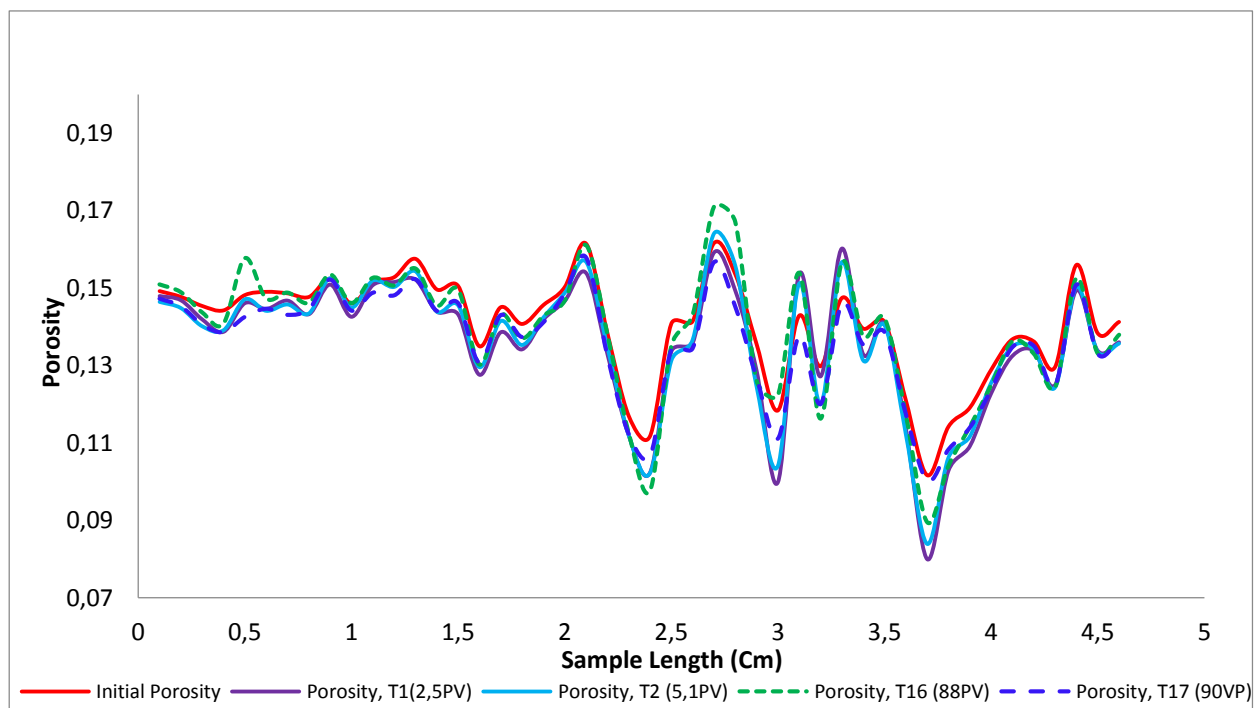


Figure 4.17 Sample Porosity variation along the sample RV6 CH2



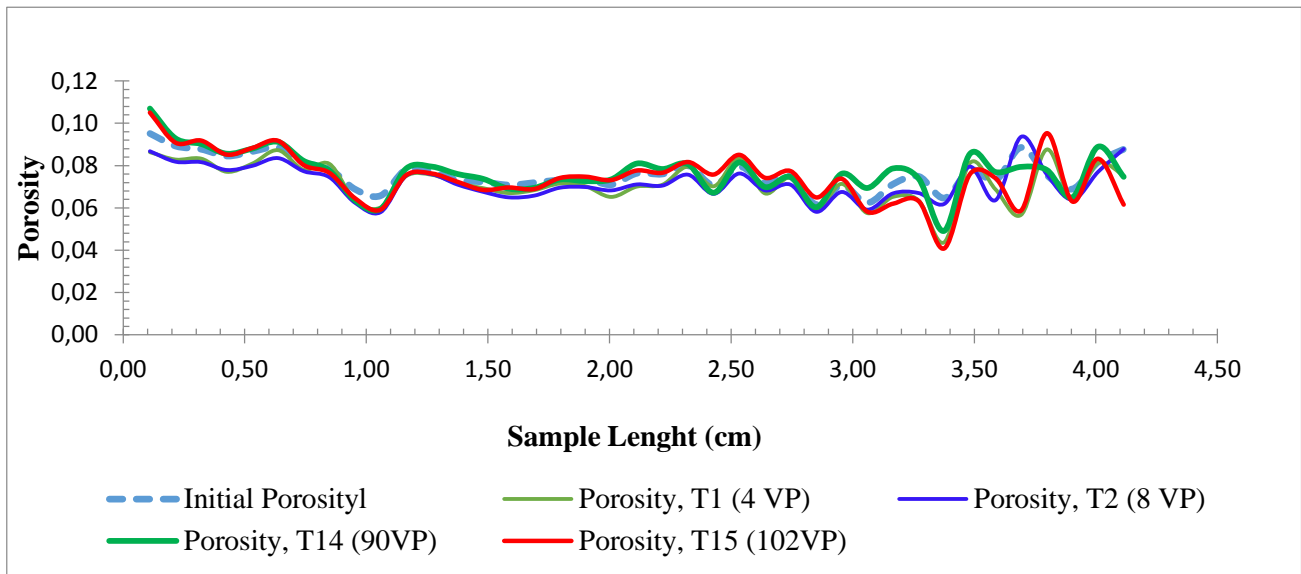


Figure 4.18 Porosity Variation along sample DH1-B in different times.

#### 4.1.4.2 Permeability

Permeability results in this experiment also can be compared with Nuñez 2017 results ( ;Error! No se encuentra el origen de la referencia. and **Figure 4.20**) It can be seen that the sample RV4 placed in the first coreholder did not show any permeability alteration. The permeability profile remains constant between 90 and 100 miliDarcys along the entire test. However, the sample RV6 at the CH2 presented a permeability decrease after injection of approximately 40 PVI. On the other hand, the permeability in the experiments with reservoir rock under the same conditions (**Figure 4.21**) show that after the injection of 102 PVI, the samples DH1-A and DH1-B show a permeability increase during the test.

It can be concluded that for both Core holders, with the reservoir rock, with initial permeability values between 10 to 18 mD has a higher increase in

permeability property that dolomite rocks with initial permeability values between 80 to 150 mD.

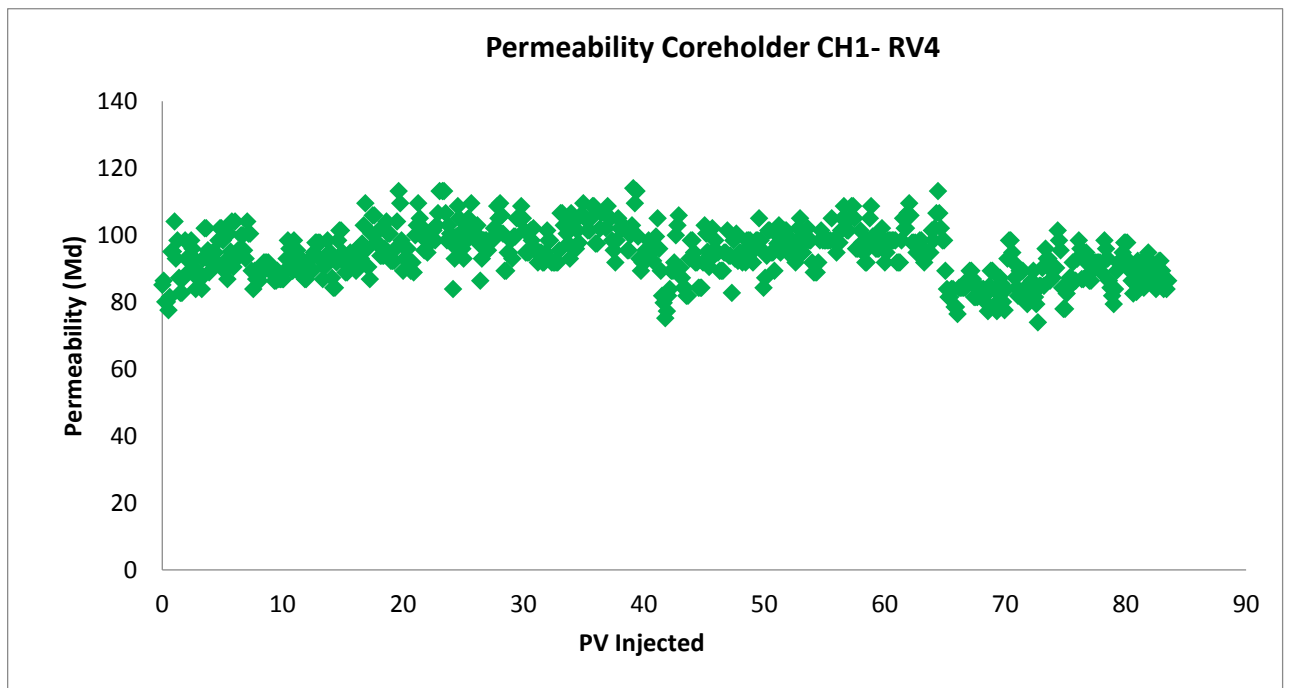


Figure 4.19 Nuñez 2017. Permeability Variation RV4 CH1

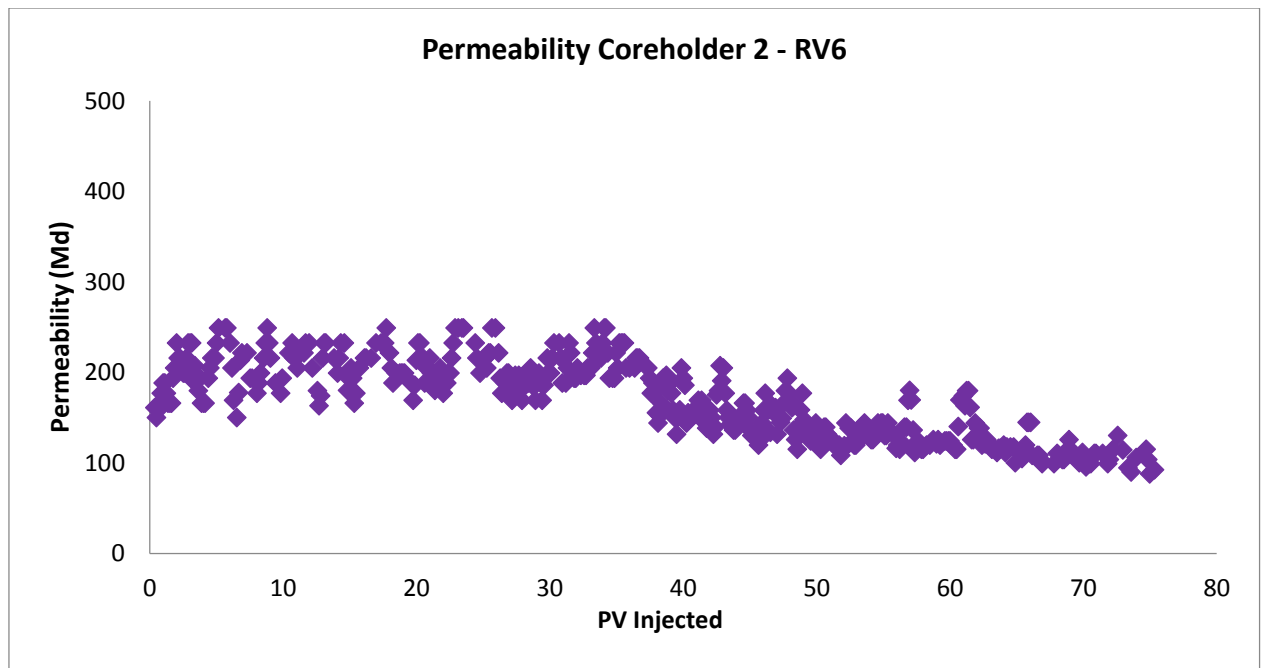


Figure 4.20. Nunez 2017. Permeability Variation RV6 CH2

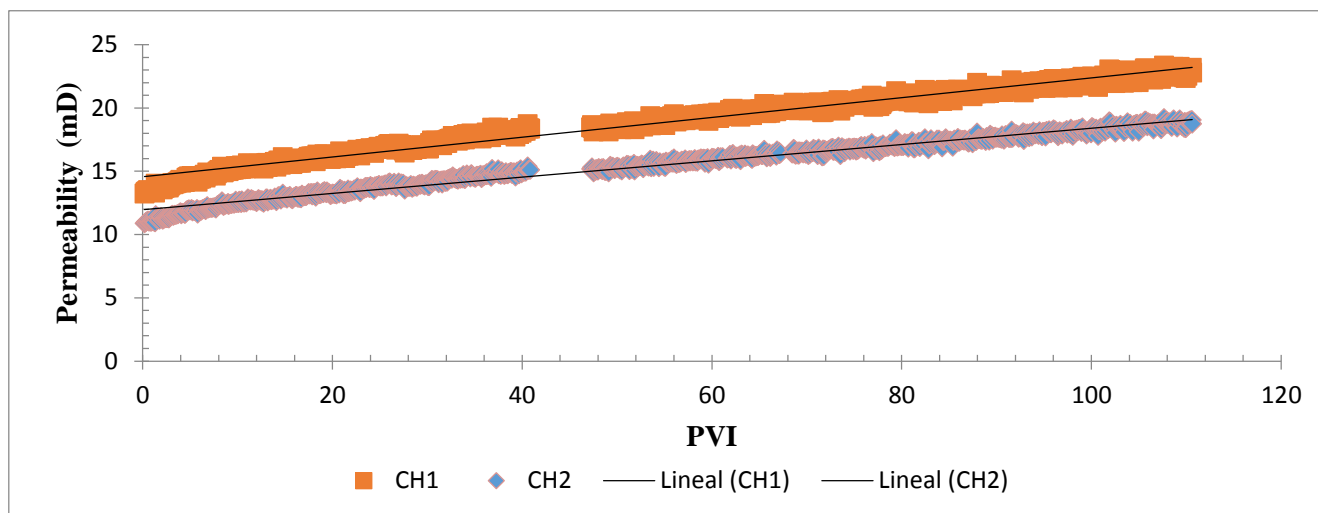


Figure 4.21 Permeability of DH1-A and DH1-B samples throughout the experiment 1.

## 4.2 Experiment #2 – Dissolution Near to Wellbore After two production years

This test had the intention to evaluate the dissolution near to the well after two years of production. To investigate the dissolution behaviour, the injection pressure changed to 7500 psi in Experiment 2.

### 4.2.1 Porosity Results

The second experiment was carried out to reply the rock dissolution that can occur near to wellbore after two production years. The operational conditions performed at the experiment are in **Table 4.4**

**Table 4.4** Experimental conditions Test #2

<b>Experiment #2</b>	
<b>Parameter</b>	<b>Experimental Condition</b>
Injeted Fluid	Brine 42 Kppm - 25% CO <sub>2</sub>
Flow Rate	1 cc /min
Injection Pressure	7500 psi
Overburden Pressure	8500 psi
Temperature	70 °C

It was performed a total of 16 CT – scans for each sample along 13 hours and each CT generated 57 images for the first sample and 73 images for the second one.

**Table 4.5** presents the initial porosity and permeability for the samples DH2-A and DH2-B.

**Table 4.5** Initial porosity (gas) and permeability (gas) of the samples for Experiment #2

<b>Sample</b>	<b>Porosity %</b>	<b>Permeability (mD)</b>
DH2-A	10.559	42.87
DH2-B	22.68	57.33

**Figure 4.22** and **Figure 4.23** show the behaviour of the average porosity of the rock DH2-A and DH2-B along the experiment #2. After 102 porous volume injected (PVI), the sample DH2-A, located in the CH1, increased the average porosity from 10.95% to 13.40%. The sample DH2-B in the CH2 increased from 20.58% to 20.94%.

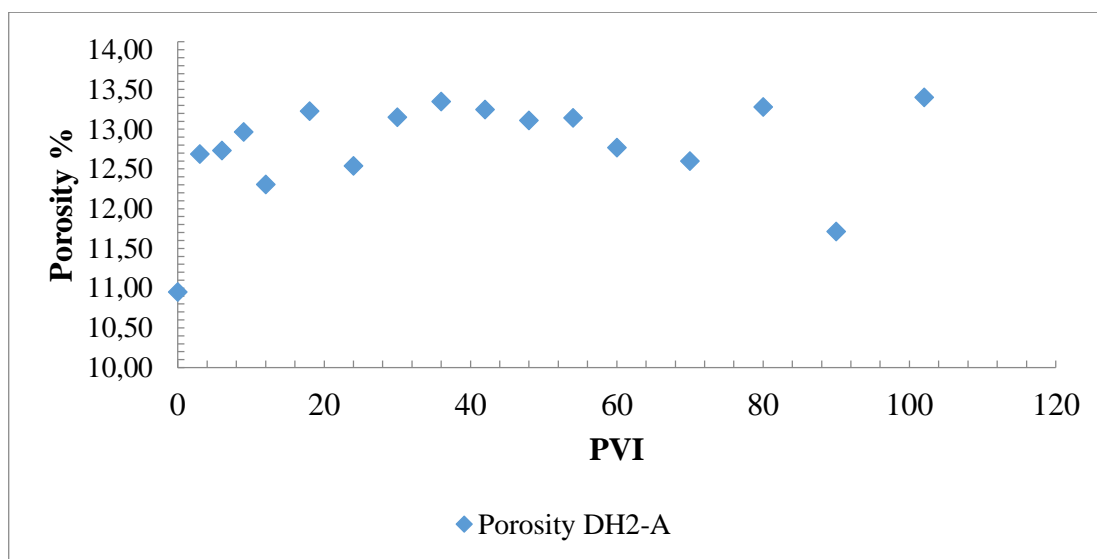


**Figure 4.22** Average Porosity Values obtained from Tomographies DH2-A

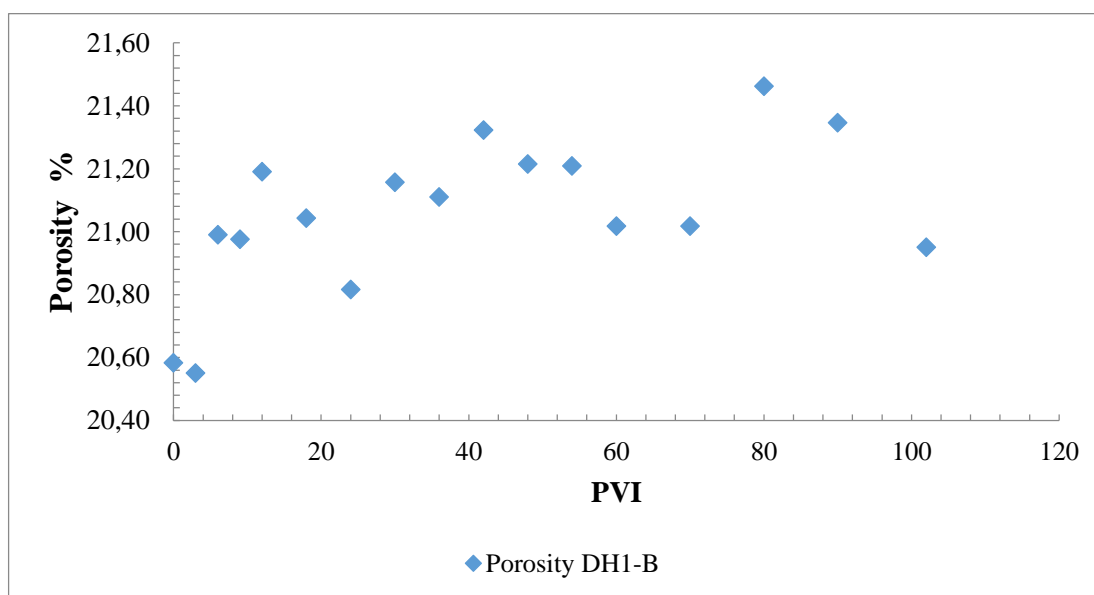


**Figure 4.23** Average Porosity Values obtained from Tomographies DH2-B.

#### 4.2.1.1 Core Holder 1 with the sample DH2-A

The porosity increased along the entire length of the sample DH2-A as can see in **Figure 4.24**. The blue line is the initial porosity, and the red line is the porosity calculated from the last tomography at 102 porous volume injected. It can conclude that the core DH1-A always had dissolution along the experiment, the red line is always above the blue line as shown in **Figure 4.30**.

**Figure 4.24** shows that the core DH2-A probably presents mineralogy and petrophysical characteristic propitious favouring the phenomenon of dissolution. It can be observed three regions in this figure. The first region (A, yellow line), from the inlet of the sample to 1.7 cm, presents initial porosity values between 7.5% and 13.90%. It can observe that this region presented high heterogeneity referring to porosity. The second region (B, green line), from 1.8 to 5.3 cm of the sample, presents initial porosity values between 8.93 % and 11.7%. This region (B) shows visual homogenous porosity behaviour. The third region (C, orange line), from 5.4 to 5.7 cm, presents porosity variations higher than the second region. The porosity values are between 8.52% and 17.30%.

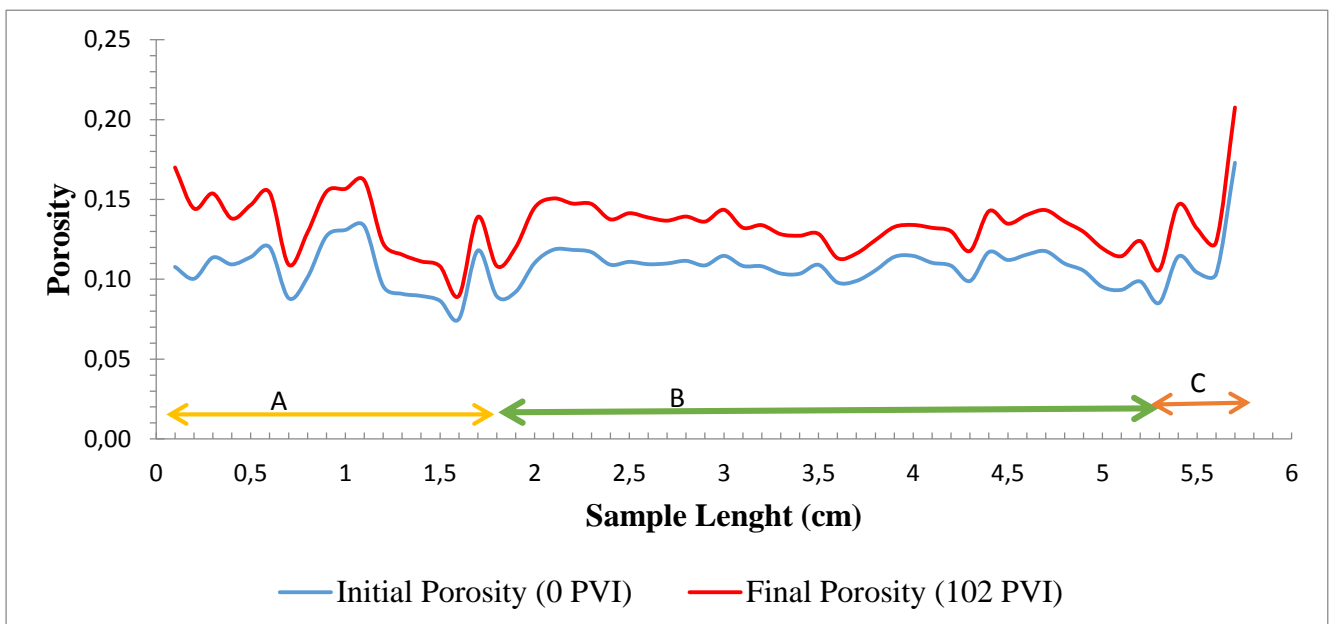


**Figure 4.24** Porosity Variation along the Sample DH2-A

#### 4.2.1.2 Core Holder 2 with the sample DH2-B

**Figure 4.25** shows the porosity along the length of the sample DH2-B for the tomography scans number 1, 2, 15 and 16. Each line represents the porosity profile for its respective tomography. It is possible to identify the tomography as follows: the blue dashed line is the initial porosity, the green line is the porosity calculated from the tomography 1 with three porous volumes injected (PVI). From

the tomography 2 with 6 PVI referred the solid blue line, the orange line is from tomography 15 with 90 PVI and, the red line is the final porosity number 16 with 102 PVI.

It is possible to see three regions in **Figure 4.25**. The first region (A, green line) from centimeter 0 to 3, shows a homogeneous porosity behavior due to the porosity profile oscillation is lower than the second region. The second region (B, red line) between centimeters 3 to 4.3 of the sample, the behavior of the porosities profiles does not maintain the same tendency as the initial porosity, a phenomenon that was also presented in the CH2 of Experiment #1. For this reason, the behavior of this region was analyzed with more details in **Figure 4.26**. The third region (C, Blue line) from centimeter 4.4 to end of the sample, the porosities came back to maintain the same tendency presented in the initial porosity profile.

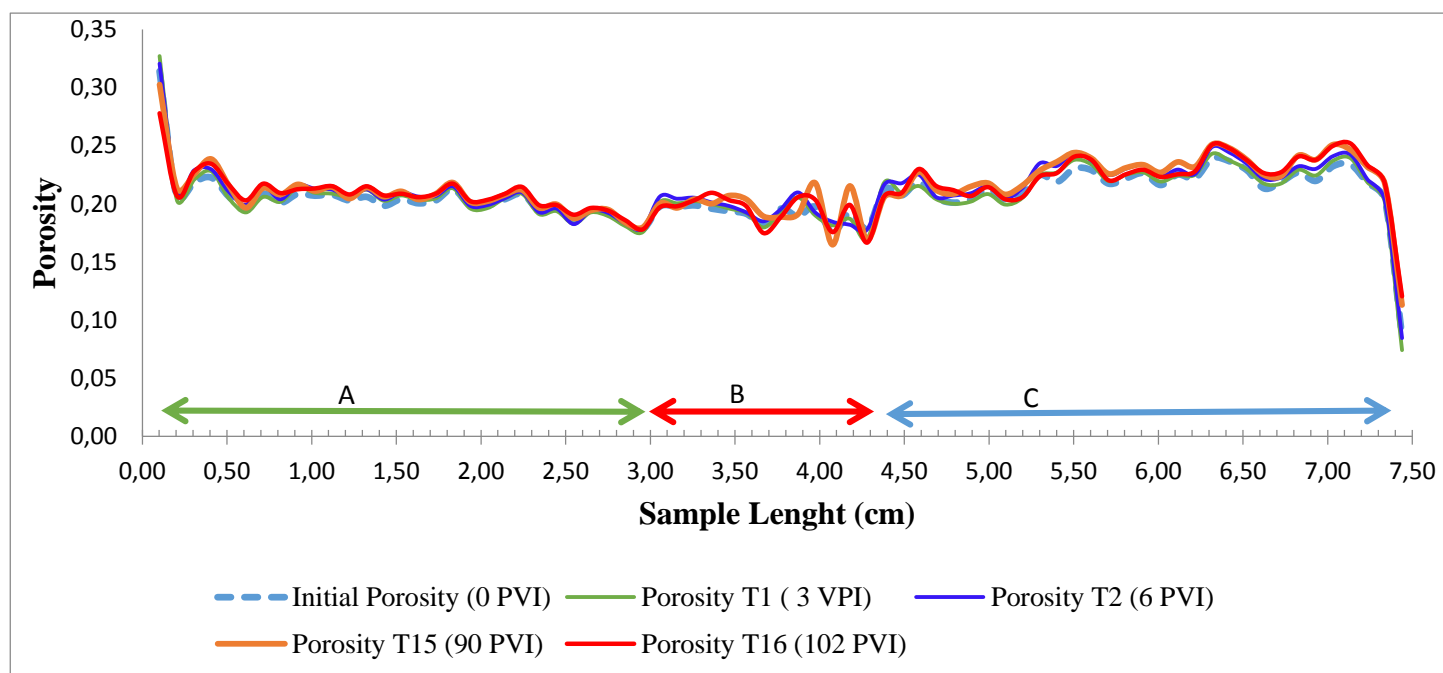


**Figure 4.25** Porosity Variation Along the Sample DH2-B

With **Figure 4.26** it was possible to corroborate that in the 3 - 4.30 cm., where the tomography scans do not follow the same sequence. This sudden alteration of the tendency can be attributed to porosity changes along the sample in this region.

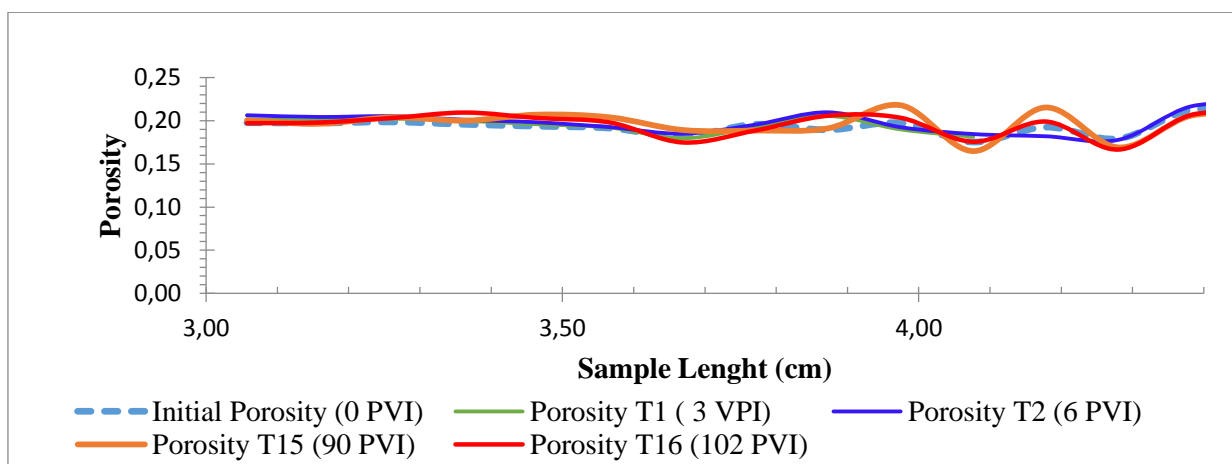


**Figure 4.26** Porosity Variation Along the Sample ( 3 - 4.3 cm) DH2-B

In **Figure 4.27** was analyzed the porosities calculates at different times with the CT scan. The blue line drawn represents the initial porosities of the rock DH2-B. The markers above the blue line indicate dissolution and those which below the blue line indicate precipitation at the same point.

Also, it can be seen that for the interval of 3.0 to 3.1 centimeters, the dissolution occurred all the time. There were precipitation and dissolution at different times from 3.3 until 3.7 centimeters, while in the 3.8 cm happened dissolution in all time, in others words, the porosity increased in this point.

We can suggest that the fluid (carbonated water) arrived in the point 3.8 (red frame) sub-saturated (fluid contains less rock minerals dissolved than could be dissolved) for that reason dissolved. After that, the rock began to reach a geochemical equilibrium with the fluid, and the dissolution began to decrease.

The behavior of precipitation and dissolution reactions for range 3 to 4.3 cm depends on the several properties. These properties can not be easily estimate once they are related to mineralogy, the transport conditions, the concentration of reactants and rock reactivity. In the case of the zone presents high heterogeneity can exist the combination of one or more factors mentioned affecting the behavior of reactivity and the porosity profiles. For example in the position from 3.67 cm to 3.77cm, it was noted that the increase (dissolution) or decrease (precipitation) of porosity change in the different VPI. If the points *Ia* and *Ib* (p3) were compared, it can be concluded that in the point *Ia* occurred precipitation (porosity decrease) and the fluid flow out to next point can be equilibrated or sub-saturated.



If the fluid were sub-saturated, it could promote the dissolution of the other minerals as it occurs in the point *1b*.

However, in the same position but for distinct PVI, it can be observed that the point *2a* (p16) and *2b*(p16) show dissolution and the first point has a lower intensity than the second one. Finally, in the same position, the point *3a* (p15) presents a high dissolution and the fluid come out super-saturated and in the next point (*3b*) the porosity returns to initial porosity value, which indicates the precipitation occurrence.

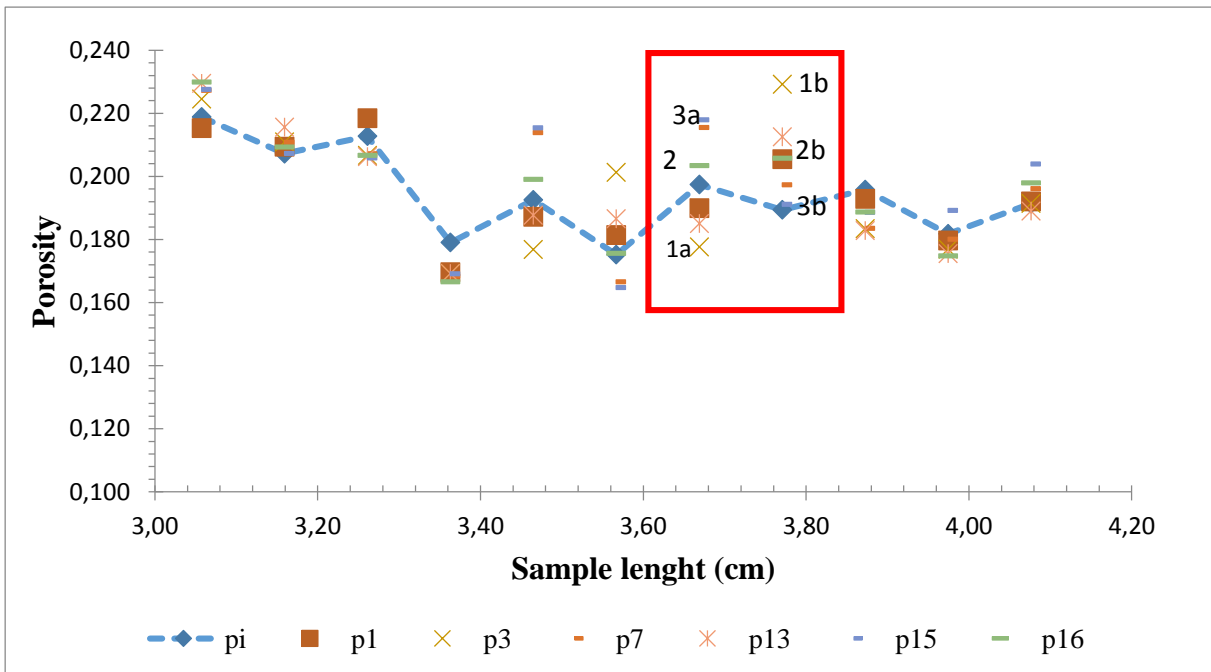


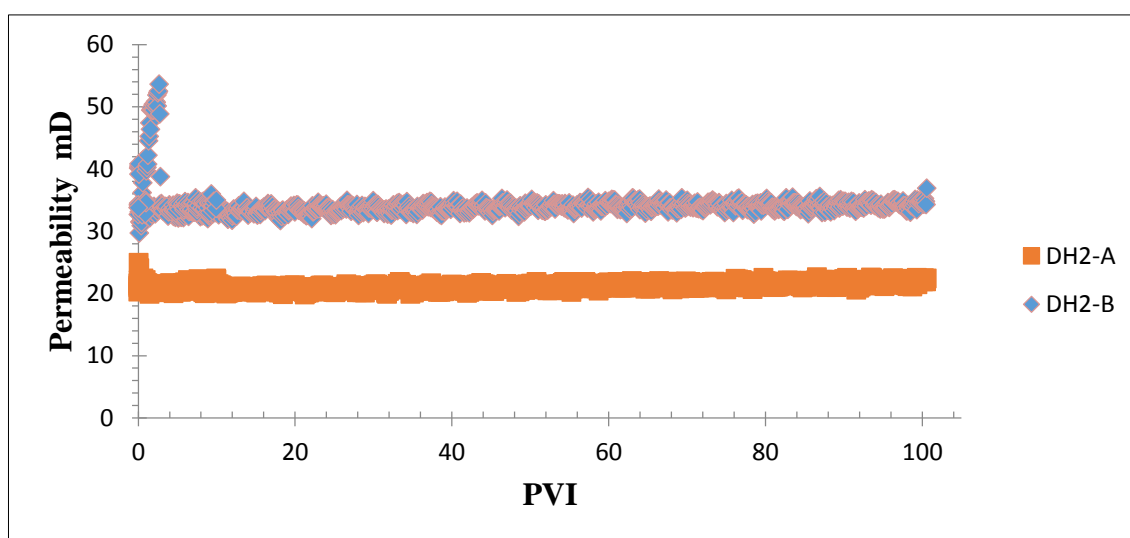
**Figure 4.27** Porosities Rock DH2-B calculates at different times with the CT scan

#### 4.2.2 Permeability Results

**Figure 4.28** shows the evolution of the permeability during the test. The permeability shows the same behaviour in the two core holders. The sample DH2-A assembled in the CH1 presented 42.8 mD using the gas permeabilimeter and 24.9 mD calculated by the pressure drop registered by the first measurement registered in the pressure transducer. The permeability varied between 20 and 21 mD through the whole experiment (102 VPI). It can conclude that there was no significant increase during the test.

The DH2-B sample located in CH2 presents a gas permeability of 57.33 mD and 34.52 was the permeability value calculated from pressure differential. It was observed that the first 20 minutes, the sample DH2-B suffered a permeability increase until 51.88 mD, and then it had a sudden descent from 48 to 38 mD, and after that, it stabilized in 34 mD along the test.

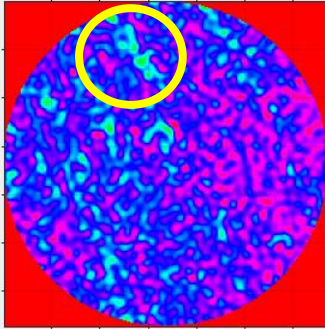
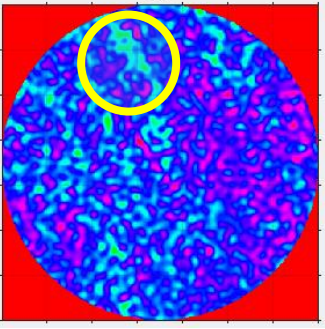
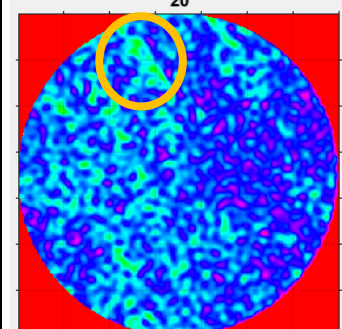
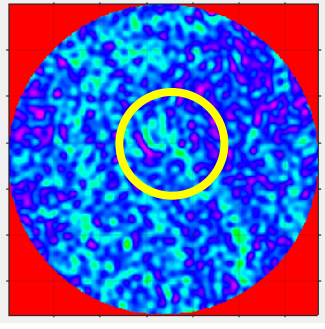
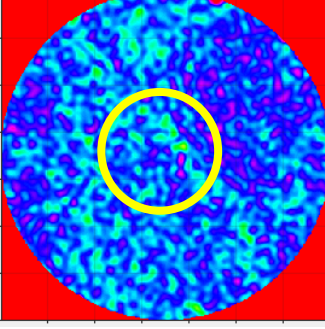
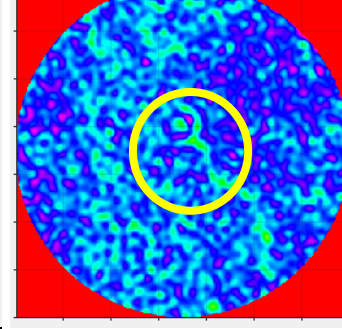
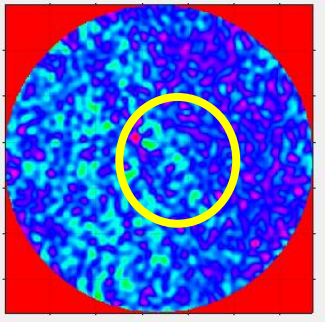
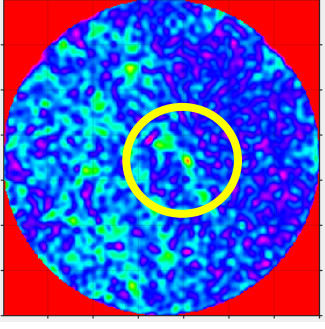
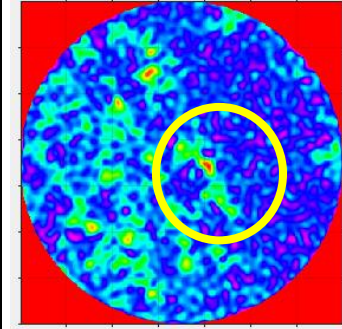
It suggests this permeability behaviour is due to the first 20 minutes of injection (approximately three porous volume injected). During this time, it is possible to open the secondary channels that increased the permeability, but after the increment the quantity of pore volumes injected, the mineral saturation in the fluid increased and precipitated causing decreasing the permeability.



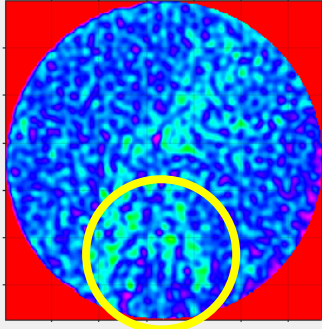
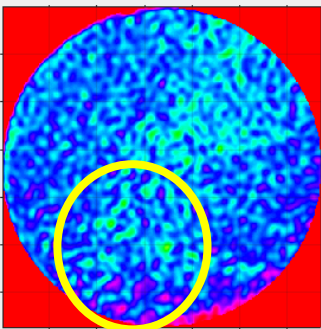
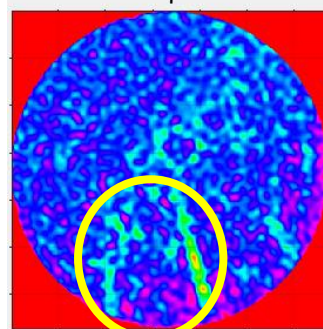
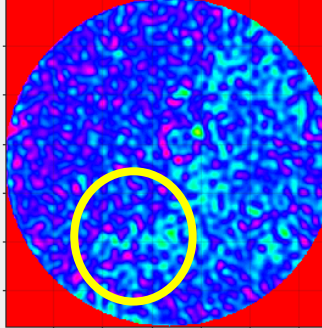
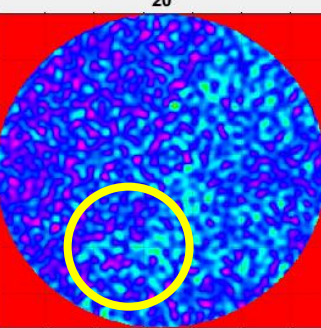
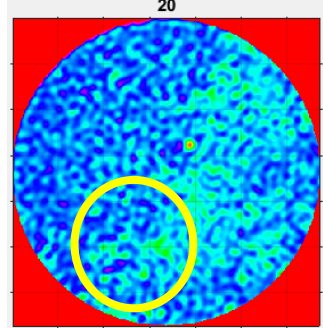
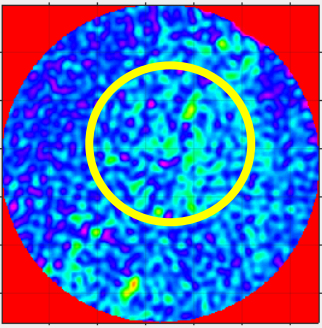
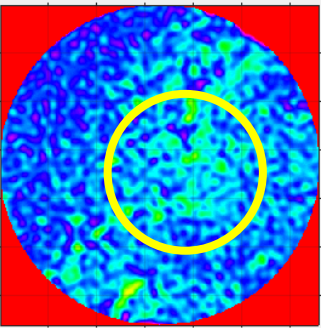
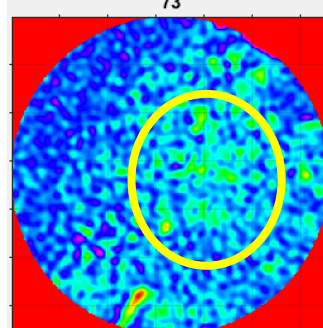
**Figure 4.28** Permeability Experiment #2

**Table 4.6** and **Table 4.7** shows that the porosity increments in the images took place at distinct positions around the sample. Following the comments suggested by images different analyzed in these tables, it can be concluded that there was not the creation of preferential path ( wormhole), which could increase the permeability value. However, it is believed that the permeability measurements for sample 1 are correct.

**Table 4.6** Position of the rock at the beginning, middle and end of the experiment CH1

<b>Core Holder 1 – DH2-A</b>			
<b># Image</b>	<b>Tomography #1</b>	<b>Tomography #8</b>	<b>Tomography #16</b>
20	20 	20 	20 
30	30 	30 	30 
57	57 	57 	57 

**Table 4.7** Position of the rock at the beginning, middle and end of the experiment CH2

<b>Core Holder 2 – DH2-B</b>			
<b># Image</b>	<b>Tomography #1</b>	<b>Tomography #8</b>	<b>Tomography #16</b>
1	1 	1 	1 
20	20 	20 	20 
73	73 	73 	73 

### 4.2.3 Ion Chromatography Result Experiment #2

Ionic Chromatography results are presented in **Table 4.8** with the ions concentrations mg/L **Figure 4.29** to **Figure 4.30** show the production curve for each ion: Mg and Ca.

The concentration of magnesium ion presented in **Figure 4.29** shows that the effluents collected at outlet of CH1 and CH2 exhibited values for concentration of this ion lower than the initial, which could suggest that the magnesium ion is staying in the rock or it is precipitating as salt.

**Figure 4.30** illustrates the production of calcium ion in the carbonated water after it went through the cores. The orange and blue lines indicate the concentration in the effluents of the core-holder 1 (CH1) and core-holder 2 (CH2), respectively. It can be seen that the concentration of calcium is higher in the outlet of CH2, it can be explained due to the high dissolution occurred in the CH1 (**Figure 4.24**), then part of these ions went into CH2 adding to the concentration of calcium in the effluents of CH2.

**Table 4.8** Calcium and Magnesium Ions Chromatography results

VP	Ca (mg/L)		Mg (mg/L)	
	CH1	CH2	CH1	CH2
4	930,19	471,20	791,64	813,25
8	888,80	1070,77	772,58	827,34
12	575,13	1091,38	720,30	784,21
16	881,72	1148,54	785,79	796,04
22	681,84	1130,72	784,42	783,26
28	829,23	1138,31	791,64	783,32
34	818,40	1145,84	794,55	783,32
40	814,19	1169,53	803,05	792,06
46	551,72	581,03	797,32	766,92
54	785,38	1152,64	791,61	789,73
62	815,48	1092,02	804,39	767,38
70	779,81	1145,44	799,22	791,16
78	775,09	1148,56	798,11	793,21
90	778,22	1112,29	804,61	787,94
102	547,84	1119,11	806,51	788,41

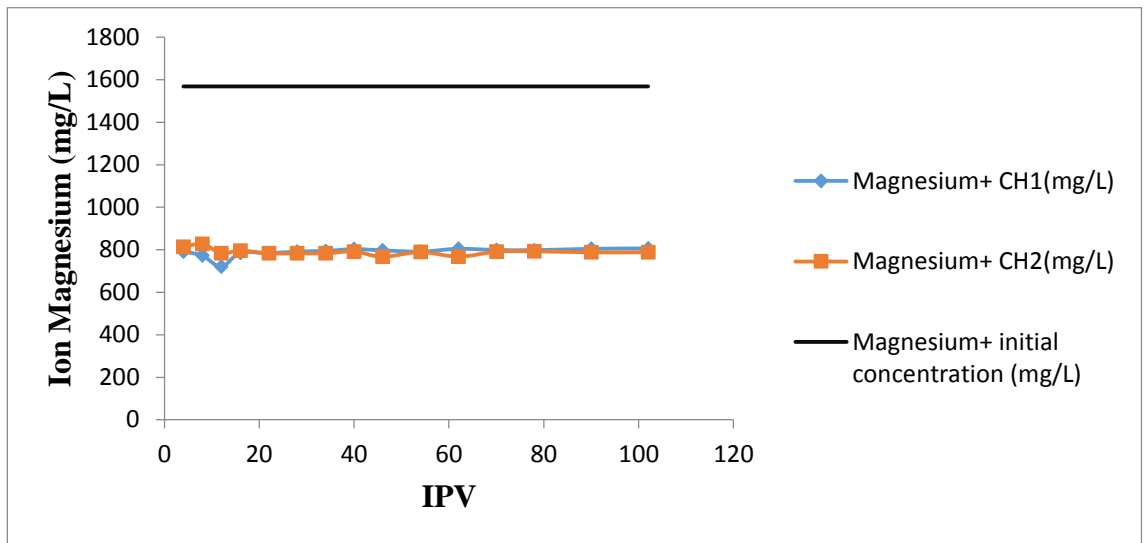


Figure 4.29 Magnesium produced CH1 and CH2.

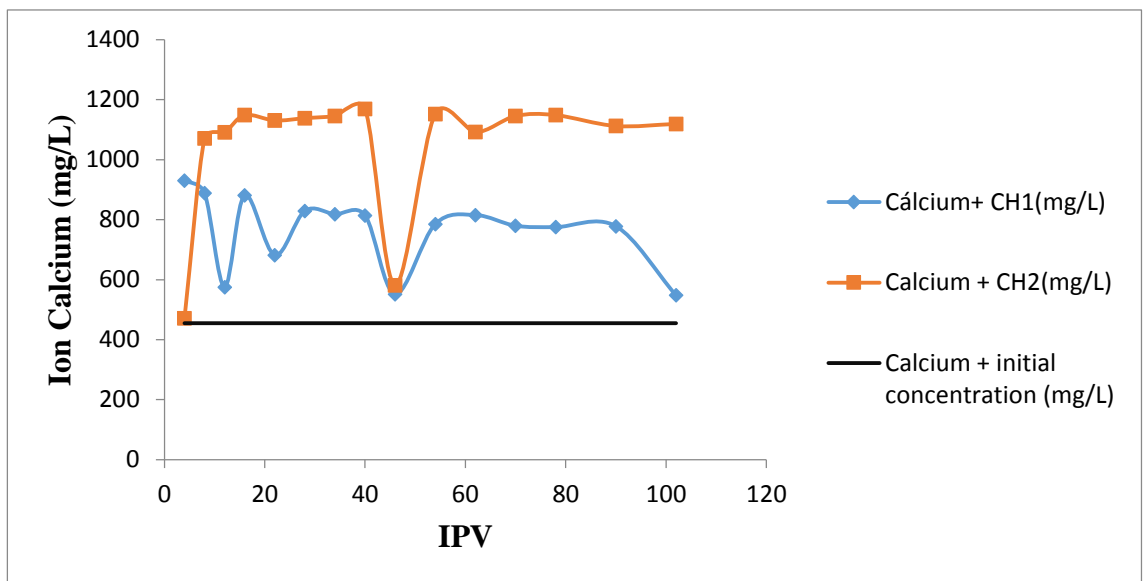


Figure 4.30 Calcium produced CH1 and CH2.

#### 4.2.4 Discussion on Experiment 2

In this section, we are going to compare the results obtained in the second experiment with the Nunez's experiment. Both tests were made under reservoir conditions, injection pressure of 7500 psi and 70°C. **Figure 4.31** and **Figure 4.33** are from the second experiment of Nuñez 2017 and the nomenclature R2N and R4N are the sample's names used for the experiment.

##### 4.2.4.1 Porosity

The Porosity results for the second experiment (7500 psi injection pressure) was compared with the experiment of Nuñez 2017 at the same conditions (**Figure 4.31** and **Figure 4.33**). Nuñez 2017 reports that the core R2N in the first core holder increase its porosity significantly, it can be seen in the first 1.2 centimeters (**Figure 4.31**) of the sample. He concluded that dissolution occurs almost immediately as injection fluid start going through the rock. On the other hand, experiments with reservoir rock (**Figure 4.32**) show that the core DH2-A not only have dissolution in the first centimeters of the rock, but its mineralogy and petrophysical characteristic promoted the dissolution of the rock along of the entire sample.

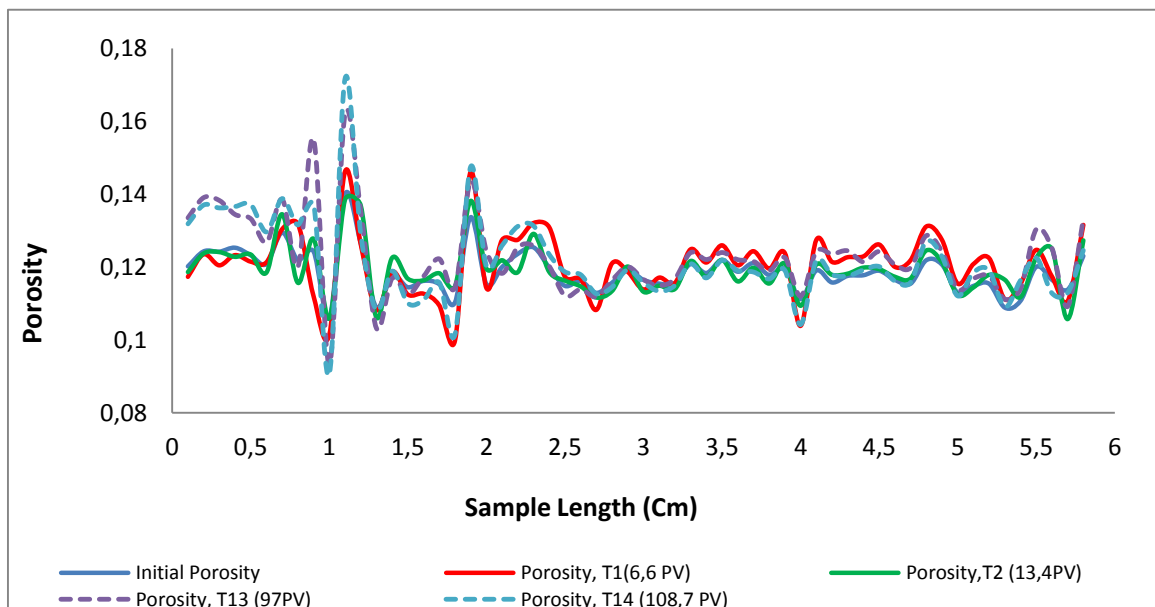


**Figure 4.31** Sample Porosity variation along the sample R2N CH1. Source: Nunez

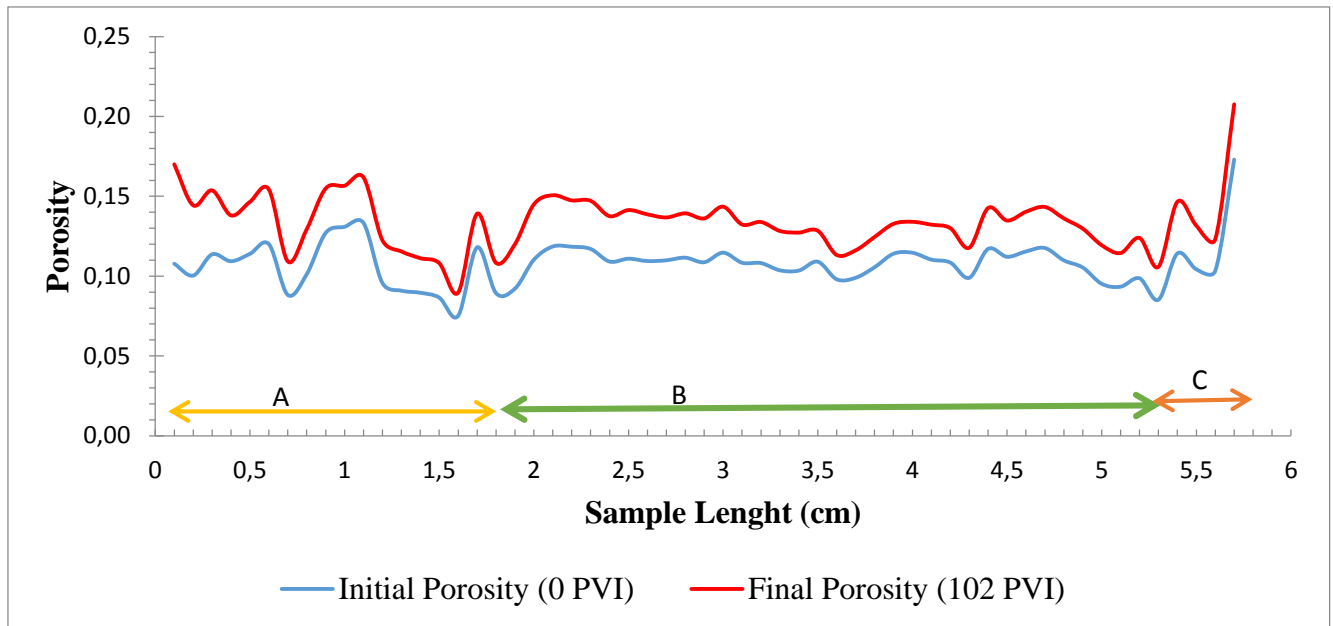


**Figure 4.32** Porosity Variation along the Sample DH2-A

According to Nuñez 2017 the CH2 **Figure 4.33** shows that the phenomena of dissolution and precipitation is associated with localized porosity heterogeneities in the sample. Besides, in the centimeters 2.4, and 3.2, the sample in the CH2 presented that the behavior of the porosity profile does not maintain the same tendency as the initial porosity. This phenomenon was also observed at reservoir rock in the region b, indicated at the **Figure 4.34**.



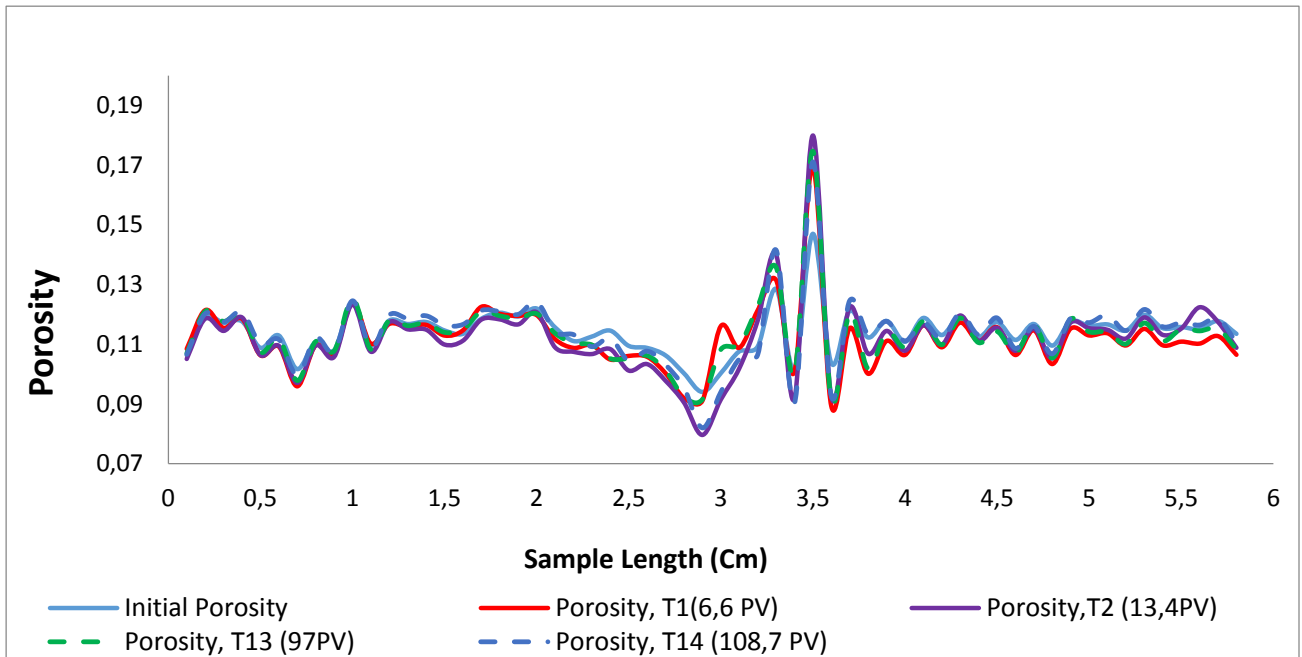


**Figure 4.33** Nunez 2017. Sample Porosity variation along the sample R4N CH2

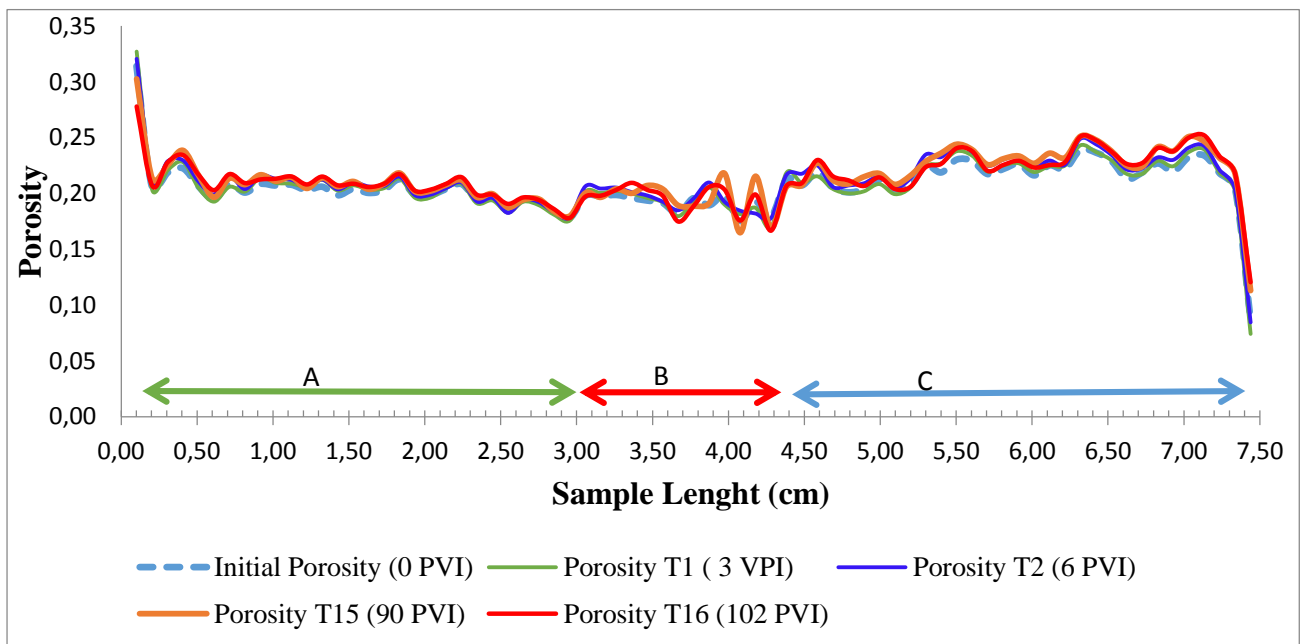


**Figure 4.34** Porosity Variation Along the Sample DH2-B

#### 4.2.4.2 Permeability

According to Nuñez 2017, the sample located in the CH1 (**Figure 4.35**), shows an decrease in permeability values after the injection of the first 10 PV. After that, the value exhibited remains constant around 65 mD along the experiment. The CH2 (**Figure 4.36**) showed a tendency to decrease in permeability along the test, similar to the observed in sample RV4 of the first experiment. However, the experiment in reservoir rock (**Figure 4.37**) permeability kept constant in the two core-holders along the test. The DH2- A varied between 20 and 21 mD and The DH2-B stabilized in 34 mD along the test.

It can be concluded that the experiments, with 7500 psi of injection pressure and 70 °C, for dolomite rocks, with initial permeability values between 60 to 120 mD , show a decreased tendency at the permeability property along to the experiment. On the hand, under the same conditions, for reservoir rock with initial permeability values show a consistent behavior along the experiment due to the permeability values do not change.

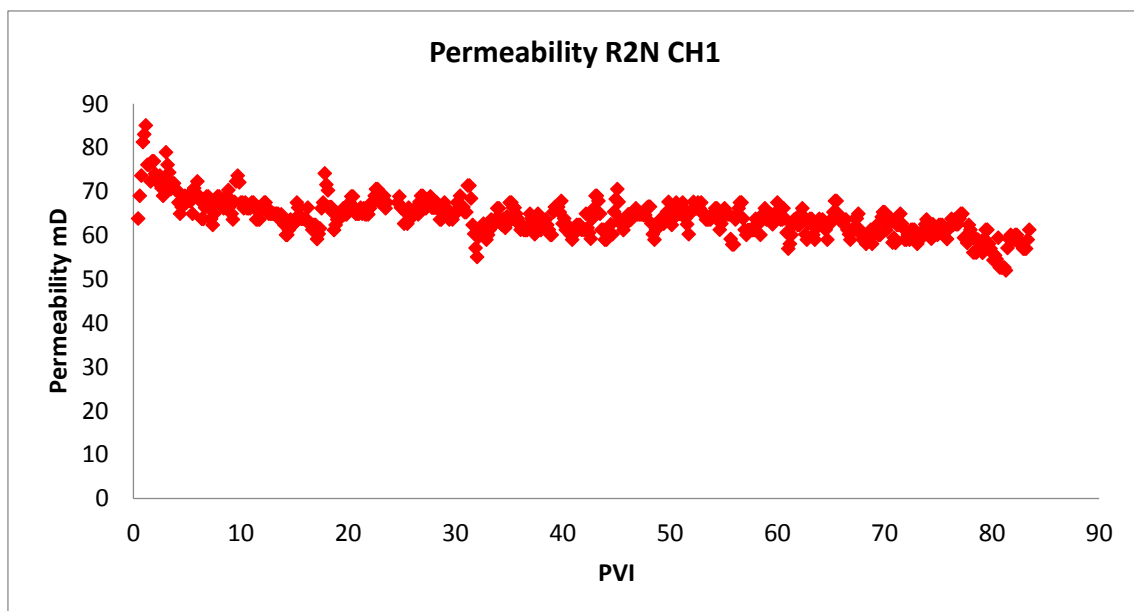


**Figure 4.35** Nunez 2017. Permeability Scatter Plot Sample R2N CH1.

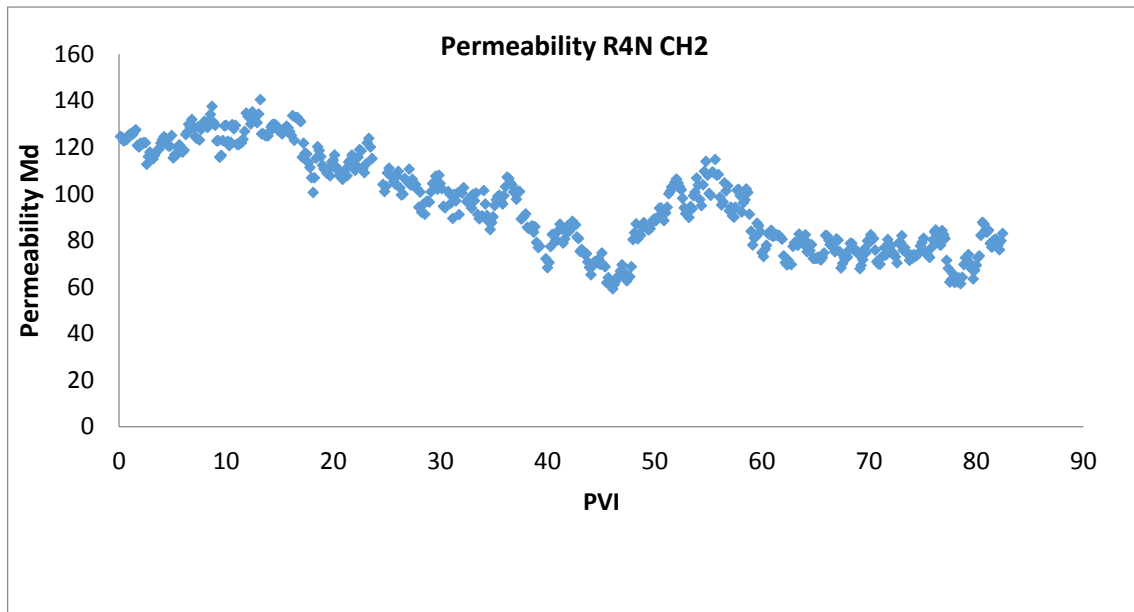


**Figure 4.36** Permeability Scatter Sample Plot R4N CH2.

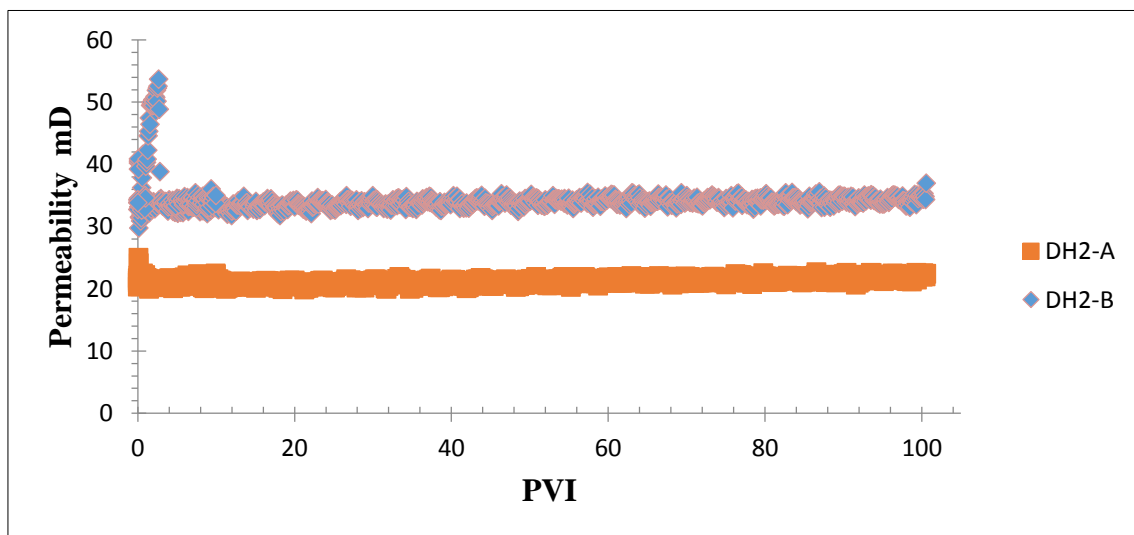


**Figure 4.37.** Permeability Results Experiment 2

### 4.3 Experiment #3 – Represents a region 100 m away from the injector well

This test had the intention to evaluate the dissolution 100 meters away from the injector well. To investigate the dissolution behaviour, the injection pressure changed to 8250 psi and the composition brine was modified. A new brine composition for the carbonated water was calculated with the geochemical simulator PHREEQC and the chromatography results of the effluents obtained in Experiment 1. The new composition corresponds to the carbonated water prevalent at 100 meters away from the wellbore.

It was planned to inject 80 porous volumes and take 11 CT scans for each sample. However, at the beginning of the test the pressure transducer used to measure the pressure drop in the second core holder overpass the pressure range putting in risk the integrity of the equipment, therefore, the second core holder was put offline. Due to those problems, it was not possible to get any information from sample assembled in the CH2.

#### 4.3.1 Porosity Results

The operational conditions performed at the experiment are in **Table 4.9**.

**Table 4.9** Experimental conditions Test #3

<b>Experiment #2</b>	
<b>Parameter</b>	<b>Experimental Condition</b>
Injeted Fluid	Brine simulate PHREEQC
Flow Rate	0.1 cc /min
Injection Pressure	8250 psi
Overburden Pressure	9250 psi
Temperature	70 °C

It was performed a total of 11 and 2 CT scans for CH1 and CH2 respectively. Experiment 3 lasted aproximately 95 hours and each CT scan generated 44 images for the first sample and 66 images for the second one.

**Table 4.10** presents initial porosity and permeability for the samples DH3-A and DH3-B.

**Table 4.10.** Initial porosity (gas) and permeability (gas) of the samples for Experiment #3

Sample	Porosity %	Permeability (mD)
DH3-A	10.1	18
DH3-B	11.3	10

**Figure 4.38** shows the behaviour of the average porosity of the rock DH3-A along the Experiment 3. The average porosity of sample DH3-A increased from 12.3% to 13.04% after 80 VPI.

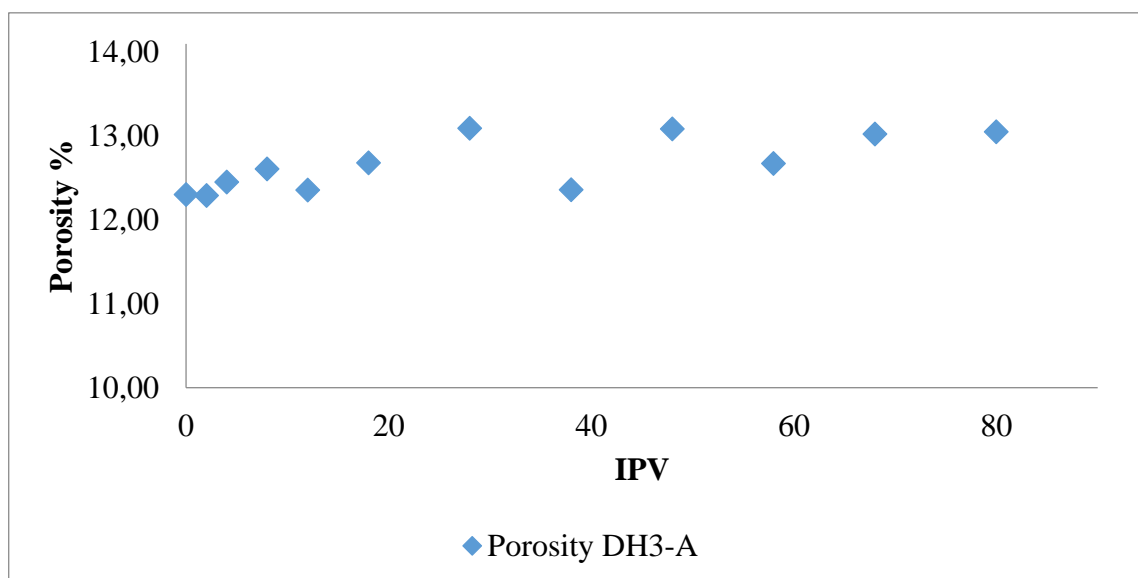


**Figure 4.38** Average Porosity Values obtained from Tomographies DH3-A

#### 4.3.1.1 Core Holder 1 with the sample DH3-A

The porosity increased in some points of the sample DH3-A as can see in **Figure 4.39**. The blue line is the initial porosity, and the red line is the porosity calculated from the last tomography at 80 porous volume injected. It can conclude the core DH1-A did not had constant dissolution however, also did not have

precipitation along the sample because the figure shows that the red line is always above the blue line.

It can conclude that the core DH1-A did not show constant dissolution along the test. Also, there was not precipitation along the sample, as can see in the Figure X where the red line is always above the blue line.

**Figure 4.39** is divided into three regions according to the porosity behavior. The region A (yellow line) goes from inlet to 1.5 cm; this region did not show significant variations due to the homogeneity of the rock, porosity in this zone is between 11% to 13%.

Region B (green line) goes from 1.5 cm to 3.5 cm, this zone presents a high heterogeneity concerning to the initial porosity due to the wide range for porosity (13% to 20 %). In this region the dissolution phenomena are stronger compared with the region A. The red line which represents the final porosity always is more significant than the initial porosity. In the zones where the porosity is high (peaks) the dissolution effect presented more magnificent and in zones with low porosity did not present any change at the final porosity value.

Finally, region C (Orange line), which goes from 3.5 to 4.7 cm displays high heterogeneity in the initial porosity. The behavior is entirely different than in region B due to the porosity values are between 15% to 7%. At the beginning of the zone is observed an alteration of the tendency, it can be attributed to mineralogy because there was only porosity variation and there was not changes on profile tendency (see region B). The final porosity did not show any variation at remaining zone, indicating that dissolution phenomena did not take place in this area.

Also, it is possible to observe that from 0.8 to 3.7 cm, the trend of the red line did not reflect the same than the blue line. It can suggest that in these points can occur mineralogical changes affecting the trends in the porosity profiles.

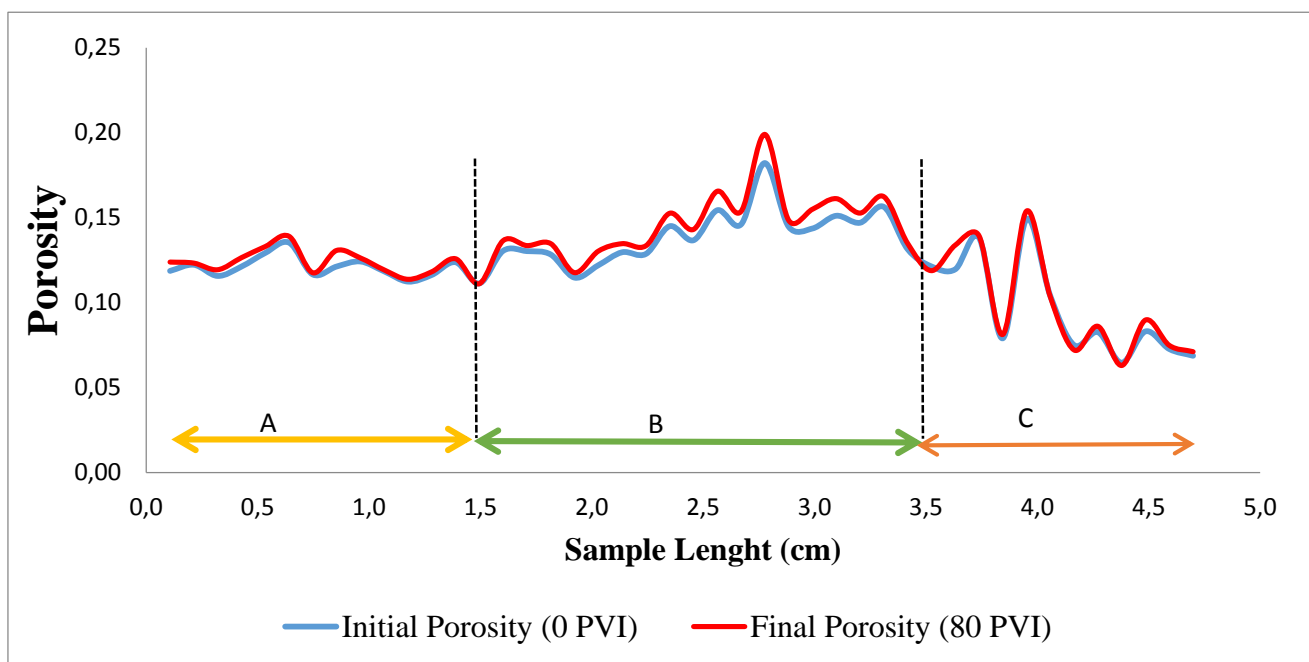


**Figure 4.39** Porosity Variation along sample DH3-A

#### 4.3.1.2 Core Holder 2 with the sample DH3-B

**Figure 4.40** describes porosity along the sample length. It can observe the initial porosity (red line), porosity calculated with tomography one (orange line) and two (green line). The figure is divided into three regions according to the porosity behavior.

Region A (Green line), from the inlet to 1,2 cm; it can identify that this region did not have dissolution due to there was no separation between the lines. From 0,5 to 1 cm, it is possible to see that has a little alteration with the tomography trend. Also, it is possible to notice that in high values of porosity do not have a dissolution.

Region B (Blue line), from 1,2 to 5,5 cm it can identify that it is a homogeneous zone due to initial porosity does not have peaks or valleys. The initial porosity values are between 9 and 10 %. In additions, in this zone did not

have predominate dissolution and precipitation phenomena. From 2,38 to 2,8 cm, exist a little dissolution.

Region C (Yellow line), from 5,5 to the outlet of the sample, in this zone is evident the trend changes between the tomographies one and two with respect to the initial porosity. How it was studied in the experiments one and two, this phenomena indicates that this zone has a mineralogy heterogeneity. With this experiments can corroborate that when the rock has mineralogy heterogeneity without porosity heterogeneity presents point where can coexist dissolution and precipitation phenomena for different porous volume injected.

Region C (Yellow line), from 5,5 to the outlet of the sample, is evident the trend changes between the tomographies one and two compared with the initial porosity these phenomena indicate the presence of mineralogy heterogeneity how it can saw in the experiments one and two. With this experiment, can corroborate that when the rock has mineralogy heterogeneity without porosity heterogeneity presents points where can coexist dissolution and precipitation phenomena for different porous volume injected (Trend changes)

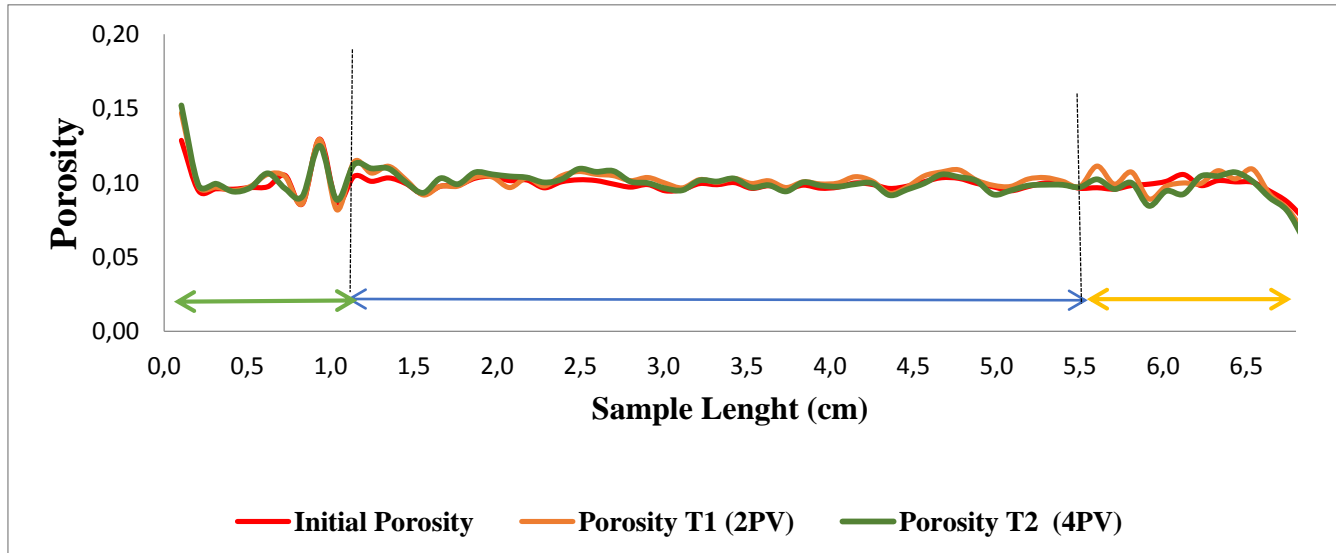


**Figure 4.40** Porosity Variation along sample DH3-B

### 4.3.2 Permeability Results

**Figure 4.41** describes the permeability behavior in the CH1 along the test. The graph shows high values of dispersion, for this reason, it was necessary to analyze the permeability each 20 PVI as shown in the to **Figure 4.45**.



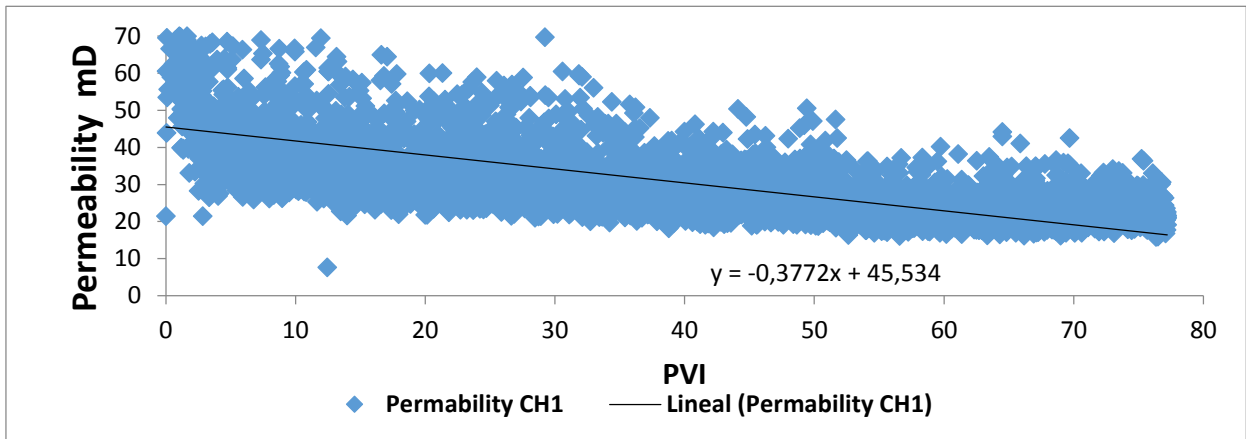


**Figure 4.41** Permeability Experiment #3

shows permeability behavior in the first 20 PVI in the sample DH3-A. The initial rock permeability had a value of 69 mD, and when the injection began, this rock property diminished oscillating between 70 to 30 mD.

In **Figure 4.43**, **Figure 4.44** and, **Figure 4.45** it is possible to see that the permeability values range is between 50 mD and 20 mD. Finally, in 77 PVI, it can be observed that the rock remains permeability between 30 md and 20md. This behavior along the experiment is due to the rock getting stuck and unstuck.

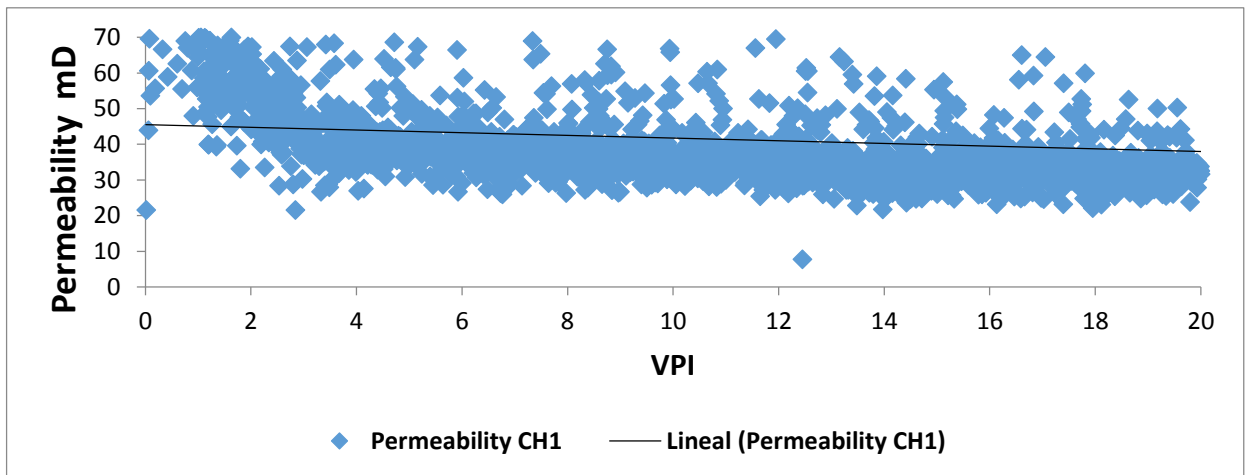


**Figure 4.42** Permeability since 0 to 20 PVI - Experiment #3

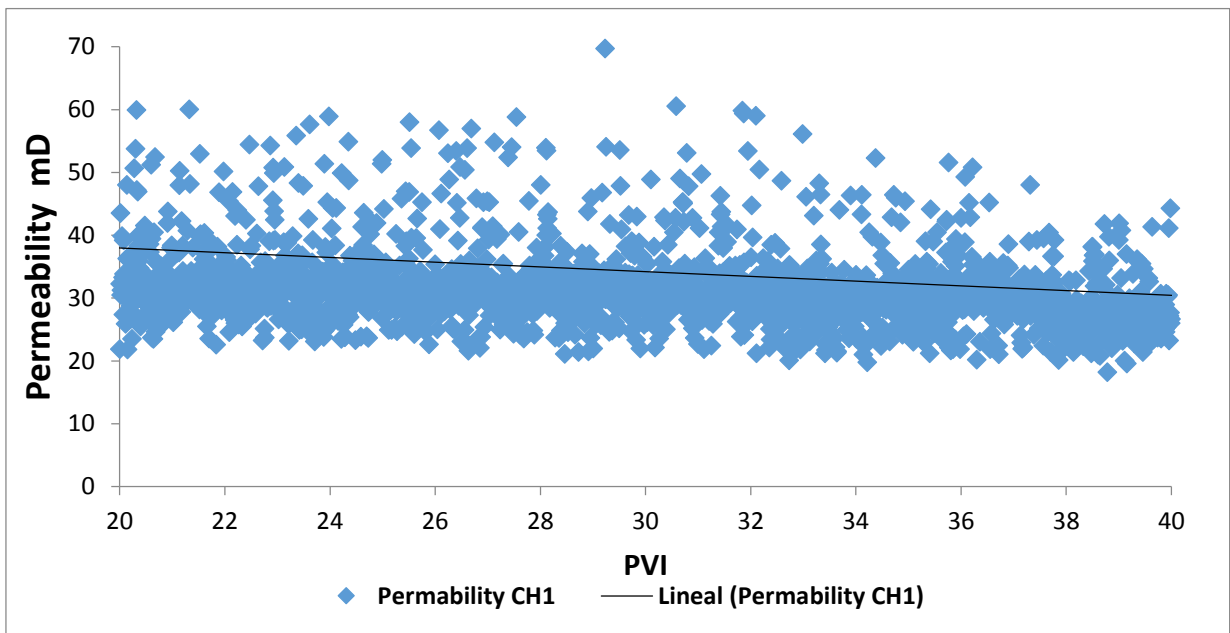


**Figure 4.43** Permeability since 20 to 40 PVI - Experiment #3

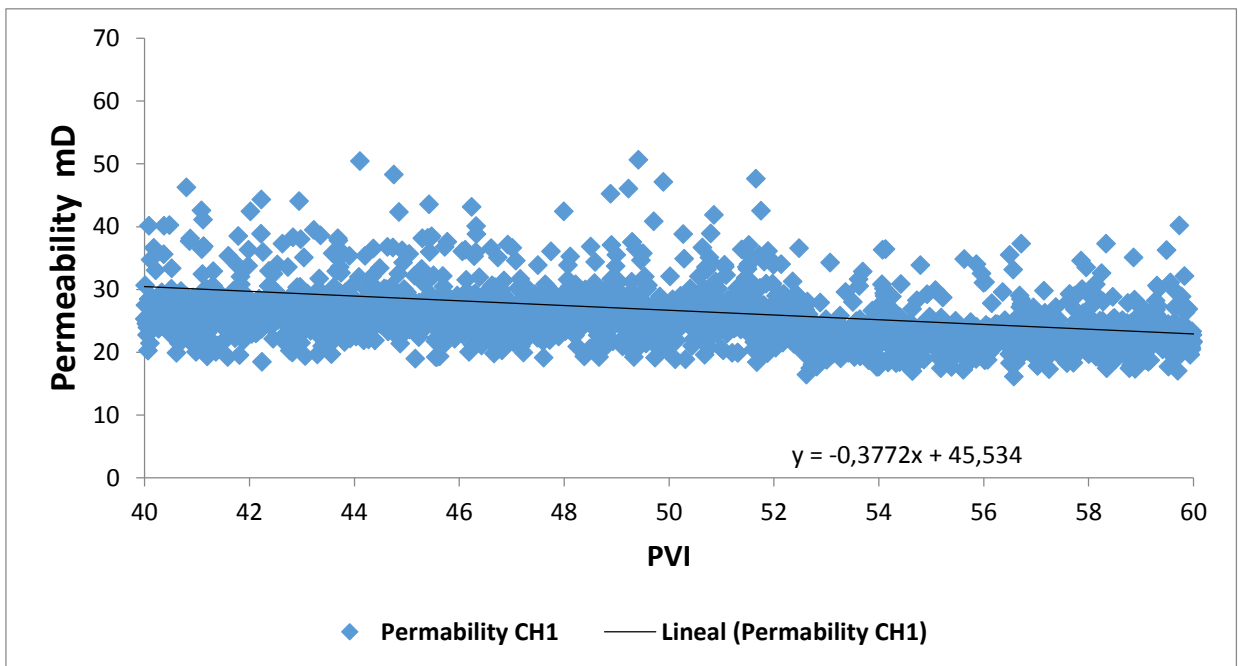


**Figure 4.44** Permeability since 40 to 60 PVI - Experiment #3

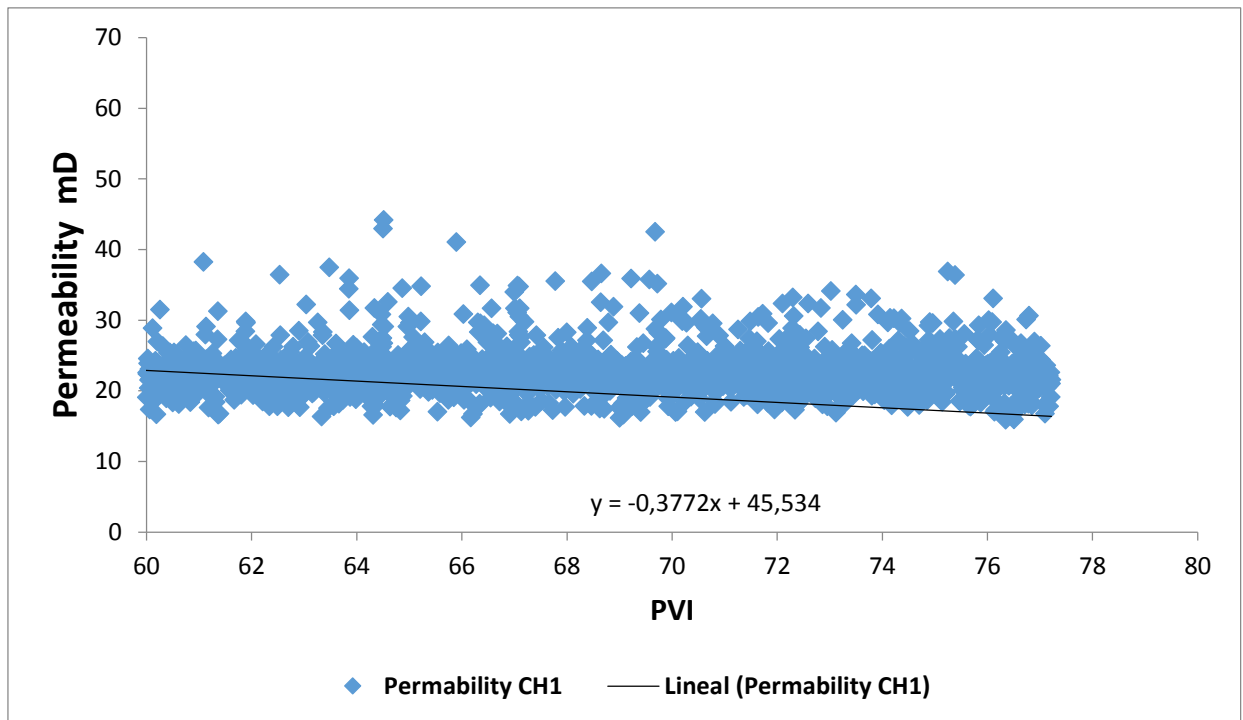


**Figure 4.45** Permeability since 60 to 77 PVI - Experiment #3

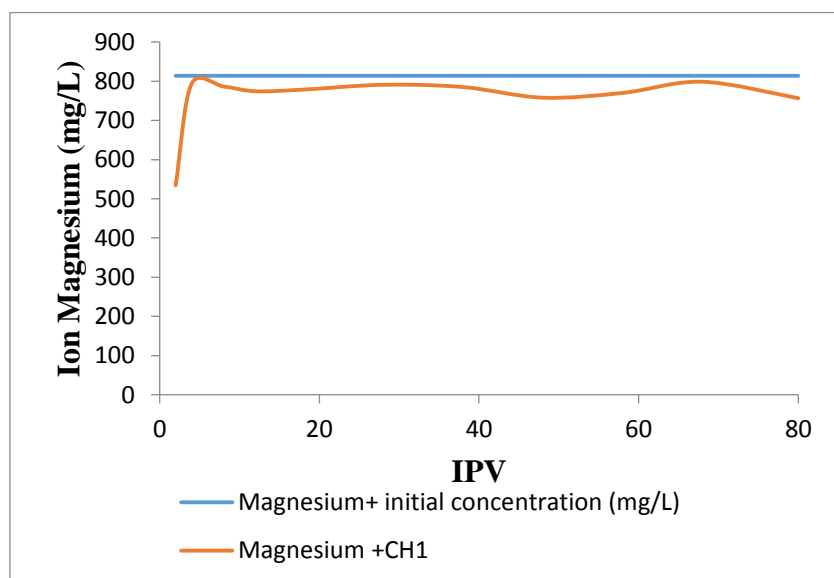
### 4.3.3 Ion Chromatography Result Experiment #3

Ionic Chromatography results are presented in **Table 4.11** with the ions concentrations mg/L. **Figure 4.46** and **Figure 4.47** show the production curve for each ion: Mg, and Ca as a function of PVI for the experiment III. In this experiment, it was collected just one effluent at the CH2 exit. The orange and blue lines indicate the ion concentrations in the effluent.

It can observe that the calcium and magnesium concentrations along the experiment are lower than the initial Brine. It could suggest that the Mg and Ca ions are staying in the rock increasing the precipitation. Therefore, this may be an explanation because the permeability showed decrease throughout the entire experiment.

**Table 4.11.** Calcium and Magnesium Ions Chromatography results

PVI	Mg (mg/L)	Ca (mg/L)
	CH1	CH1
2	534.49	836.56
4	793.34	2659.20
8	786.66	2703.46
12	774.52	2677.27
18	778.66	2381.22
28	790.92	2739.65
38	785.20	2718.94
48	758.06	2650.99
58	770.27	2596.75
68	798.69	2768.11
80	756.61	1946.67

**Figure 4.46** Magnesium produced CH1 and CH2

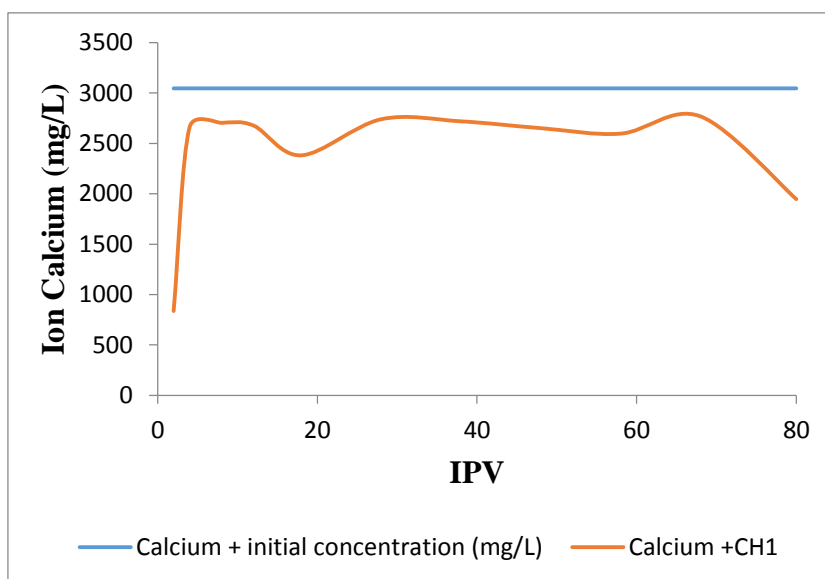


**Figure 4.47** Calcium produced CH1 and CH2

#### 4.3.4 Discussion on Experiment 3

In this section, we are going to compare the results obtained in the Third experiment of this work with the Nuñez's third experiment. Both tests were made under reservoir conditions, injection pressure of 8250 psi and 70°C. **Figure 4.48** and **Figure 4.50** show the third experiment of Nuñez 2017 and nomenclature of RN1 and RN3 are the sample's names used for the experiment.

##### 4.3.4.1 Porosity

The Porosity results in the third experiment (8250-psi injection pressure) were compared with the experiment of Nuñez in 2017 under the same conditions (**Figure 4.48** and **Figure 4.50**). Experiments with reservoir rock (**Figure 4.49** and **Figure 4.51**) did not show any precipitation in the sample DH3-A, located in CH1,. In high values of porosity, it can be seen the phenomenon of dissolution, and in lower porosity points the final porosity did not show any variation from initial porosity. On the other hand, Nuñez 2017 reports that the core RN1 in the first core holder (**Figure 4.48**) had points of precipitation along the sample (centimeters 3 to 3.5). Besides, we can observe that in high initial porosity values, there was a dissolution (centimeters 1.5 and 3.6) and in the lower points of initial porosity, there was precipitation.

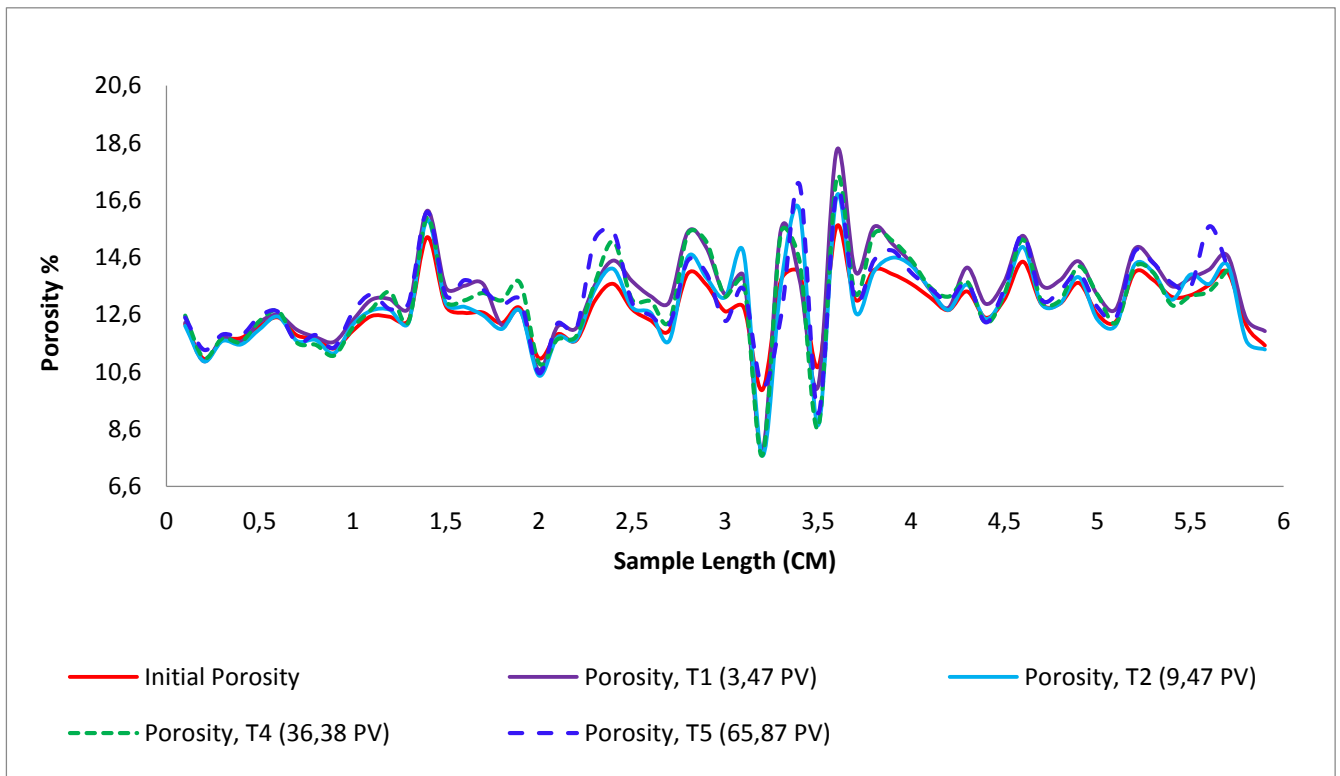


Figure 4.48 Nunez 2017. Sample Porosity variation along the Dolomite sample RN1 CH1.

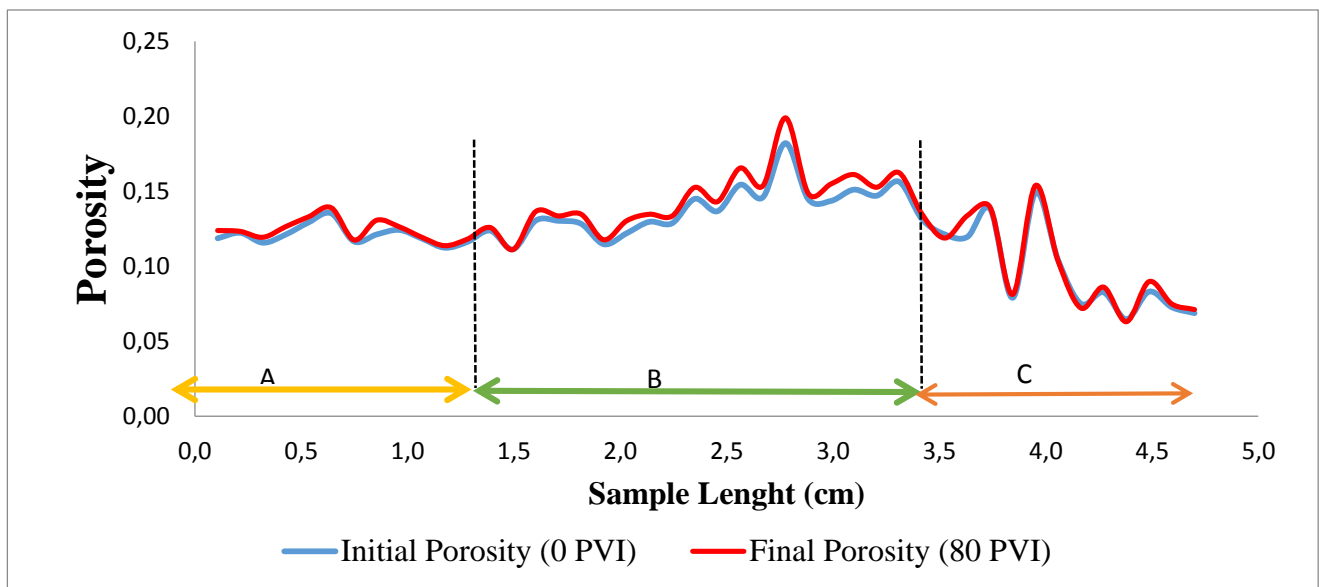
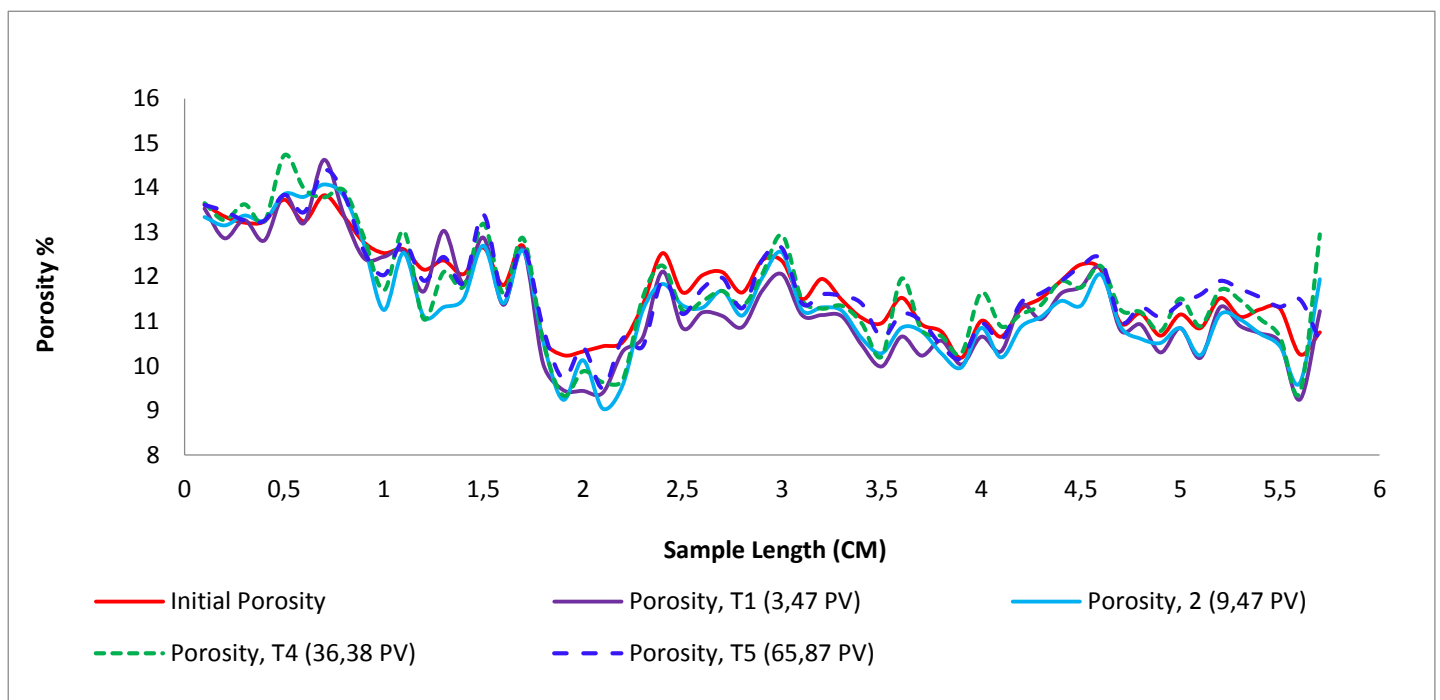
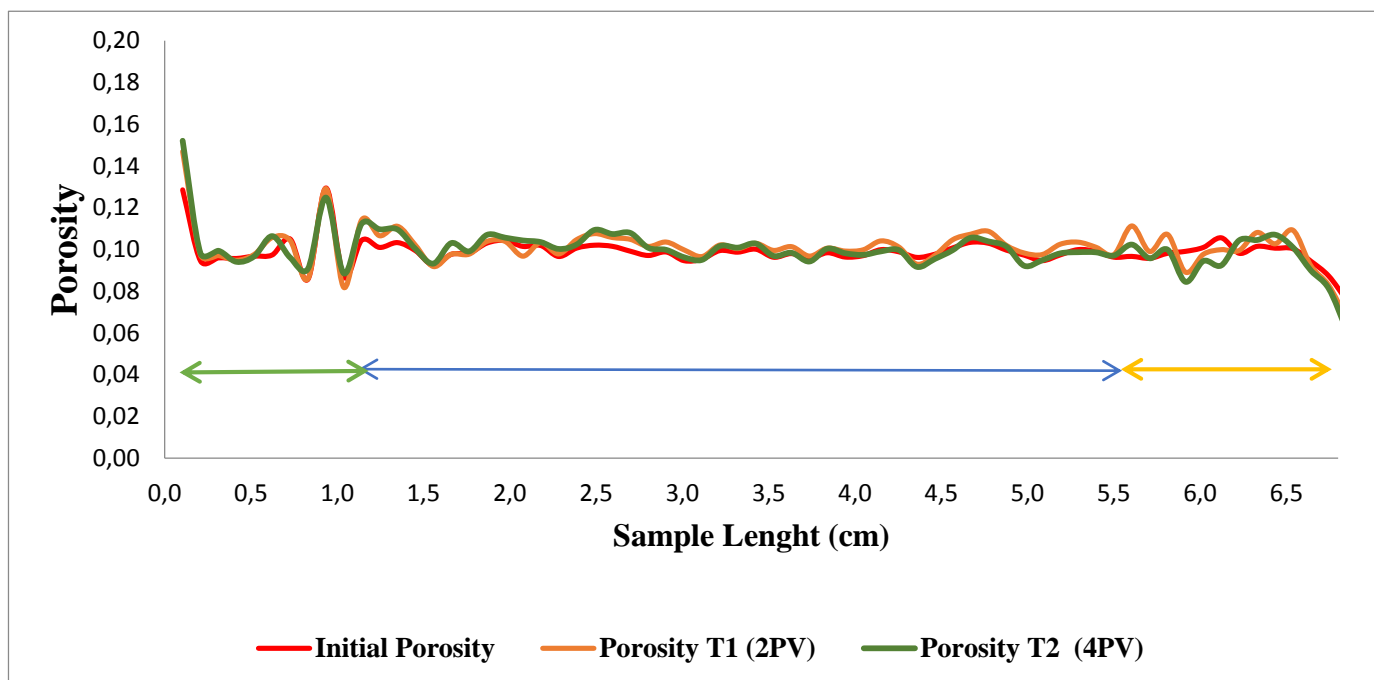


Figure 4.49 Porosity Variation along sample DH3-A

**Figure 4.51** shows the behavior of the porosity of the sample DH3-B as a function of sample length and it was possibly identified that at the last centimeters of the rock the behavior of the porosities profiles did not maintain the same tendency as the initial porosity how it can see at the CH2 in the experiments one and two. The other hand, Nuñez 2017 (**Figure 4.50**) also indicated that several points along the sample presented the behavior of the porosity where the tendency of the porosity trends did not maintain the tendency. For example at the centimeters 1.3, 2, and 5.5.



**Figure 4.50** Nunez 2017. Sample Porosity variation along the Dolomite sample R3N CH2



**Figure 4.51** Porosity Variation along sample DH3-A

#### 4.3.4.2 Permeability

Experiment with Reservoir rock (**Figure 4.55**) show that the permeability decreased along the test. The Initial permeability value was 69 mD, and the final value was 20 mD. On the other hand, Nuñez 2017 (**Figure 4.54**) indicated that permeability for the sample R1N placed in the first core holder presented a constant tendency along the entire experiment, with a value of 140 mD.

It can be concluded that the experiments, with 8250 psi of injection pressure and 70 °C, for dolomite rocks, with initial permeability value of 140 mD, show a constant tendency at the permeability property along to the experiment. On the hand, under the same conditions, for reservoir rock with an initial permeability value of 70 mD show a decrease tendency behavior along the experiment.



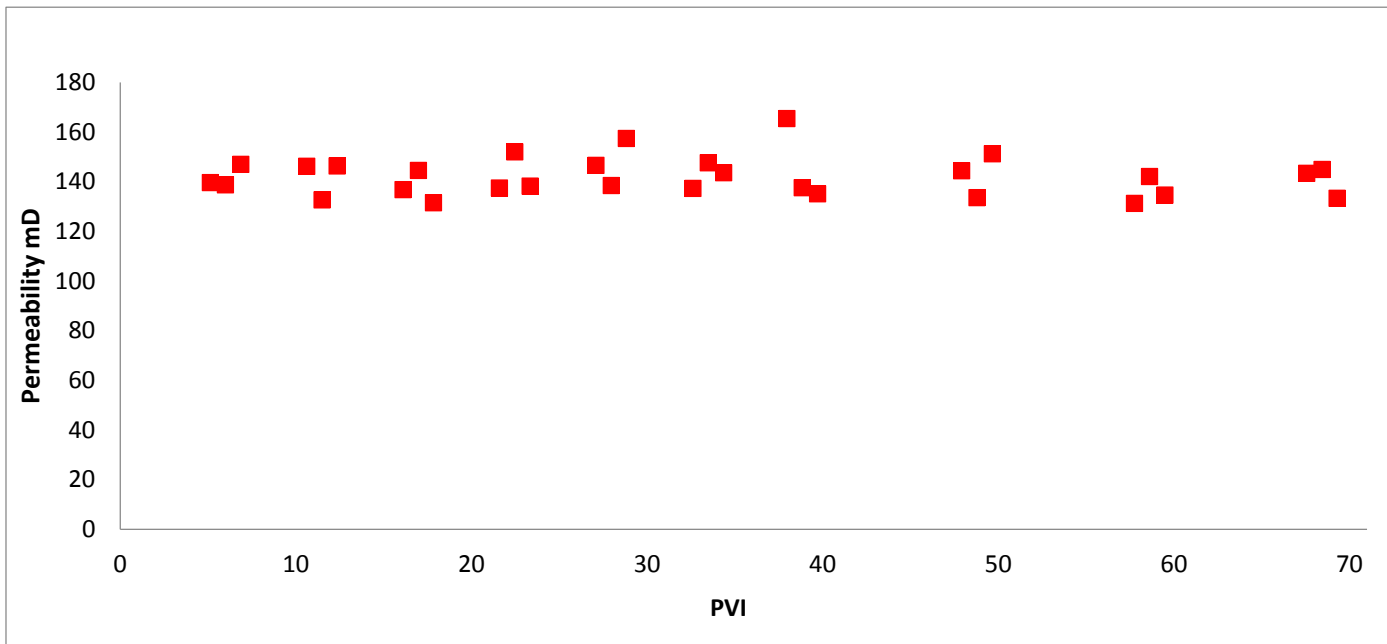


Figure 4.53 Permeability Scatter Plot of dolomite sample (R1N) CH1 by (Nuñez, 2017)

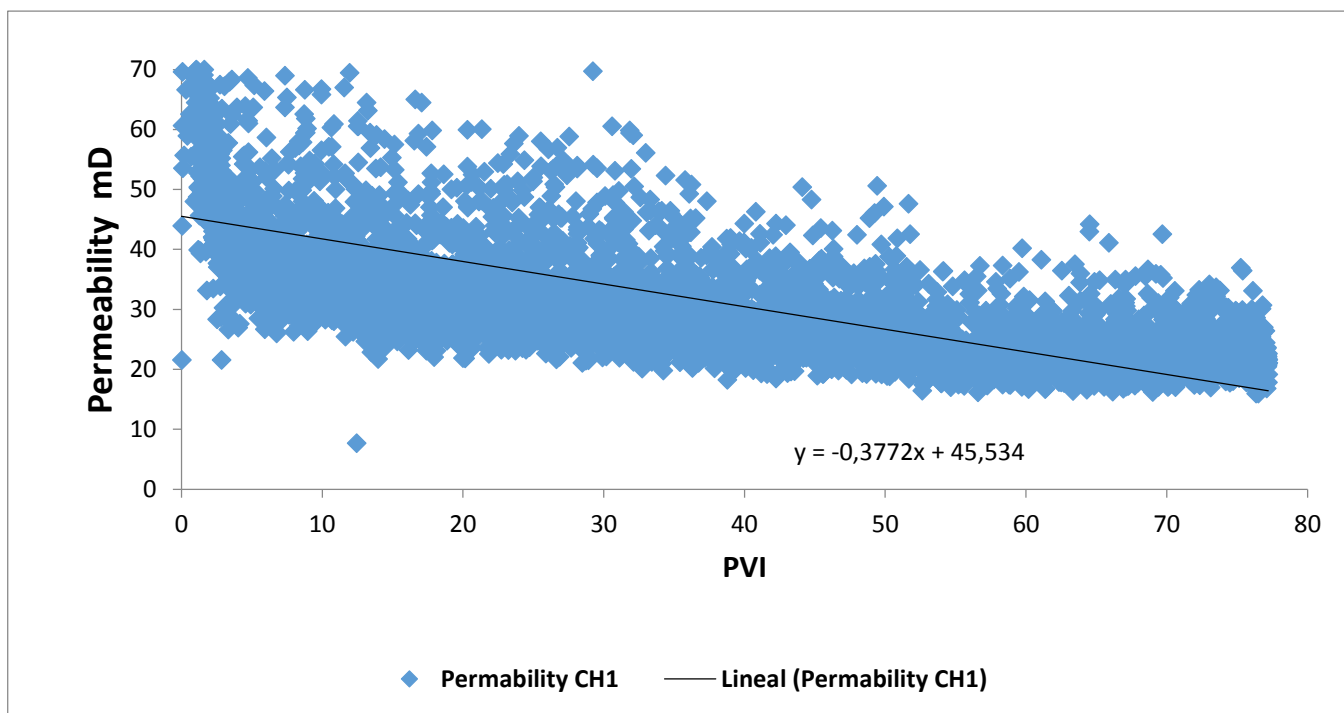


Figure 4.54 Permeability Experiment #3

#### 4.4 Dissolved Moles Results for Experiments 1, 2, and 3.

The dissolved moles for the experiments were calculated following mathematical development presented in Equation 3.6 to Equation 3.9 (section 3.2.6. Chapter 3).

For the **Equation 3.8** (section 3.2.6. Chapter 3), the % *Mineral* corresponds to mineral percentage present in the rock. We know that the rocks for our experiments are composed of calcite, dolomite, clay, and others. It was chosen the kaolinite that represent the clay.

##### 4.4.1 Experiment #1

###### 4.4.1.1 Core Holder 1 – DH1-A

For the analysis of the rocks DH1-A, the sample was divided into cells. The cell corresponds to a relationship between total core volume and number of images made by tomography of the rock – 47 for the CH1. One cell was chosen, which each represents the initial position in the porous medium (along with the rock length).

**Figure 4.55** to **Figure 4.57** show the minerals dissolved moles of cell one that corresponds to the face of the injection in the sample DH1-A. All minerals show a dissolution rate. The calcite has the highest dissolution rate compared to dolomite and kaolinite.

The **table 4.12** shows the reaction rate of minerals of cell 1 in the sample DH1-A.

**Table 4.12** Mineral Reaction Rate at the Cell 1 in the Sample DH1-A

Mineral	Reaction Rate
Calcite	$4 \times 10^{-6}$
Dolomite	$2 \times 10^{-6}$
Kaolinite	$5 \times 10^{-8}$

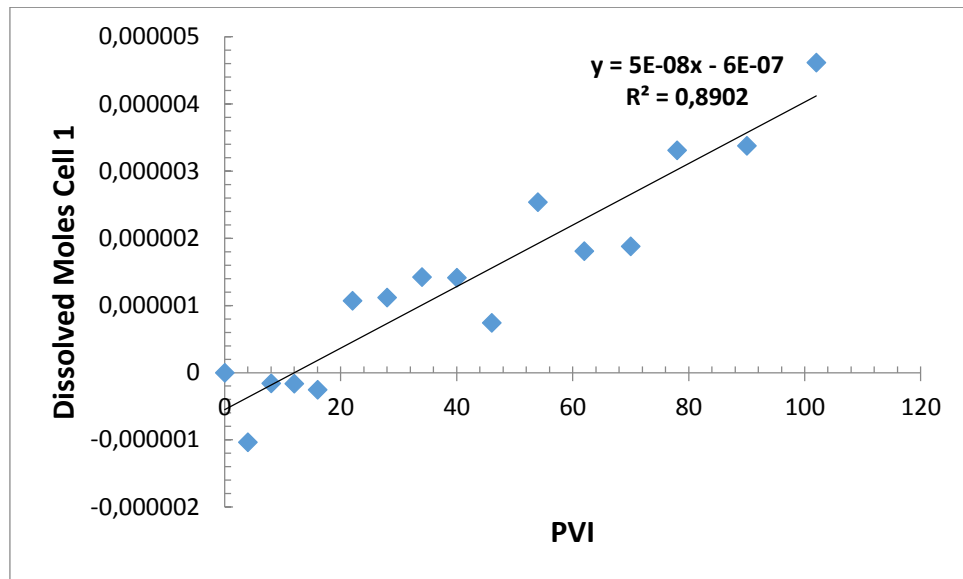


**Figure 4.55** Evolution of Dissolved moles of Kaolinite Sample DH1-A – Cell 1.

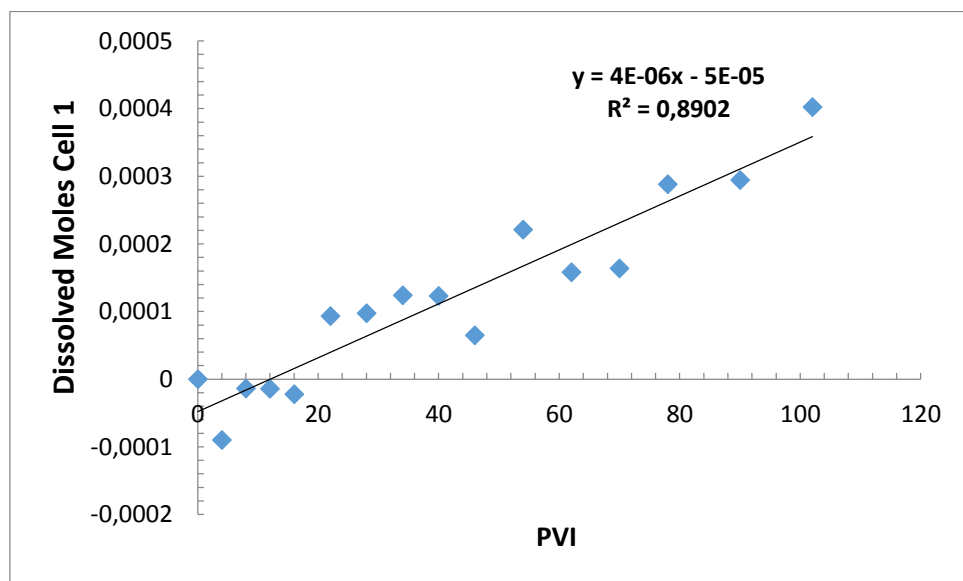


**Figure 4.56** Evolution of Dissolved moles of Calcite Sample DH1-A –Cell 1

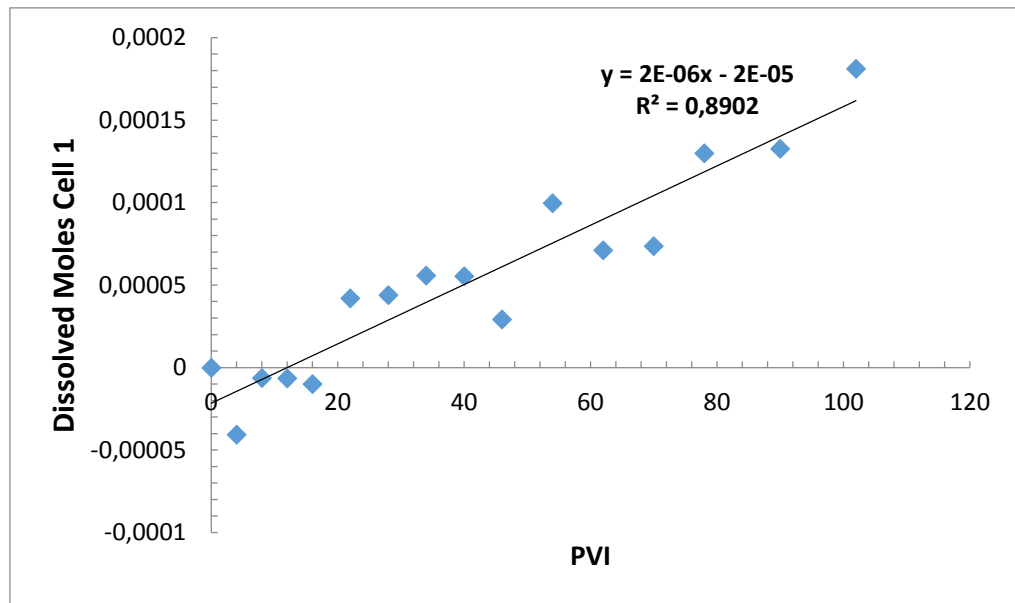


**Figure 4.57** Evolution of Dissolved moles of Dolomite Sample DH1-A – Cell 1

#### 4.4.1.2 Core Holder 2 – DH1-B

The same study for the sample DH1-B was made analyzing the cell one at the entrance of the injection. The **Table 4.13** corresponds to the Mineral Percentage DH1-B located CH2.

**Table 4.13** Mineral Percentage DH1-B located CH2

Mineral Name	% Mineral
Clay	1.35
Dolomite	37.9
Calcite	45.2
Others	15.5

**Figure 4.58** to **Figure 4.60** show the dissolved moles of the kaolinite, calcite and dolomite minerals behaviours to the cell 1 CH2. In this case, the highest

dissolution rate is for the calcite followed by dolomite, and the kaolinite. The calcite rate has the same order of magnitude of  $10^{-6}$  that the calcite rate at the CH1.

**Table 4.14** presents the dissolution rate for calcite, dolomite, and kaolinite. It can be observed that the dissolution rates values for all minerals showed that calcite has the highest dissolution rate, followed for the dolomite and kaolinite.

**Table 4.14** Mineral Reaction Rates at the Cell 1 in the Sample DH1-B

Mineral	Dissolution Rate
Calcite	$3 \times 10^{-6}$
Dolomite	$1 \times 10^{-6}$
Kaolinite	$3 \times 10^{-8}$

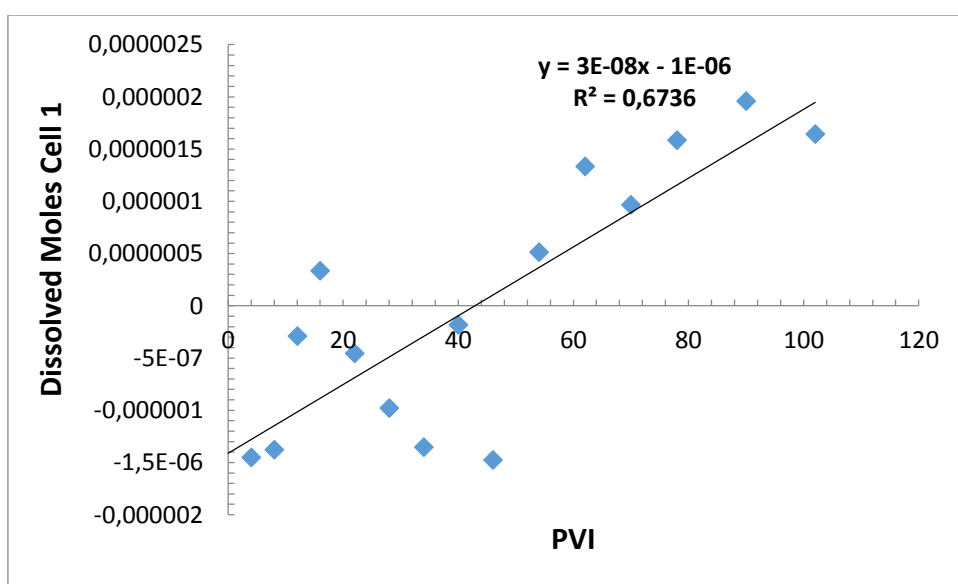


**Figure 4.58** Evolution of Dissolved moles of Kaolinite Sample DH1-B – Cell 1

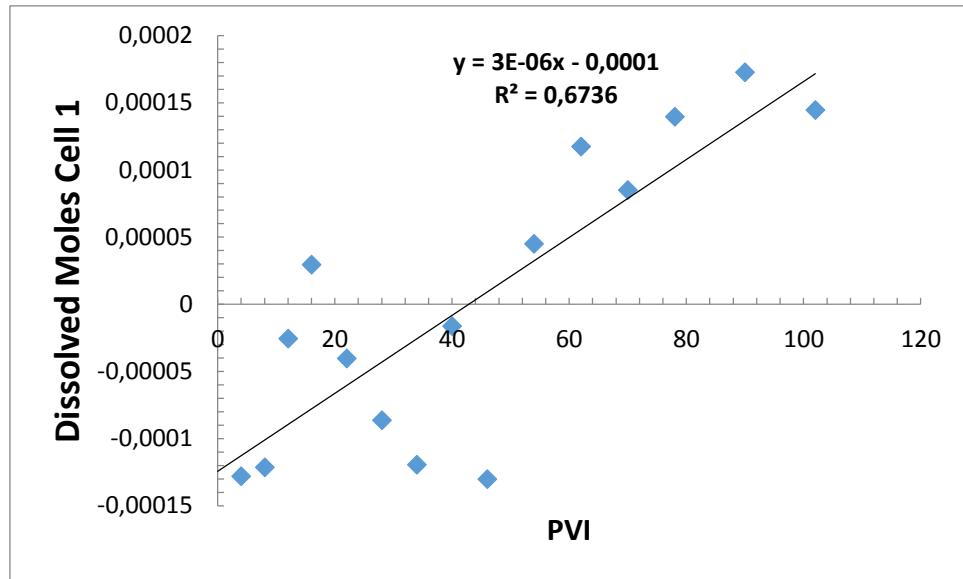


**Figure 4.59** Evolution of Dissolved moles of Calcite Sample DH1-B –Cell 1

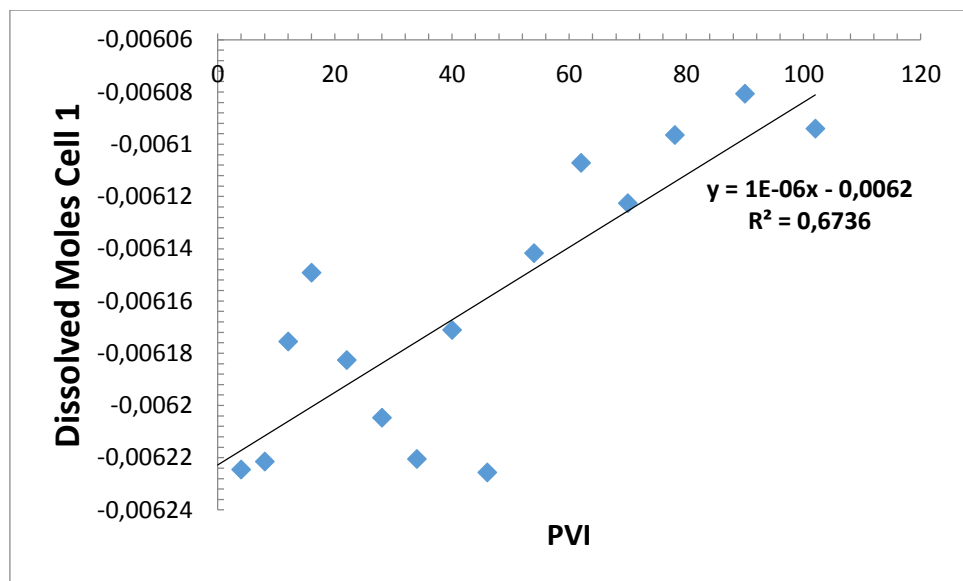


**Figure 4.60** Evolution of Dissolved moles of Dolomite Sample DH1-B – Cell 1

## 4.4.2 Experiment #2

### 4.4.2.1 Core Holder 1- DH2-A

The CT scan of sample DH2-A provided images of 57 transversal slices with 1 mm of length. Each slice was called cell. The study of the dissolved moles was

performed analyzing the cell one at the entrance of the injection. The same study for the sample DH1-B was performed analysing the cell one at the entrance of the injection.

The **Table 4.15** reports the mineral composition of sample DH2-A located CH1.

**Table 4.15.** Mineral Percentage DH2-A located CH1

Mineral Name	% Mineral
Clay	3.68
Dolomite	9.8
Calcite	77.22
Others	9.18

**Figure 4.61** to **Figure 4.63** present the reaction rate of the three minerals that the rock is composed. The rate shows an increasing linear behavior and positive slope in all three cases, which would also indicate the presence of dissolution phenomena and consequently a porosity growth in that cell. The **Table 4.16** shows the reaction rate for calcite, dolomite, and kaolinite. It can be observed that the calcite has the highest dissolution rate compared to dolomite and kaolinite. The three minerals in this cell presented the same behaviour than the cell 1-CH1 of experiment 1.

**Table 4.16** Mineral Reaction Rate at the Cell 1 in the Sample DH2-A

Mineral	Reaction Rate
Calcite	$6 \times 10^{-6}$
Dolomite	$2 \times 10^{-6}$
Kaolinite	$1 \times 10^{-7}$

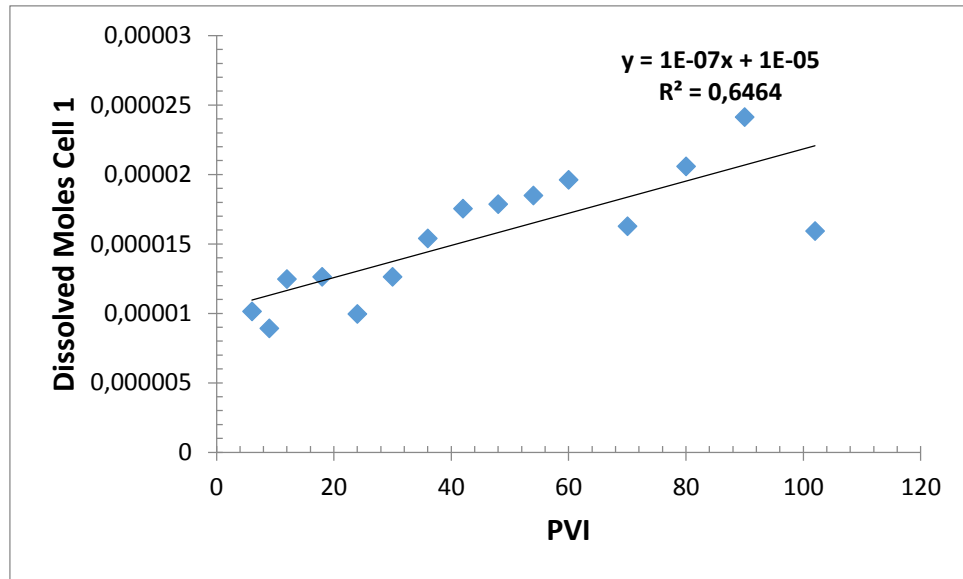


**Figure 4.61** Evolution of Dissolved moles of Kaolinite Sample DH2-A – Cell 1.

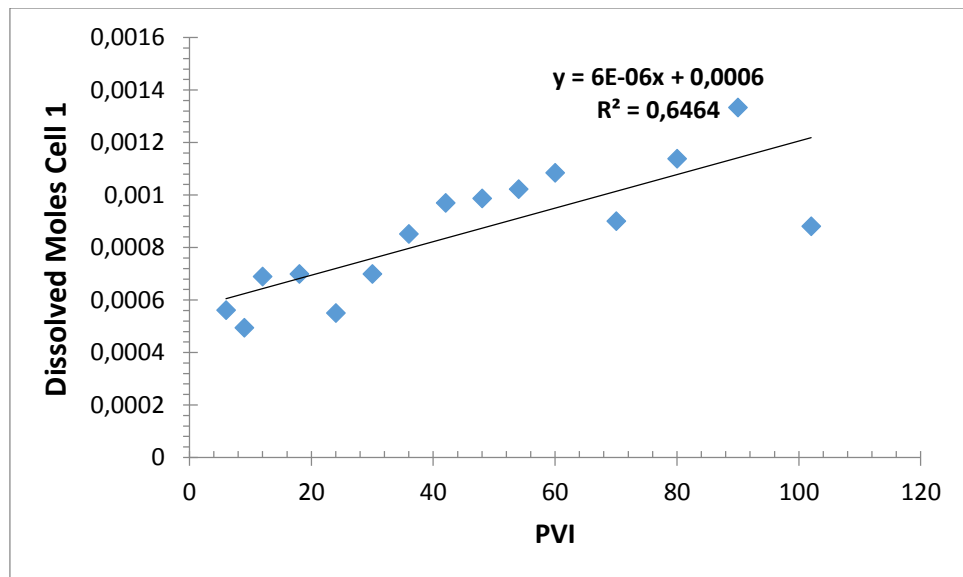


**Figure 4.62** Evolution of Dissolved moles of Calcite Sample DH2-A – Cell 1



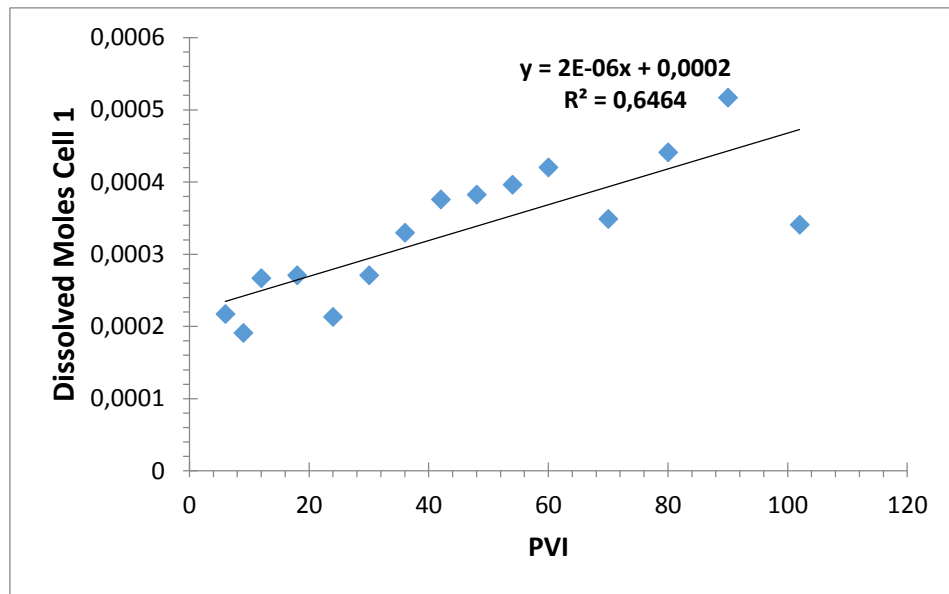


**Figure 4.63** Evolution of Dissolved moles of Dolomite Sample DH2-A – Cell 1

#### 4.4.2.2 Core Holder 2 – DH2-B

The **Table 4.17** shows composition in Mineral Percentage of sample DH2-B located CH2.

**Table 4.17.** Mineral Percentage DH2-B located CH2

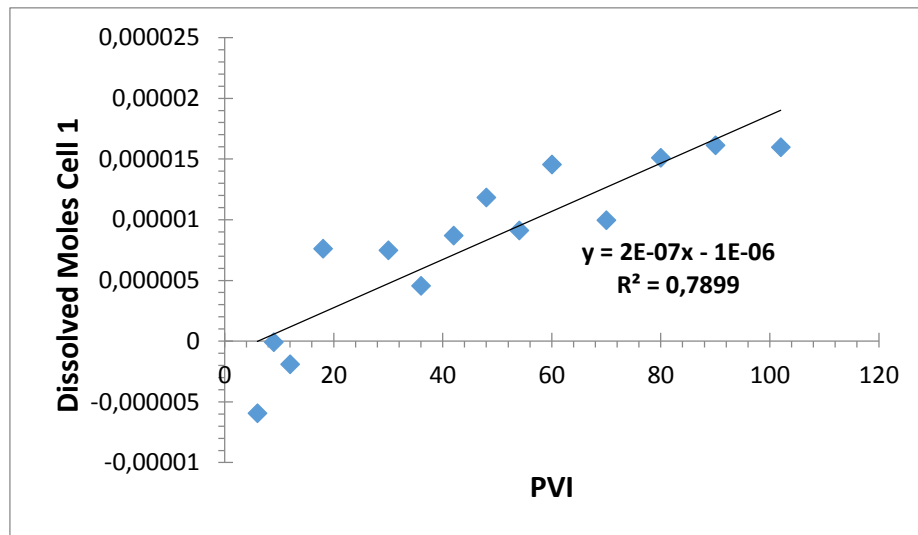
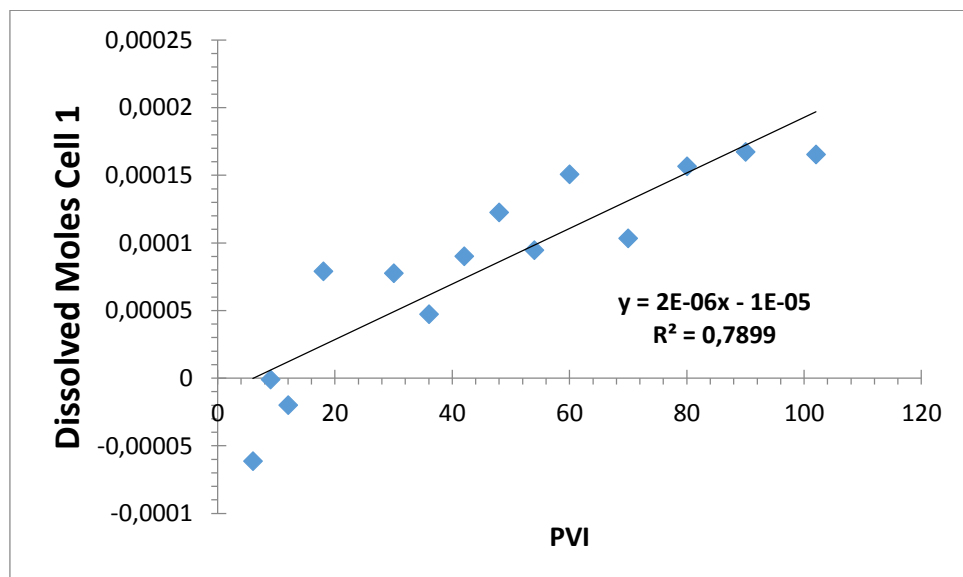
Mineral Name	% Mineral
Clay	4.76
Dolomite	64.31
Calcite	18.74
Others	12.19

**Figure 4.64** to **Figure 4.66** present dissolved moles as a function of porous volume injected of the three minerals that the rock is composed.

**Table 4.18** presented the reaction rate of minerals that contain the sample DH2-B. In this case, the dolomite has the highest dissolution rate compared to calcite and kaolinite. Dolomite has a higher reaction rate than the dolomite in the DH2-A

**Table 4.18** Mineral Dissolution Rate at the Cell 1 in the Sample DH2-B

Mineral	Dissolution Rate
Dolomite	$4 \times 10^{-6}$
Calcite	$2 \times 10^{-6}$
Kaolinite	$2 \times 10^{-7}$

**Figure 4.64** Evolution of Dissolved moles of Kaolinite Sample DH2-B – Cell 1**Figure 4.65** Evolution of Dissolved moles of Calcite Sample DH2-B – Cell 1

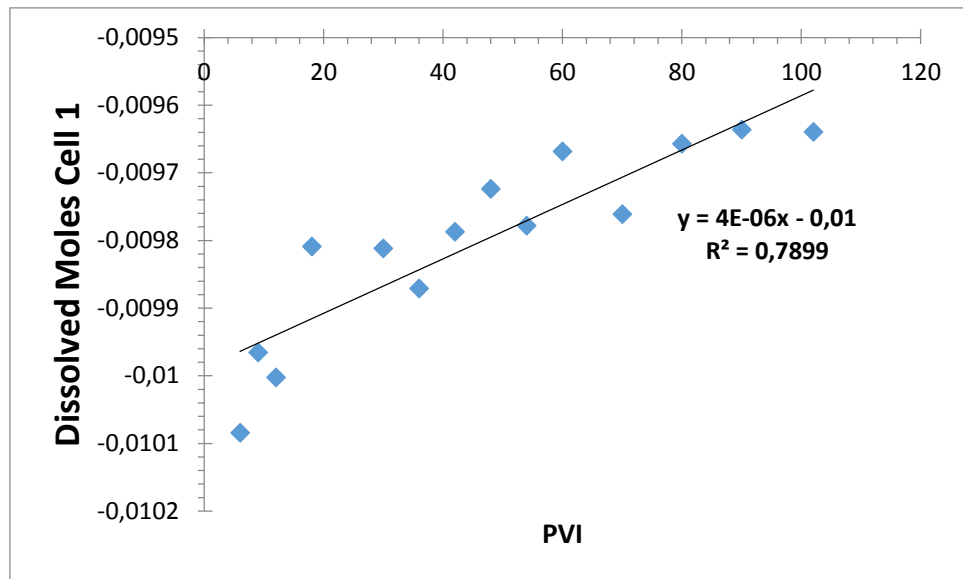


**Figure 4.66** Evolution of Dissolved moles of Dolomite Sample DH2-B – Cell 1

#### 4.4.3 Experiment #3

##### 4.4.3.1 Core Holder 1- DH3-A

The CT scan of sample DH3-A provided images of 44 transversal slices with 1 mm of length. The study of the dissolved moles was performed analyzing the cell one at the entrance of the injection, and the **Table 4.19** corresponds to the mineral percentage DH3-A located CH1.

**Table 4.19** Mineral Percentage DH3-A located CH1

Mineral Name	% Mineral
Clay	4.3
Dolomite	5.3
Calcite	84.1
Others	6.3

**Table 4.20** presents the reaction rate for calcite, dolomite, and kaolinite. The reaction rate was taken from the slope of the **Figure 4.67** to **Figure 4.69** that present the dissolution rate of the three minerals that the rock is composed.

It can notice that the calcite has the highest dissolution rate (positive reaction rate) compared to dolomite and kaolinite. The three minerals in this cell presented the same behaviour than experiment 1 –CH1-Cell 1.

**Table 4.20** Mineral Reaction Rate at the Cell 1 in the Sample DH3-A

Mineral	Reaction Rate
Calcite	$3 \times 10^{-6}$
Dolomite	$8 \times 10^{-7}$
Kaolinite	$5 \times 10^{-8}$

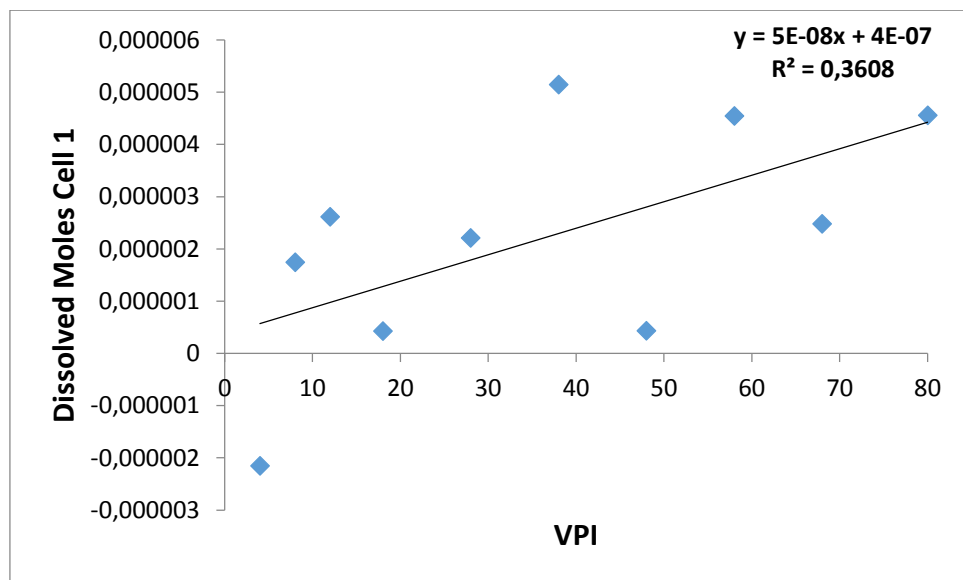


**Figure 4.67** Evolution of Dissolved moles of Kaolinite Sample DH3-A – Cell 1.

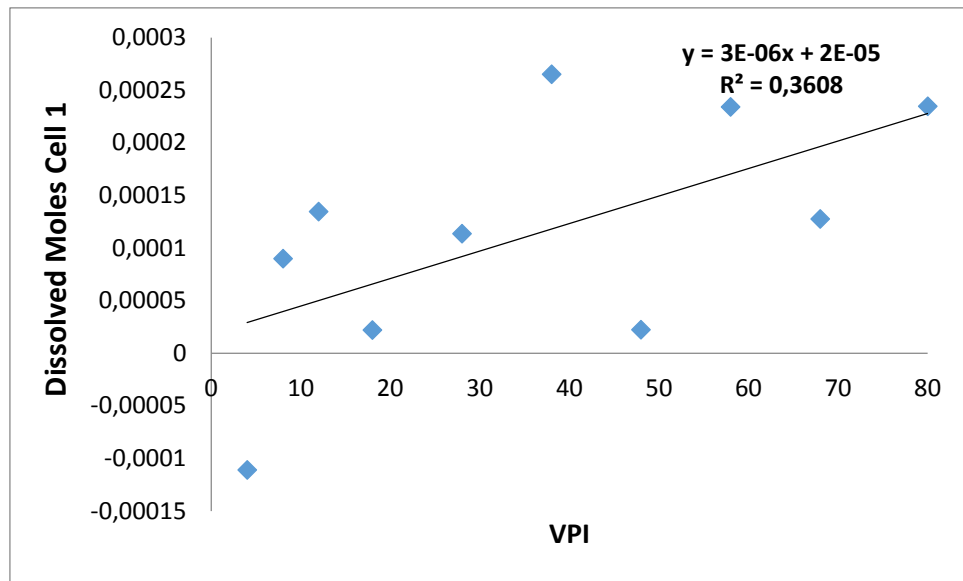


**Figure 4.68** Evolution of Dissolved moles of Calcite Sample DH3-A –Cell 1

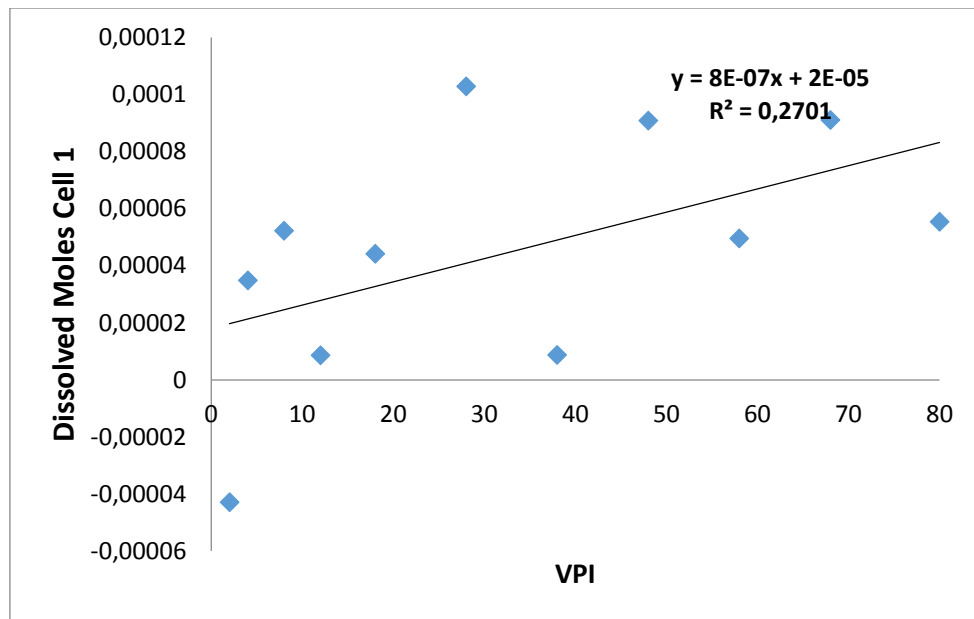


**Figure 4.69** Evolution of Dissolved moles of Dolomite Sample DH3-A – Cell 1

#### 4.4.4 Discussion of Results

Pokrovsky et al., 2005 indicated that dissolution rates of calcite and dolomite were measured at 25 ° C and PH from 3 to 4 as a function of salinity between 0.001 and 1 M [NaCl] and partial pressure of CO<sub>2</sub> between 10 -3.5 and 55 atm ( 0.05143 and 808.25 psi). Experiments on Calcite and dolomite were performed in a batch reactor controlled hydrodynamic conditions using the

rotating disk technique. The PH was measured in-situ an electrode in a cell without the liquid junction. He concluded that for the two minerals, the effect of the pressure of CO<sub>2</sub> had been found to insignificant compared with the PH. Also, he said that calcite dissolution rate depends on stirring between 200 and 2000 rpm at 2, 10, and 50 atm of the pressure of CO<sub>2</sub> suggesting mass transport at these conditions. For dolomite dissolution rates increase with increasing the pressure of CO<sub>2</sub> from 1 to 10 atm, and it stays constant when the pressure increased to 50 atm. The results of dissolution rates from the two minerals are presented in the from **Table 4.21**

**Table 4.21** Dolomite and Calcite rates measured at 25°C in rotaring disk experiments.

R <sub>mgmol/cm<sup>2</sup>/s</sub>	pCO <sub>2</sub> , atm (1,2)	pCO <sub>2</sub> , atm (10)	pCO <sub>2</sub> , atm (35)	pCO <sub>2</sub> , atm (50)
Dolomite	3.77e <sup>-10</sup>	1.21e <sup>-09</sup>	1.07e <sup>-09</sup>	1.02e <sup>-09</sup>
Calcite	4.74e <sup>-09</sup>	2.13e <sup>-08</sup>	1.80e <sup>-08</sup>	1.70e <sup>-08</sup>

In this work, it was injected carbonate water enriched with 25 % of CO<sub>2</sub>, into a carbonate rock, composed of dolomite, calcite, and shale, at different pressures 8500, 7500, and 8250 psi simulating some regions between the injector and producer well. **Table 4.22** and **Table 4.23** show the calcite and dolomite dissolution rates at different pressure from CH1 and CH2.

**Table 4.22** Dolomite and Calcite Rates measured at 70 °C in carbonate water injection experiment at CH1

R <sub>mgmol/cm<sup>2</sup>/s</sub>	pCO <sub>2</sub> , psi (8500) atm (578.38)	pCO <sub>2</sub> , psi (7500) atm (510.34)	pCO <sub>2</sub> , psi (8250) atm (561.37)
Dolomite	2 e <sup>-6</sup>	2 e <sup>-6</sup>	8 e <sup>-7</sup>
Calcite	4 e <sup>-6</sup>	6 e <sup>-6</sup>	3 e <sup>-6</sup>

**Table 4.23** Dolomite and Calcite Rates measured at 70 °C in carbonate water injection experiment at CH2

$R_{\text{mgmol/cm}^2/\text{s}}$	pCO <sub>2</sub> , psi (8500)	pCO <sub>2</sub> , psi (7500)
	atm (578.38)	atm (510.34)
Dolomite	$1 \text{ e}^{-6}$	$4 \text{ e}^{-6}$
Calcite	$3 \text{ e}^{-6}$	$2 \text{ e}^{-6}$

Both works were performed at different experiment conditions, Pokrovsky et al., 2005 worked with 25°C and pressure between 0.05 and 808 psi. On the other hand, this work is at 70°C and pressure from 7500 to 8500 psi. From both studies, it can be concluded for lower injected pressures, and lower temperatures; it is obtained lower calcite and dolomite dissolution rates.

## 5 CONCLUSIONS

This chapter presents the conclusions obtained by this work after of evaluating the phenomenon of dissolution and precipitation during carbonated water injection saturated with 25 % of CO<sub>2</sub> in Brazilian pre-salt carbonate rocks composed by calcite dolomite and clay at reservoir conditions in three different scenarios.

- In this research, the modifications carried out in order to improve the experimental methodology developed by Nunez (2017) and Vaz (2017) displayed to reach results successfully. The installation of transducers with high precision, and the injection of a carbonated water assembled in a single accumulator provided confiability on acquisition data .
- Experiment I showed that the main dissolution just occurred in the first sample (CH1) and in its first centimeters, the dissolution phenomenon was verified by porosity and permeability increase tendency.
- Experiment II indicated that the sample DH2-A, located in the first core holder, presented just right mineralogical composition for the study of dissolution phenomenon due to the rock presented dissolution along all sample's length. On the other hand, permeability presented a constant tendency along the experiment.
- Experiment II, in the second core holder, and I show a behavior where the porosity trends did not follow the initial porosity trend in some places at the rock. In others words, the rock has points where to different porous volume injected the sample presented dissolution or precipitation. This behavior had not been seen in the previous studies with outcrop carbonate rocks presented by Nunez (2017) and Vaz (2017).
- Analysing the behavior occurred at the second sample (CH2) of the Experiments I and II, it can be concluded that the principal factors that affect the behavior of the porosity trends are the heterogeneity according to the porosity and the mineralogical heterogeneity along the sample rock. When the heterogeneities in



porosity and mineralogy are in the same place of the rock, the porosity tendency did not match the initial porosity due to dissolution and precipitation phenomena coexist in the same point throughout the test.

- The sample DH3-A (Experiment III -Dissolution far from wellbore), located at the first core holder, did not show a significant porosity increment in the first centimeters and at the end of the test, as observed at the Experiment I and II. This behavior can be associated with the decrease amount of carbonic acid present in the projected carbonated water at 100 m.
- Permeability and porosity in experiment III, showan inversely proportional relationship due to porosity showed at an increasing tendency, and permeability had a decreased tendency.
- The ion calcium and ion magnesium were displayed changes in concentration at the end of the experiments I, II, and III. This performance was expected and it is related directly with the dissolution of the calcite, and the precipitation of the dolomite.
- Experiment I, II, and III show that the dissolution rate of the calcite is higher than the dissolution rates of the dolomite and kaolinite. For the first cell of each core holder at the three experiments, The calcite dissolution rate is on the order of  $10^{-6}$ , the dolomite dissolution rate is on the order of  $10^{-6}$  and  $10^{-7}$ , and the mineral with the lower dissolution rate is the kaolinite with values on the order of  $10^{-7}$  and  $10^{-8}$ .

## 6 REFERENCES

AL ADASANI, A.; BAI, B. Analysis of EOR projects and updated screening criteria. **Journal of Petroleum Science and Engineering**, v. 79, n. 1–2, p. 10–24, 2011.

ANDRÉ, L.; RABEMANANA, V.; VUATAZ, F. D. Influence of water-rock interactions on fracture permeability of the deep reservoir at Soultz-sous-Forêts, France. **Geothermics**, v. 35, n. 5–6, p. 507–531, 2006.

API. Recommended Practices for Core Analysis RB 40. **Api**, n. February, p. 236, 1998.

BACCI, G.; KORRE, A.; DURUCAN, S. An experimental and numerical investigation into the impact of dissolution/precipitation mechanisms on CO<sub>2</sub> injectivity in the wellbore and far field regions. **International Journal of Greenhouse Gas Control**, v. 5, n. 3, p. 579–588, 2011.

CHILINGARIAN, G. V. et al. **Interrelationships among surface area, permeability, porosity, pore size, and residual water saturation**. [s.l: s.n.]. v. 30

COTO, B. et al. Effects in the solubility of CaCO<sub>3</sub>: Experimental study and model description. **Fluid Phase Equilibria**, v. 324, p. 1–7, 2012.

CUI, G. et al. Injection of supercritical CO<sub>2</sub> for geothermal exploitation from sandstone and carbonate reservoirs: CO<sub>2</sub>–water–rock interactions and their effects. **Journal of CO<sub>2</sub> Utilization**, v. 20, n. May, p. 113–128, 2017.

DR. KARL JOUSTEN, DR. JÜRGEN DIRSCHERL, DR. RUDOLF LACHENMANN, DR. ALFONS JÜNEMANN, DR. -ING. FRIEDRICHSEN, DR. ERIK LIPPELT, D. I. B. K. Handbook of Vacuum Technology. In: [s.l: s.n.].

EGERMANN, P.; BAZIN, B.; VIZIKA, O. An Experimental Investigation of Reaction-Transport Phenomena During CO<sub>2</sub> Injection. **SPE Middle East Oil and Gas Show and Conference**, 2005.

FOGLER, H. S. Pore Evolution and Channel Formation During Flow and Reaction in Porous Media Pore Evolution and Channel Formation During Flow and Reaction in Porous Media. v. 34, n. October, p. 45–54, 1988.

GOLFIER, F. et al. On the ability of a Darcy-scale model to capture wormhole formation during the dissolution of a porous medium. **Journal of Fluid Mechanics**, v. 457, p. 213–254, 2002.

GOUZE, P.; LUQUOT, L. X-ray microtomography characterization of porosity, permeability and reactive surface changes during dissolution. **Journal of Contaminant Hydrology**, v. 120–121, n. C, p. 44–55, 2011.

GOZALPOUR, F.; REN, S. R.; TOHIDI, B. CO<sub>2</sub> EOR and storage in oil reservoirs. **Oil and Gas Science and Technology**, v. 60, n. 3, p. 537–546, 2005.

HOLM, L. W. Carbon Dioxide Solvent Flooding for Increased Oil Recovery. **Petroleum Transaction, AIME**, v. 216, p. 225–231, 1959.

IZGEC, O. et al. CO<sub>2</sub> injection in carbonates. **SPE Western Regional Meeting, Proceedings**, p. 231–239, 2005.

KALENDER, W. A. X-ray computed tomography. **Physics in medicine and biology**, v. 51, n. 13, p. R29–R29, 2006.

KANE, A. V. Performance Review of a Large-Scale CO<sub>2</sub>-WAG Enhanced Recovery Project, SACROC Unit Kelly-Snyder Field. **Journal of Petroleum Technology**, v. 31, n. 02, p. 217–231, 1979.

KECHUT, N. I. et al. Tertiary Oil Recovery and CO<sub>2</sub> Sequestration by Carbonated Water Injection (CWI). **SPE International Conference on CO<sub>2</sub> Capture, Storage, and Utilization**, 2010.

KHATHER, M. et al. Experimental investigation of changes in petrophysical properties during CO<sub>2</sub> injection into dolomite-rich rocks. **International Journal of Greenhouse Gas Control**, 2017.

LASAGA, A. C. Chemical kinetics of water-rock interactions. **Journal of Geophysical Research: Solid Earth**, v. 89, n. B6, p. 4009–4025, 1984.

LUQUOT, L.; GOUZE, P. Experimental determination of porosity and permeability changes induced by injection of CO<sub>2</sub> into carbonate rocks. **Chemical Geology**, v. 265, n. 1–2, p. 148–159, 2009.

MANRIQUE, E. J.; MUCI, V. E.; GURFINKEL, M. E. EOR Field Experiences in Carbonate Reservoirs in the United States. **SPE Reservoir Evaluation & Engineering**, v. 10, n. 06, p. 667–686, 2007.

MATLAB. High-Performance Numeric Computation and Visualization Software. Reference Guide version 4.2. Reading: The Mathworks Inc., 2016.

MCPHERSON, B.; LICHTNER, P. CO<sub>2</sub> sequestration in deep aquifers. ...

**on Carbon Sequestration, ...**, 2001.

MENKE, H. P. et al. Reservoir condition imaging of reactive transport in heterogeneous carbonates using fast synchrotron tomography - Effect of initial pore structure and flow conditions. **Chemical Geology**, v. 428, p. 15–26, 2016.

MONGER, T. G.; TRUJILLO, D. E.; U, L. S. Organic Deposition During CO<sub>2</sub> and Rich-Gas Flooding. n. February, 1991.

MOSAVAT, N.; TORABI, F. Performance of Secondary Carbonated Water Injection in Light Oil Systems. **Industrial & Engineering Chemistry Research**, v. 53, n. 3, p. 1262–1273, 2014.

MOSAVAT, N.; TORABI, F. Micro-optical analysis of carbonated water injection in irregular and heterogeneous pore geometry. **Fuel**, v. 175, p. 191–201, 2016.

NUÑEZ R.G, J. A. VARGAS, O.V. TREVISAN, R. VAZ, KOROISHI, E. T. Investigation of Dissolution Effects on Dolomite Porous Media Under Carbonated Water Injection. 2017.

NUÑEZ, R. R. B. **Investigation of Dissolution effects on Dolomite Porous Media Under Carbonated Water Injection**. [s.l.] Universidade Estadual de Campinas, 2017.

OUDEN, L. DEN et al. Tu B08 Calcite Dissolution Behaviour During Low Salinity Water Flooding in Carbonate Rock. **SPE Asia Pacific Enhanced Oil Recovery Conference**, n. AUGUST, p. 14–16, 2015.

PICHA, M. S. SPE 105425 Enhanced Oil Recovery by Hot CO<sub>2</sub> Flooding. 2007.

POKROVSKY, O. S.; GOLUBEV, S. V.; SCHOTT, J. Dissolution kinetics of calcite, dolomite and magnesite at 25 °C and 0 to 50 atm pCO<sub>2</sub>. **Chemical Geology**, v. 217, n. 3–4 SPEC. ISS., p. 239–255, 2005.

QAJAR, J.; ARNS, C. H. Characterization of reactive flow-induced evolution of carbonate rocks using digital core analysis- part 1: Assessment of pore-scale mineral dissolution and deposition. **Journal of Contaminant Hydrology**, 2016.

SHOGENOV, K. et al. Reservoir quality and petrophysical properties of Cambrian sandstones and their changes during the experimental modelling of CO<sub>2</sub> storage in the Baltic Basin. **Estonian Journal of Earth Sciences**, v. 64, n. 3, p. 199, 2015.

SHU, G. et al. Improvement of CO<sub>2</sub>EOR performance in water-wet reservoirs by adding active carbonated water. **Journal of Petroleum Science and Engineering**, v. 121, p. 142–148, 2014.

SOHRABI, M. et al. Carbonated Water Injection (CWI) - A productive way of using CO<sub>2</sub> for oil recovery and CO<sub>2</sub> storage. **Energy Procedia**, v. 4, p. 2192–2199, 2011.

TAYLOR, K. C.; MEHTA, S.; ARAMCO, S. SPE 89417 Anomalous Acid Reaction Rates in Carbonate Reservoir Rocks. **SPE Journal**, n. January 2004, p. 1–17, 2006.

TRAVIS, JEFFREY; KRING, J. **LabVIEW for Everyone**. [s.l: s.n.].

VAZ, R. G. et al. Carbonate Rock Dissolution under Carbonated Water Injection (CWI). p. 1–9, 2017.

VERMA, M. K. Fundamentals of Carbon Dioxide-Enhanced Oil Recovery (CO<sub>2</sub>-EOR)—A Supporting Document of the Assessment Methodology for Hydrocarbon Recovery Using CO<sub>2</sub>-EOR Associated with Carbon Sequestration. **U.S. Geological Survey Open-File Report**, p. 19, 2015.

W. WRIGHT. MARLOW, MICHAEL S., HOMA J. LEE, AND A. Physical properties of sediment from the Lesser Antilles margin along the Barbados Ridge: results from Deep Sea Drilling Project Leg 78A. p. 549–558, 1984.

YASUDA, E. Y. et al. Investigation on the Petrophysical Changes on a Coquina Core Under Carbonate Water Injection Assisted By Computerized Tomography. p. 1–9, 2017.

YASUDA, E. Y.; SANTOS, R. G. DOS; VIDAL TREVISAN, O. Kinetics of carbonate dissolution and its effects on the porosity and permeability of consolidated porous media. **Journal of Petroleum Science and Engineering**, v. 112, p. 284–289, 2013.

YUJI YASUDA, E. et al. Evaluation of Permeability Changes in a Carbonate Rock under Carbonate Water Flow. **Applied Mechanics and Materials**, v. 830, p. 65–70, 2016.

ZEKRI, A. Y.; SHEDID, S. A.; ALMEHAIDEB, R. A. Investigation of supercritical carbon dioxide, asphaltenic crude oil, and formation brine interactions in carbonate formations. **Journal of Petroleum Science and Engineering**, v. 69, n. 1–2, p. 63–70, 2009.

ZINSMEYER, T. M. et al. Back Pressure Valve. 1993.